Electrokinetic Detection of Sepsis Biomarkers in Dehydrated/Rehydrated Hydrogel

Electrokinetic Detection of Sepsis Biomarkers in Dehydrated/Rehydrated Hydrogel

By Shadi Shahriari, B.Sc.

A Thesis Submitted to the School of Graduate Studies in Partial Fulfilment of the Requirements for the Degree
Doctor of Philosophy

DOCTOR OF PHILOSOPHY (2024)

Graduate Program in

McMaster University, Hamilton, Ontario, Canada

TITLE: Electrokinetic Detection of Sepsis Biomarkers in Dehydrated/Rehydrated Hydrogel

AUTHOR: Shadi Shahriari

SUPERVISOR: Dr. P. Ravi Selvaganapathy

PAGES: 143

Abstract

According to the third international consensus definition (sepsis-3), sepsis is characterized as life-threatening organ dysfunction resulting from an uncontrolled host response to infection. Sepsis stands as a prominent contributor to worldwide mortality. A study revealed approximately 50 million reported cases of sepsis and 11 million associated deaths worldwide, constituting nearly 20% of all global fatalities. Various biomarkers have been investigated for sepsis prognosis including Procalcitonin (PCT), C-reactive protein (CRP), interleukin-1β (IL-1β), interleukin-6 (IL-6), and protein C. In addition to proteomic markers genomic biomarkers have also been investigated for sepsis. For instance, research indicates a substantial rise in plasma cell-free DNA (cfDNA) and total circulating histones levels during sepsis, correlating with its severity and mortality. The complexity arises in creating a measurement tool for sepsis, given the diverse nature of these biomarkers, each requiring distinct detection methods.

The objective of this doctoral thesis is to develop a low-cost fully integrated microfluidic device for detecting a genomic biomarker (cfDNA) and a proteomic biomarker (total circulating histones) using a new method for integration of hydrogels inside microfluidic devices during the fabrication process. This method involves using porous and fibrous membranes as scaffolds to support gels. The scaffold facilitates the drying and reconstitution of these gels without any loss of shape or leakage, making it advantageous in various applications, especially in point-of-care (POC) devices where long-term storage of gels inside the device is required. This hydrogel integration method was applied to demonstrate gel electrophoretic concentration and isoelectric trapping of cfDNA and histones respectively in rehydrated agarose gates with proper pH embedded in a porous membrane in a microfluidic device. Then, these two detections were performed in a single fully integrated microfluidic device. Additionally, nonspecific fluorescent dyes were incorporated

within the device, eliminating the necessity for off-chip sample preparation. This enables direct testing of plasma samples without the need to label DNA and histones with fluorescent dyes beforehand. In all the fabrication steps of the microfluidic device, xurography, a cost-effective and rapid fabrication method, was utilized. This device demonstrated the effective separation of cfDNA and histones in the agarose gates in a total time of 20 minutes, employing 10 and 30 Volts for cfDNA and histone accumulation, respectively. This device could be further developed to create a POC device for the quantification of cfDNA and histones simultaneously in severe sepsis patients plasma sample.

Acknowledgements

I am grateful to everyone who has supported me during my Ph.D. journey. First and foremost, I would like to express my sincere gratitude to my supervisor, Dr. Ravi Selvaganapathy for his constant support, guidance, and encouragement. I have not only gained extensive knowledge in my professional endeavors but have also experienced significant personal growth under his guidance. He provided me with a flexible research environment, allowing me to thrive both professionally and personally.

I extend my heartfelt appreciation to my committee members, Dr. Ching and Dr. Howlader, for taking the time to provide me with guidance and insights over the course of the Ph.D. Their valuable suggestions greatly enriched the quality of this research. I would also like to thank Dr. Alison E. Fox-Robichaud, Dr. Patricia C. Liaw, Dr. Dhruva J. Dwivedi, and Dr. Jaskirat Arora for helping me better understand the clinical side of the project and providing me the clinical samples.

I would like to thank my friends and past and current CAMEF group members, who made my Ph.D. a more enjoyable and memorable journey. Thank you for all your help, friendship, and unforgettable memories both in and outside of the laboratory. Special thanks go to my friend, Elaheh. Her friendship has been a source of intellectual stimulation and emotional support.

Finally, I would like to express my gratitude to my family for their unwavering love and support. Without them none of this would have been possible. Their encouragement and belief in my abilities have been a constant source of motivation.

At the end, I want to express my deepest gratitude to all those whose names may not appear here but have, in various ways, contributed to the successful completion of this thesis.

Thank you all for being an integral part of this academic endeavor.

Table of Contents

List of figures and tables

List of abbreviations

BSA – Bovine serum albumin

CE – Capillary Electrophoresis

cfDNA – Cell free deoxyribonucleic acid

CRP – C-reactive protein

DAMPs – Damage-associated molecular patterns

DC – Direct current

DCM – Dichloromethane

DEP – Dielectrophoresis

dIEF/ cIEF – digital/ capillary isoelectric focusing

DI water – Deionized water

dPCR – Digital PCR

ELISA – Enzyme-linked immunosorbent assay

EP – Electrophoresis

FAS – Field-amplified stacking

ICP – Ion concentration polarization

ICU – Intensive care unit

IEF – Isoelectric focusing

IET – Isoelectric trapping

IL – Interleukin

ITP – Isotachophoresis

LOD – Limit of detection

LOS – Length of stay

PAAM – Polyacrylamide

PAGE – Polyacrylamide gel electrophoresis

PAMPs – Pathogen-associated molecular patterns

PCL – Polycaprolactone

PCR – Polymerase chain reaction

PCT – Procalcitonin

PDMS – Polydimethylsiloxane

PEG – Polyethylene glycol

PET – Polyethylene Terephthalate

pI – Isoelectric point

PI – Polyimide

pNIPAAM – Poly-N-isopropyl acrylamide

POC – Point of Care

PS – Polystyrene

PSA – Pressure sensitive adhesive

PTFE – Polytetrafluoroethylene

PVA – Polyvinyl alcohol

PVC – Polyvinyl chloride

qPCR – Quantitative PCR

qSOFA – Quick SOFA

RNA – Ribonucleic acid

SEM – Scanning electron microscopy

SOFA – Sequential Organ Failure Assessment

SPE – Solid phase extraction

TAE – Tris-acetate-EDTA

TNF-α – Tumor necrosis factor-α

UV – Ultraviolet

1 Chapter 1 Introduction

Sections: 1.2 Microfluidics and 1.2.2 Fabrication techniques of microfluidic devices; full Citation: Shahriari, S.; Patel, V.; Selvaganapathy, P.R. Xurography as a Tool for the Fabrication of Microfluidic Devices. Journal of Micromechanics and Microengineering 2023.

1.1 Sepsis

Based on third international consensus definition (sepsis-3), sepsis is defined as "life-threatening organ dysfunction caused by a dysregulated host response to infection"[1]. Sepsis is one of the leading causes of mortality worldwide [2,3]. Based on a study in 2017, around 50 million sepsis cases and 11 million deaths related to sepsis were reported worldwide, accounting for near 20% of all global deaths [4]. Some studies have demonstrated annual decline in sepsis-related mortality rates. However, in low and middle-income countries, a significant mortality rate as high as 80% persists [5]. Sepsis also creates a greater strain on hospitals resources. In U.S. the average length of stay (LOS) of septic patients in hospitals is about 75% more than other medical conditions and the sepsis management expenses stand as the most expensive. For example, in 2013, 13% of the overall U.S. hospital costs was related to sepsis and it accounted for over $24 billion (~$18,244 per hospitalization). Similar to mortality and LOS, it was demonstrated that there was a significant rise in average daily hospital costs as the severity of sepsis increased [6]. In Canada, it is estimated that one year costs of sepsis to the Ontario healthcare system is near $1 billion [7]. Delayed diagnosis and treatment result in unfavorable sepsis outcomes. Studies demonstrated that delay in first antibiotic administration was correlated with increased sepsis mortality [8–10]. On average, every hour of delay was linked to a roughly 7% decrease in survival rates [10].

1.1.1 Current diagnosis and prognosis methods

Sequential Organ Failure Analysis (SOFA) assessment is a scoring system for determining organ dysfunction and it helps health care professionals to evaluate and track the extent of organ failure in sepsis patients. SOFA score is based on several parameters such as oxygen level, platelet, bilirubin, and creatinine level, Glasgow Coma Scale score, and mean arterial pressure [11]. If there is no organ dysfunction, SOFA score is zero. As the SOFA score rises, it indicates general

deterioration and a score of 2 or more is linked with higher mortality [12]. However, as SOFA needs several laboratory information which are not immediately available at the bedside, a simpler and quicker scoring system is needed to help with clinical assessments. Quick SOFA (qSOFA) enables a simple and rapid evaluation in the settings like pre-hospital, clinic, or emergency department [11,12]. The qSOFA system allocates one point for each of these conditions: systolic blood pressure of 100 mmHg or lower, respiratory rate of 22 per minute or higher, and altered mental status (Glasgow Coma Scale score of 13 or lower) [13]. A qSOFA score of 2 or greater with a suspected infection is considered as a signal for closer monitoring and potentially ICU admission to prevent worsening outcomes [11,13]. Although qSOFA is helpful in identifying organ dysfunction and mortality risk in sepsis, it necessitates cautious interpretation for defining sepsis. One issue is qSOFA sensitivity for early risk assessment as it relies on the clinician's skill to recognize infection as the underlying reason for organ dysfunction, which might not be easily noticeable in the initial stages. Furthermore, qSOFA's validation has been primarily conducted outside of the ICU and may not useful for the patients already admitted to ICU unit [11]. Therefore, the mentioned factors can contribute to delayed or incorrect diagnosis and prognosis of sepsis. The development of sepsis biomarkers can help in diagnosis and prognosis of sepsis and monitoring treatment responses.

1.1.2 Sepsis Biomarkers

Biomarkers play a valuable role for diagnosis, prognosis, early organ dysfunction recognition, and identification of suitable treatment for patients with sepsis or suspected sepsis. A variety of biomarkers have been identified for sepsis. They include acute-phase proteins, fluid phase pattern recognition molecules (PRMs), damage-associated molecular patterns (DAMPs), cytokines, chemokines, endothelial cell markers, cell membrane receptors, non-coding RNAs, miRNA, and

soluble receptors, and metabolites [14]. Sepsis begins when the innate immune cells constituted by macrophages, monocytes, and neutrophils, detect the presence of damage-associated molecular patterns (DAMPs) or pathogen-associated molecular patterns (PAMPs). The detection of DAMPs or PAMPs is carried out by pattern-recognition receptors present on host cells. This leads to activation of intracellular signal transduction pathways which triggers the release of various mediators, including pro-inflammatory and anti-inflammatory molecules such as tumor necrosis factor-α (TNF-α), interleukin-1β (IL-1β), and interleukin-6 (IL-6) [15]. Sepsis also results in rise in the levels of acute phase proteins. These proteins include procalcitonin (PCT), calprotectin, pro-adrenomedulin, pentraxin-3, and C-reactive protein (CRP). Moreover, the concentrations of glycoproteins found on the surfaces of cells, such as presepsin, soluble triggering receptor expressed on myeloid cell 1 (sTREM-1), and soluble urokinase plasminogen activator receptor (suPAR), could potentially be elevated. CD64 index, an immunoglobulin receptor, also increases in the early stages of activation of the innate immune response. Many of these molecules have been considered as sepsis biomarkers. Particularly, procalcitonin (PCT) and C-reactive protein (CRP) are widely recognized as biomarkers used in diagnosis and prognosis of sepsis [5]. CRP is a protein in blood plasma which is synthesized and released by the liver [16]. CRP is a clinical marker of inflammation and infection independent of the underlining cause. Therefore, the main limitation of CRP is its lack of specificity for sepsis diagnosis, as it also increases in other inflammatory conditions such as autoimmune diseases and cancer [17]. PCT is another biomarker of sepsis that was initially identified in 1993. Serum concentration of PCT in healthy individuals is below 0.1 ng/mL and it increases significantly in response to a bacterial infection [18]. However, PCT might not consistently serve as a dependable prognostic indicator and often holds limited significance as a standalone value [19]. Therefore, it is common for healthcare professionals to

use a combination of laboratory tests and multiple biomarkers to diagnose and manage sepsis effectively.

In a recent review, 258 biomarkers have been identified for sepsis, of these 69 were mainly evaluated for their diagnostic value, 100 for sepsis prognosis, and 89 for both diagnosis and prognosis [20]. Studies have shown that apoptotic biomarkers (cell-free DNA, nucleosomes, histones) represent the cumulative organ injury and systemic inflammation. Therefore, they have the potential to offer independent and additive predictive capabilities when combined with conventional biomarkers and scoring systems. Level of apoptotic biomarkers which indicate cellular apoptosis activity, was higher in sepsis non-survivors compared to survivors [21]. Thus, two of the recently proposed prognostic biomarkers for sepsis are cell-free DNA (cfDNA) and histones [22–27]. Nucleosome contains an octamer consisting of two dimers of histone H2A and H2B and a tetramer of histone H3 and H4 forms a core around which 147 bp of DNA is wrapped ±1.67 times. The structural arrangement of nucleosomes is crucial in the regulation of gene transcription and supports effective compaction of chromatin at higher levels. Widespread cell death during sepsis contributes to extracellular release of DNA and histones. Circulating levels of nucleosomes, cfDNA, and histones are increased in sepsis [28–31].

1.1.2.1 Cell-free DNA

Free circulating DNA or cell-free DNA (cfDNA) was discovered in 1948 by Mandel and Metai in human blood plasma [32]. cfDNA is comprised of short-lived fragments (50–200 base pair (bp)) of DNA, wrapped around histones and is released to the blood circulation from a number of cells, including neutrophils, eosinophils, and macrophages, as a result of necrosis, apoptosis or other forms of cellular damage [33]. Increased levels of cfDNA in blood is a result of various conditions such as cancer, trauma, stroke or sepsis [34]. Lately, there has been growing interest in utilizing

cfDNA as a biomarker for prediction of mortality in sepsis patients. Studies have revealed that patients who do not survive exhibit higher concentrations of cfDNA compared to those who survive [18,25]. Based on a study on patients with severe sepsis, the mean cfDNA level in survivors was 1.16±0.13 μg/mL which was similar to healthy volunteers (0.93±0.76μg/mL), however, for non-survivors was 4.65±0.48μg/mL [23]. cfDNA with a cut-off of 2.35 μg/mL exhibits an 88% sensitivity and a 94% specificity in predicting ICU mortality.

1.1.2.2 Current methods for cfDNA quantification

There is a requirement for accurate and easily applicable methods to quantify cfDNA. Currently, there are multiple methods for measurement of cfDNA level including spectrophotometry, fluorometry, quantitative PCR (qPCR), digital PCR (dPCR), and electrophoresis [32,35]. UV Spectrometry is the most popular and simplest way to measure DNA concentration. DNA has an absorbance peak at 260nm; therefore, by using Lambert-Beer's law, the concentration of the sample can be obtained through its absorbed UV light intensity. The UV spectrometry method has several limitations, such as the need for pure DNA in order to be measured accurately. Also, most of the instruments using UV spectrometry method are able to measure only concentrations higher than 2μg/mL [36].

Quantitative PCR (qPCR) is a method combining conventional PCR amplification technique and fluorescent quantification to measure DNA concentrations. In this technique, by measuring fluorescence intensity after each cycle, the amount of DNA amplicons in the that cycle is obtained [37]. There are several limitations for using this method; such as its high cost and requirement for prior sequence information about the particular gene of interest [38,39]. Also, qPCR necessitates specific reagents such as primers, probes, enzymes, and fluorescent dyes. qPCR requires skilled

personnel to conduct the entire process. This requirement can pose challenges to its application in settings with limited resources [38].

Digital PCR (dPCR) is a new technique for measuring absolute and relative numbers of copies of the template DNA. In dPCR individual DNA molecules disperse into thousands of smaller units, and each unit can contain one to several molecules or even no DNA template. After the amplification of the DNA in the partitions, the number of units which have amplified DNA is counted. This is performed based on the existence or absence of fluorescence signal (recognized as 1 or 0). Based on the proportion of positive partitions, the number of the target molecule in the origin solution is obtained [36,40]. dPCR needs only small amounts of sample and it has high sensitivity; however, the cost of dPCR analysis is higher than other methods [41]. In all of the PCR based methods, only the DNA that corresponds to the selected primers is quantified and they do not provide information about the total amount of DNA in a sample.

Fluorescent dyes which bind to DNA specifically are commonly used in quantification. This DNA quantification method is able to detect a much lower concentration of DNA and is more sensitive [42]. The available fluorescent dyes such as PicoGreen and Qubit assays which specifically bind to double-stranded DNA (dsDNA) offer a detection accuracy of pg/mL. Fluorometric quantification delivers easy workflow and is less time consuming as compared to other methods. Quantification of cfDNA with fluorescent dyes is mostly combined with EP or DEP based extraction methods in microfluidic devices. In this case, after EP or DEP cfDNA isolation and removing impurities, the concentrated cfDNA is detected directly on chip. For example, Sonnenberg et al. used a DEP-based device for rapid isolation of cfDNA from blood samples of chronic lymphocytic leukemia (CLL) patients and quantified using fluorescent dye [43].

1.1.2.3 Histone

Histones are chromatin subunits, and they are classified into core histones (H2A, H2B, H3, and H4) and linker histones (H1 and H5). Histones have N-terminal tail that contains amino acids rich in lysine and arginine, contributing to the positively charged nature of histones. This positive charge facilitates the binding of histones to the negatively charged DNA [26]. Histones typically have an isoelectric point around 11 and exhibit a molecular weight ranging from 10−22 kDa, depending on the specific fraction [44]. Histones can be released from nucleus into the extracellular space, where they may act as damage-associated molecular pattern (DAMP) molecules, contributing to inflammation and tissue damage. The extracellular release of histones necessitates the disruption of both nuclear and plasma cell membranes, resembling the necrosis commonly observed in acute organ injury. Similarly, regulated forms of necrosis specific to immune cells, such as NETosis in neutrophils and eTosis in other granulocytes or macrophages, also play a role in the generation of circulating histones [26,45,46].

High concentrations of circulating histones have been associated with disease severity and mortality in certain medical conditions such as sepsis. Therefore, extracellular histones have been identified as prognostic biomarkers for sepsis. [22,24,26,27,47–50]. It has been demonstrated that the total circulating histone level was significantly higher in septic patients who died within 28 days of ICU admission (32.7 μg/mL) compared to survivors (20.1 μg/mL) ($P < 0.0001$). In contrast, the total circulating histone concentration for healthy persons was much lower (1.3 μg/mL) [22]. Therefore, monitoring histone levels in the bloodstream may offer insights into the progression of sepsis and guide physicians in identifying patients who may benefit from a more aggressive care plan.

1.1.2.4 Current methods for histone quantification

Several methods are employed to detect the presence of circulating histones and their quantification. Immunoblot assays (western blotting) are commonly used, allowing the visualization of histones in patient samples; however, they lack the ability to distinguish between freely circulating histones, histones bound to DNA, or those within nucleosome complexes. Enzyme-linked immunosorbent assay (ELISA), on the other hand, has been developed to quantify specific histone subtypes, often utilizing polyclonal antibodies, making it challenging to exclusively detect free histones. Roche's Cell Death Detection ELISA employs a monoclonal anti-histone antibody as a catching antibody and a monoclonal anti-DNA antibody for detection. Therefore, it detects the amount of cleaved DNA/histone complexes [29]. Additionally, the ELISA assays are expensive and time-consuming. Therefore, alternative methods, may prove beneficial for developing devices capable of accurately distinguishing total circulating histones in various clinical scenarios.

A point-of-care (POC) device for detection of cfDNA and total histones in plasma need to be low-cost and rapid with minimized number and complexity of steps which reduces the need for manual intervention and trained personnel. This can be most effectively accomplished by using microfluidics which allows the integration of various steps and the simultaneous detection of multiple biomarkers in an affordable and rapid format.

1.2 Microfluidics

Microfluidics is the field that deals with the flow of fluids in structures at the sub-millimeter scale. This field has been investigated intensely over the past few decades and has been applied in several areas from biology, medicine, chemistry, engineering, and the environment [51,52]. Various components such as micromixers [53–56], micropumps [57–60], microvalves [57,61], biosensors

[62,63], droplet generators [64–66], and separation devices [67–69] have been developed to control and handle fluid flow at the sub millimeter scale in microfluidic devices. Microfluidic devices have several advantages such as low cost, small size, ability to handle small sample volume and low power consumption that can improve their analytical performance and sensitivity compared to the conventional size systems [51,70].

Recently, sample preparation steps, such as extraction, concentration, labeling, and separation have been performed on-chip by integrating them into microfluidic devices [69]. This leads to decreasing manual sample handling and improving diagnostic accuracy. Sample type (e.g, whole blood, serum, or saliva), the type of analysis, and the target analyte affect the complexity of the preparation step [71].

1.2.1 Microfluidics for separation and detection of biomarkers

Sample extraction and preconcentration in microfluidics can be classified into two categories: electrophoretic and nonelectrophoretic methods. Electrophoretic methods mostly include field-amplified stacking (FAS), isotachophoresis (ITP), and isoelectric focusing (IEF) [72]. Nonelectrophoretic methods consist of solid phase extraction (SPE), antibody-based extraction, and aptamer-based extraction [69].

1.2.1.1 Electrokinetic methods

Electrokinetic methods deal with the movement of fluid and ions in electric fields. Mostly in this method, the equipment is simple as only high voltage is needed for separation of the target and there is no need to use pumps; therefore, it is the preferred separation method to be implemented in microfluidic devices [73].

1.2.1.2 Electrophoretic Separation

Electrophoresis is the movement of particles to the opposite electrode under the influence of an electric field. Particles move depending on their electrophoresis mobility. Electrical mobility depends on the zeta potential (ζ_p) and viscosity of the fluid. Electrophoresis force is written as:

$$F_{EP} = 6\pi\zeta_p\varepsilon_f \mathrm{aE} \quad (1)$$

Where a is the particle radius, ε_f is the permittivity of the medium and E is the electric field. In microfluidics, this method is frequently employed to separate and analyze biomolecules, such as DNA and proteins. By applying an electric field across a microchannel, charged particles experience a force proportional to their charge, size, and the electric field strength, facilitating their precise movement within the microfluidic device [74].

1.2.1.3 Isoelectric Trapping

One technique employed for the separation of proteins is isoelectric trapping (IET), a method falling within the category of isoelectric focusing techniques designed to separate proteins based on their isoelectric point (pI). Unlike a continuous pH gradient, IET involves the creation of a stepwise pH gradient using a series of buffering membranes. The use of discrete pH gates in IET facilitates the targeted separation of proteins [75]. Commercially available IET devices often face limitations in heat dissipation and have prolonged operation times ranging from 3 to 24 hours. However, Lim et al. demonstrated an enhancement in addressing heat dissipation issues and reducing separation time to a range of 20–60 minutes [76]. Microscale immobilized pH-specific membranes have been developed to address some of the disadvantages of macroscale IET devices. Using microscale IET, stable and precisely defined pH-specific membranes can be arranged in a microfluidic device, however, high running voltages (~100 V/cm) was still required. These

microfluidic devices, featuring integrated isoelectric gates, have the capability to isolate and trap the analyte of interest from other species in the sample for diverse applications.

1.2.1.4 Non-electrokinetic methods

Solid Phase Extraction (SPE) is one of the most common non-electrophoretic preconcentration methods performed in microfluidic devices. In this technique, the analyte is retained using a stationary phase material and then eluted by a proper solvent [77]. The SPE support can be integrated into microchannels by particle packing or monolith fabrication [78]. In SPE of nucleic acids, most stationary phases are based on silica and many microfluidic devices have integrated various silica microstructures. The main goal of these silica microstructures, which is common among all of them is to maximize the surface area to have more contact for binding [79]. Silica absorptive extraction has some disadvantages such as, multiple wash and elution steps are needed, device fabrication is costly, and the extraction efficiency is significantly dependent on surface to volume ratio which is based on the fabrication process [79,80].

Antibody-based extraction is another group of non-electrophoretic extraction methods. Antibodies are used for extraction of molecules in microfluidics due to their selectivity and specificity towards their antigen [81]. Antibodies can be integrated into a microfluidic device by surface modification of the setup, or through a solid support such as beads, porous monoliths, or nanoparticles [69].

Aptamer-based extraction is one of the most recently non-electrophoretic concentration techniques. Aptamers are specific single-stranded artificial nucleotides, which are able to bind to their targets. They also have been used for extraction and concentration in microfluidics. Aptamers have advantages such as high stability and low cross reactivity compared to antibodies [82]. One limitation associated with these methods is that antibodies or aptamers are not available with the required selectivity at an affordable cost all of the time [74].

1.2.2 Fabrication techniques of microfluidic devices

Photolithography is an established microfabrication technique in which light is used to create patterns on a photosensitive material coated on a silicon or glass surface. This process is mostly performed in a clean room environment. The photosensitive material itself can be either used as the structural features of the microfluidic device or as the master mold for transferring the patterns onto a soft polymeric material such as polydimethylsiloxane (PDMS). This process is called soft lithography [83,84]. To date, photolithography followed by soft lithography has been the most popular method for the fabrication of microfluidic devices [51]. Although this method is versatile and rapid with resolution sufficient for microfluidic applications, it still requires expensive equipment, specialized personnel, and clean room facilities for the fabrication of the master mold. These limitations led to the search for rapid, simple, and low-cost alternatives for the fabrication of microfluidic devices that don't require the use of cleanroom facilities. Micro milling, 3D printing, laser ablation, and xurography are some examples of rapid and lower cost microfabrication and prototyping techniques that have been used both to fabricate microfluidic devices by themselves or to make molds for soft lithography [85,86]. Although rapid prototyping techniques such as xurography do not provide as high a resolution as photolithography methods, they enable scalable manufacturing [87]. Moreover, they provide the ability to test new device designs much faster and subsequently enhance the speed of development cycles [85].

Xurography also known as craft cutting (or writing) or razor writing, was first introduced as a microfabrication method by Bartholomeusz et al. in 2005 [88]. Xurography utilizes a cutting plotter for cutting various materials such as thin adhesives, polymer films, metal foils, and paper using a physical blade. Xurography is a rapid, simple, and low-cost (both in equipment and materials) microfabrication technique which eliminates the need for clean rooms facilities and

specialized personnel [84]. Full fabrication using the xurography method takes a matter of minutes. Therefore, various repetitions of a design can be tested quickly and efficiently.

Cutting plotters compared to laser cutters which are also employed for cutting layers of tapes, plastic, and paper for creating microdevices, provide less resolution and have limitation in the selection of the material and its thickness, however, their price is significantly less and they are easier to setup [89]. Moreover, laser cutters require a vacuum pump for clearing debris. Leaving burn residue is another issue associated with laser cutters which have been shown to inhibit some reactions such as polymerase chain reaction (PCR). However, cutting plotters need no vacuum pump and leave no burn residues [87].

Xurography was first performed using expensive industrial cutters which cost around $4000 USD for macroscale applications such as the production of large advertisement signs mostly from vinyl adhesive, however, in recent years they have become broadly commercialized, and the cost of equipment has dropped to almost $200 USD for a desktop sized cutting equipment. This price reduction has not affected the cutting resolution and is more associated with scaling down the cutting area [90,91]. For instance, Silhouette and Cricut are two of the desktop size cutting plotter providers. The price of their machines starts from $200 USD and the cutting performance is comparable to more expensive ones [91]. Moreover, the cost of materials used in xurography is much less than the other techniques. For example, in the case of soft lithography; silicon wafers are $6–20 each (University Wafer), UV masks are $84 (Fine Line Imaging), and a PDMS kit is $92/kg (Krayden); whereas in rapid prototyping methods such use xurography, plastics and adhesives are ~$5/sq ft (McMaster Carr) and $2/sq ft (Amazon.com) respectively [87]. Therefore, microdevices fabricated using this method are cheaper. For example, it was estimated that six tape-bonded microchips cost less than $2.00 [92].

Several approaches have been taken in using xurography to fabricate microfluidic devices such as creating laminated multi-layer microfluidic devices, fabricating micromolds, producing masks, and integration of electrodes into microdevices. Various materials such as pressure-sensitive adhesives (PSAs), polymers, paper, and metal films have been used in these fabrication techniques. Most of the xurography-based microfluidic devices are created by bonding and laminating multiple cut layers using pressure-sensitive adhesives. The simplest microfluidic device consists of three layers; the top one which composes inlet and outlet, the middle one forms the flow channel, and the bottom layer encloses the device. The thickness of the material used defines the height of microchannels. After cutting, individual layers are aligned mostly using an alignment tool. Alignment holes are created in each layer in the cutting process [89].

Microfluidic devices fabricated using xurography were also used for biomolecule preconcentration [93,94]. Preconcentration within a microfluidic device can be performed using processes including controlled evaporation [95], and concentration polarization [93,94]. A disposable and portable microfluidic device was fabricated using the xurography method for viral sample concentration in less than 30 minutes. A multilayer device was fabricated to preconcentrate biomolecules based on ion concentration polarization (ICP) [94]. The device was constructed using a patterned double-sided adhesive, two glass slides and a Nafion membrane. The material was patterned, and the device was assembled in less than 15 minutes which makes the method suitable for rapid prototyping preconcentrators with different designs. Later, a study introduced a paper-based channel along with Nafion for controlled fluid handling and effective reagent storage [93]. The device was fabricated using xurography in less than 20 minutes and can attain preconcentration within 200s. A recent study has fabricated miniaturized isoelectric gates using agarose to separate biomarker proteins and concentrate and quantify them within 20 minutes. The device was

fabricated using patterned PET sheets bonded with adhesive tapes and the agarose was pipetted into the channels to create the isoelectric gates [96]. Later, a 3-reservoir device was fabricated using PET sheets and adhesive tape to separate protein C from human plasma samples. The device was modified for two-stage separation by immobilizing beads on a polyester membrane [97].

1.3 Methods for integration of hydrogels into microfluidic devices

Hydrogels are tri-dimensional materials with a network of hydrophilic polymer chains. They are capable of absorbing a large amount of water. Hydrogels provide several advantages in microfluidics such as free diffusion for molecules, increasing fluid resistance, and creating an optically clear region. Hydrogels are divided into two classes: natural and synthetic. Natural hydrogels such as gelatin, collagen, alginate, chitosan, and agarose; synthetically derived ones such as polyethylene glycol (PEG) and polyvinyl alcohol (PVA) [98,99]. Hydrogels play a crucial role in various microfluidic devices designed for biomolecule concentration and separation, including electrophoretic methods [100,101], as well as in microdevices utilized for isoelectric focusing separation [102,103].

There are two approaches for combining microfluidics and hydrogels; one is embedding hydrogel inside a microfluidic device and the other one is making microchannels inside the hydrogel bulk [98,99]. Various techniques have been employed to incorporate hydrogels into microfluidic devices, including the utilization of gel photopolymerization for microstructure formation and the integration based on flow-solidification. The latter method involves the use of hydrophilic or hydrophobic surfaces for localized hydrogel integration. This approach controls gel solidification through surface tension. For instance, hydrophobic and hydrophilic surfaces were introduced in the device [99]. Chung et al. obtained hydrophobic regions by drying the PDMS chip at 80 °C for 24 h and filled the specified region with gel. They studied cell migration and coculturing in the gel

integrated device [104]. In another example, Kim et al. used H-shaped microfluidic channel for integration hydrogel and performed plasma treatment on PDMS for rendering the surface hydrophilic [105]. However, implementing this approach is not always a straightforward process and may introduce complexity to the fabrication.

Another major method for embedding hydrogels inside microfluidics is photopolymerization of the UV-curable gels [106–109]. Some UV-curable hydrogels include polyethylene glycol diacrylate (PEG-DA), poly-N-isopropyl acrylamide (pNIPAAM), and polyacrylamide (PAAM). This technique has high resolution; however, UV-curable hydrogels are limited, and they are expensive [98,99]. More importantly, this technique requires multiple post-processing steps such as rinsing the device from unpolymerized gels. In this method, the microchannels are first filled with precursor. Then, the desired regions are photopolymerized using an exposure system and uncrosslinked gel precursor is rinsed from the channels. Therefore, this method requires post-polymerization steps such as removing uncrosslinked gel after exposure using pumping systems which makes this technique relatively complicated [110].

Similarly, one main method for integrating the pH specific gates into microfluidic chips is in situ photopolymerization. Immobilines which are some nonamphoteric buffering compounds and combined with the backbone of a polyacrylamide upon polymerization were used [76,111]. Photopolymerization rises the cost and complexity of the device, as there are numerous steps for incorporating pH specific membrane and rinsing the unpolymerized solution from the device. Photopolymerization with two methods was used for integrating pH membranes into the microfluidic device. In the first method, for fabricating each of the membranes three steps were performed after fabrication of the device. The monomer solutions were introduced in the channels sequentially. After filling the channels with first monomer solution, the membrane region for the

first gate was exposed to UV for photopolymerization. Then, unpolymerized solution was flushed from the channels using vacuum. The same steps were repeated for the next isoelectric membranes. In the second method, first a monomeric pH gradient is formed in the main channel and simultaneous photopolymerization of membranes was performed. Then, the desired regions for pH membranes were exposed through a mask. After polymerization, similar to the first method unpolymerized regions were rinsed from the device. Although in the second method only one exposure UV step is needed, both methods require tedious steps of photopolymerization and rinsing the channels from un-crosslinked solutions.

Thus, most of the current methods for integration of gels and pH-specific membranes into microfluidic devices require post-processing steps that will add extra complexity and cost to the fabrication process. Therefore, having a technique which can integrate gels as part of the fabrication process flow will be very beneficial.

Objectives of the thesis

This thesis introduces an innovative method for the integration of hydrogels into microfluidic devices, addressing challenges associated with complexity and cost in conventional methods such as photopolymerization with post-processing steps. The proposed method utilizes porous membranes as scaffolds, patterned with xurography, enabling local integration of hydrogels during the fabrication process. This method facilitates drying and reconstitution of hydrogels without shape loss or leakage.

The application of this hydrogel integration method is demonstrated in the context of gel electrophoretic concentration and quantification of cfDNA in rehydrated agarose embedded in electrospun membranes. The potential extension of this technique to create a point-of-care device for detecting cfDNA, a prognostic biomarker for severe sepsis, is also explored.

Additionally, the thesis addresses the need for a simple, low-cost, and rapid method for detecting histones, another sepsis prognosis biomarker. A microfluidic device is developed by incorporating an isoelectric membrane made of dehydrated agarose gel embedded in a porous membrane for the rapid isoelectric trapping of histones. This novel approach involves integrating isoelectric gates formed by gels loaded in a scaffold directly into the fabrication process, showing the versatility of the method.

Finally, the fully integrated microfluidic device is designed to detect both cfDNA and total circulating histones using a common platform. The device employs dehydrated agarose gates loaded with pH-specific agarose, along with fluorescent dyes, eliminating the need for off-chip sample preparation. The integration of both biomarkers and dye immobilization into a single device enhances its clinical utility, addressing the critical need for rapid sepsis prognosis.

Thesis organization

The thesis contains of 5 main chapters in a "sandwich" thesis format as following:

Chapter 1: This chapter reviews the background and motivation behind the development of microfluidic device for sepsis prognosis. This includes an overview of the sepsis biomarkers with the focus on cfDNA and histone along with their current detection methods. The necessity for a rapid method for detection of cfDNA and histone is explained. Xurography, the fabrication method for microfluidic devices is described with its advantages. The current methods for integration of gels into microfluidics and their limitations are also discussed.

Chapter 2: In this chapter, we present a novel and cost-effective approach to locally integrate hydrogels into microfluidic devices during fabrication, using porous and fibrous electrospun membranes as scaffolds. Our method utilizes xurography to pattern electrospun membranes,

capable of holding hydrogels during the fabrication process. The electrospun scaffold aids in the drying and reconstitution of hydrogels without shape loss or leakage, allowing for long-term storage as a critical feature for point-of-care devices. We also demonstrate the efficacy of our hydrogel integration method by applying it to gel electrophoretic concentration and quantification of short DNA fragments. This technology can potentially be developed further for the quantification of cfDNA, a prognostic biomarker for severe sepsis patients.

Chapter 3: In this chapter, a microfluidic device containing isoelectric gates made of dehydrated agarose gel embedded in a porous membrane for trapping histones was introduced. This device, fabricated using xurography, offers an inexpensive and rapid solution for histone trapping and detection for a potential POC device for sepsis.

Chapter 4: This chapter addresses the challenge of detecting both cfDNA and histone as sepsis biomarkers by introducing a fully integrated microfluidic device. The microfluidic device uses dehydrated pH-specific agarose gates to trap cfDNA and histones. The device is capable of simultaneously detecting cfDNA and total circulating histones from plasma in a common platform with the immobilized corresponding dyes.

Chapter 5: This chapter includes the conclusion of the thesis and suggested future works.

References

1. Singer, M.; Deutschman, C.S.; Seymour, C.W.; Shankar-Hari, M.; Annane, D.; Bauer, M.; Bellomo, R.; Bernard, G.R.; Chiche, J.-D.; Coopersmith, C.M. The Third International Consensus Definitions for Sepsis and Septic Shock (Sepsis-3). *Jama* **2016**, *315*, 801–810.
2. Vincent, J.-L.; Marshall, J.C.; Ñamendys-Silva, S.A.; François, B.; Martin-Loeches, I.; Lipman, J.; Reinhart, K.; Antonelli, M.; Pickkers, P.; Njimi, H. Assessment of the

Worldwide Burden of Critical Illness: The Intensive Care over Nations (ICON) Audit. *The lancet Respiratory medicine* **2014**, *2*, 380–386.

3. Fleischmann, C.; Scherag, A.; Adhikari, N.K.; Hartog, C.S.; Tsaganos, T.; Schlattmann, P.; Angus, D.C.; Reinhart, K. Assessment of Global Incidence and Mortality of Hospital-Treated Sepsis. Current Estimates and Limitations. *American journal of respiratory and critical care medicine* **2016**, *193*, 259–272.
4. Rudd, K.E.; Johnson, S.C.; Agesa, K.M.; Shackelford, K.A.; Tsoi, D.; Kievlan, D.R.; Colombara, D.V.; Ikuta, K.S.; Kissoon, N.; Finfer, S.; et al. Global, Regional, and National Sepsis Incidence and Mortality, 1990–2017: Analysis for the Global Burden of Disease Study. *The Lancet* **2020**, *395*, 200–211, doi:10.1016/S0140-6736(19)32989-7.
5. Kim, M.-H.; Choi, J.-H. An Update on Sepsis Biomarkers. *Infection & chemotherapy* **2020**, *52*, 1.
6. Paoli, C.J.; Reynolds, M.A.; Sinha, M.; Gitlin, M.; Crouser, E. Epidemiology and Costs of Sepsis in the United States—an Analysis Based on Timing of Diagnosis and Severity Level. *Critical care medicine* **2018**, *46*, 1889.
7. Farrah, K.; McIntyre, L.; Doig, C.J.; Talarico, R.; Taljaard, M.; Krahn, M.; Fergusson, D.; Forster, A.J.; Coyle, D.; Thavorn, K. Sepsis-Associated Mortality, Resource Use, and Healthcare Costs: A Propensity-Matched Cohort Study. *Critical Care Medicine* **2021**, *49*, 215–227.
8. Whiles, B.B.; Deis, A.S.; Simpson, S.Q. Increased Time to Initial Antimicrobial Administration Is Associated with Progression to Septic Shock in Severe Sepsis Patients. *Critical care medicine* **2017**, *45*, 623.

9. Ferrer, R.; Martin-Loeches, I.; Phillips, G.; Osborn, T.M.; Townsend, S.; Dellinger, R.P.; Artigas, A.; Schorr, C.; Levy, M.M. Empiric Antibiotic Treatment Reduces Mortality in Severe Sepsis and Septic Shock from the First Hour: Results from a Guideline-Based Performance Improvement Program. *Critical care medicine* **2014**, *42*, 1749–1755.

10. Kumar, A.; Roberts, D.; Wood, K.E.; Light, B.; Parrillo, J.E.; Sharma, S.; Suppes, R.; Feinstein, D.; Zanotti, S.; Taiberg, L. Duration of Hypotension before Initiation of Effective Antimicrobial Therapy Is the Critical Determinant of Survival in Human Septic Shock. *Critical care medicine* **2006**, *34*, 1589–1596.

11. Dugar, S.; Choudhary, C.; Duggal, A. Sepsis and Septic Shock: Guideline-Based Management. *Cleve Clin J Med* **2020**, *87*, 53–64.

12. Wentowski, C.; Ingles, D.P.; Nielsen, N.D. Sepsis 2021: A Review. *Anaesthesia & Intensive Care Medicine* **2021**, *22*, 676–684.

13. Thompson, K.; Venkatesh, B.; Finfer, S. Sepsis and Septic Shock: Current Approaches to Management. *Internal Medicine Journal* **2019**, *49*, 160–170.

14. Barichello, T.; Generoso, J.S.; Singer, M.; Dal-Pizzol, F. Biomarkers for Sepsis: More than Just Fever and Leukocytosis—a Narrative Review. *Critical Care* **2022**, *26*, 14.

15. Gyawali, B.; Ramakrishna, K.; Dhamoon, A.S. Sepsis: The Evolution in Definition, Pathophysiology, and Management. *SAGE open medicine* **2019**, *7*, 2050312119835043.

16. Faix, J.D. Biomarkers of Sepsis. *Critical reviews in clinical laboratory sciences* **2013**, *50*, 23–36.

17. Chesi, G.; Vazzana, N.; Giumelli, C. Biomarkers for Sepsis: Past, Present and Future. *Italian Journal of Medicine* **2016**, *10*, 301–307.

18. Biron, B.M.; Ayala, A.; Lomas-Neira, J.L. Biomarkers for Sepsis: What Is and What Might Be? *Biomarker insights* **2015**, *10*, BMI-S29519.

19. Yunus, I.; Fasih, A.; Wang, Y. The Use of Procalcitonin in the Determination of Severity of Sepsis, Patient Outcomes and Infection Characteristics. *PloS one* **2018**, *13*, e0206527.

20. Pierrakos, C.; Velissaris, D.; Bisdorff, M.; Marshall, J.C.; Vincent, J.-L. Biomarkers of Sepsis: Time for a Reappraisal. *Critical Care* **2020**, *24*, 1–15.

21. Duplessis, C.; Gregory, M.; Frey, K.; Bell, M.; Truong, L.; Schully, K.; Lawler, J.; Langley, R.J.; Kingsmore, S.F.; Woods, C.W. Evaluating the Discriminating Capacity of Cell Death (Apoptotic) Biomarkers in Sepsis. *Journal of intensive care* **2018**, *6*, 1–11.

22. Cheng, Z.; Abrams, S.T.; Alhamdi, Y.; Toh, J.; Yu, W.; Wang, G.; Toh, C.-H. Circulating Histones Are Major Mediators of Multiple Organ Dysfunction Syndrome in Acute Critical Illnesses. *Critical care medicine* **2019**, *47*, e677–e684.

23. Dwivedi, D.J.; Toltl, L.J.; Swystun, L.L.; Pogue, J.; Liaw, K.-L.; Weitz, J.I.; Cook, D.J.; Fox-Robichaud, A.E.; Liaw, P.C. Prognostic Utility and Characterization of Cell-Free DNA in Patients with Severe Sepsis. *Critical care* **2012**, *16*, 1–11.

24. Eichhorn, T.; Linsberger, I.; Lauková, L.; Tripisciano, C.; Fendl, B.; Weiss, R.; König, F.; Valicek, G.; Miestinger, G.; Hörmann, C. Analysis of Inflammatory Mediator Profiles in Sepsis Patients Reveals That Extracellular Histones Are Strongly Elevated in Nonsurvivors. *Mediators of Inflammation* **2021**, *2021*.

25. Jing, Q.; Leung, C.H.C.; Wu, A.R. Cell-Free DNA as Biomarker for Sepsis by Integration of Microbial and Host Information. *Clinical Chemistry* **2022**, *68*, 1184–1195.

26. Li, Y.; Wan, D.; Luo, X.; Song, T.; Wang, Y.; Yu, Q.; Jiang, L.; Liao, R.; Zhao, W.; Su, B. Circulating Histones in Sepsis: Potential Outcome Predictors and Therapeutic Targets. *Frontiers in Immunology* **2021**, *12*, 650184.

27. Wildhagen, K.C.; Wiewel, M.A.; Schultz, M.J.; Horn, J.; Schrijver, R.; Reutelingsperger, C.P.; van der Poll, T.; Nicolaes, G.A. Extracellular Histone H3 Levels Are Inversely Correlated with Antithrombin Levels and Platelet Counts and Are Associated with Mortality in Sepsis Patients. *Thrombosis research* **2015**, *136*, 542–547.

28. Gould, T.; Lysov, Z.; Liaw, P. Extracellular DNA and Histones: Double-edged Swords in Immunothrombosis. *Journal of Thrombosis and Haemostasis* **2015**, *13*, S82–S91.

29. Marsman, G.; Zeerleder, S.; Luken, B.M. Extracellular Histones, Cell-Free DNA, or Nucleosomes: Differences in Immunostimulation. *Cell death & disease* **2016**, *7*, e2518–e2518.

30. van der Meer, A.J.; Kroeze, A.; Hoogendijk, A.J.; Soussan, A.A.; van der Schoot, C.E.; Wuillemin, W.A.; Voermans, C.; van der Poll, T.; Zeerleder, S. Systemic Inflammation Induces Release of Cell-Free DNA from Hematopoietic and Parenchymal Cells in Mice and Humans. *Blood advances* **2019**, *3*, 724–728.

31. Zeerleder, S.; Stephan, F.; Emonts, M.; De Kleijn, E.D.; Esmon, C.T.; Varadi, K.; Hack, C.E.; Hazelzet, J.A. Circulating Nucleosomes and Severity of Illness in Children Suffering from Meningococcal Sepsis Treated with Protein C. *Critical care medicine* **2012**, *40*, 3224–3229.

32. Krasic, J.; Abramovic, I.; Vrtaric, A.; Gabaj, N.; Kralik-Oguic, S.; Bojanac, A. Impact of Preanalytical and Analytical Methods on Cell-Free DNA Diagnostics. Front Cell Dev Biol. 2021; 9: 686149. **2021**.

33. Charoensappakit, A.; Sae-khow, K.; Rattanaliam, P.; Vutthikraivit, N.; Pecheenbuvan, M.; Udomkarnjananun, S. Cell-Free DNA as Prognostic and Diagnostic Biomarkers for Adult Sepsis: A Systematic Review and Meta-Analysis. **2023**.

34. Rannikko, J.; Seiskari, T.; Huttunen, R.; Tarkiainen, I.; Jylhävä, J.; Hurme, M.; Syrjänen, J.; Aittoniemi, J. Plasma Cell-free DNA and qSOFA Score Predict 7-day Mortality in 481 Emergency Department Bacteraemia Patients. *Journal of Internal Medicine* **2018**, *284*, 418–426.

35. Jeon, K.; Lee, J.; Lee, J.-S.; Kim, M.; Kim, H.-S.; Kang, H.J.; Lee, Y.K. Quantification of Cell-Free DNA: A Comparative Study of Three Different Methods. *Journal of Laboratory Medicine and Quality Assurance* **2019**, *41*, 214–219.

36. Bhat, S.; Curach, N.; Mostyn, T.; Bains, G.S.; Griffiths, K.R.; Emslie, K.R. Comparison of Methods for Accurate Quantification of DNA Mass Concentration with Traceability to the International System of Units. *Analytical chemistry* **2010**, *82*, 7185–7192.

37. Kralik, P.; Ricchi, M. A Basic Guide to Real Time PCR in Microbial Diagnostics: Definitions, Parameters, and Everything. *Frontiers in microbiology* **2017**, *8*, 108.

38. Allard, M.W.; Binet, R.; Brown, E.W.; Cao, G.; Deng, X.; Grim, C.; Hammack, T.S.; Hoffmann, M.; Miller, J.; Pettengill, J. Molecular Techniques in Foodborne Disease Surveillance. **2023**.

39. Smith, C.J.; Osborn, A.M. Advantages and Limitations of Quantitative PCR (Q-PCR)-Based Approaches in Microbial Ecology. *FEMS microbiology ecology* **2009**, *67*, 6–20.

40. Jing, R.; Wang, H.; Ju, S.; Cui, M. Reference Materials for Molecular Diagnostics: Current Achievements and Future Strategies. *Clinical Biochemistry* **2018**, *56*, 11–17.

41. Mao, X.; Liu, C.; Tong, H.; Chen, Y.; Liu, K. Principles of Digital PCR and Its Applications in Current Obstetrical and Gynecological Diseases. *American journal of translational research* **2019**, *11*, 7209.

42. Nielsen, K.; Mogensen, H.; Eriksen, B.; Hedman, J.; Parson, W.; Morling, N. Comparison of Six DNA Quantification Methods.; Elsevier, 2006; Vol. 1288, pp. 759–761.

43. Sonnenberg, A.; Marciniak, J.Y.; Rassenti, L.; Ghia, E.M.; Skowronski, E.A.; Manouchehri, S.; McCanna, J.; Widhopf, G.F.; Kipps, T.J.; Heller, M.J. Rapid Electrokinetic Isolation of Cancer-Related Circulating Cell-Free DNA Directly from Blood. *Clinical chemistry* **2014**, *60*, 500–509.

44. Gargano, A.F.; Shaw, J.B.; Zhou, M.; Wilkins, C.S.; Fillmore, T.L.; Moore, R.J.; Somsen, G.W.; Paša-Tolić, L. Increasing the Separation Capacity of Intact Histone Proteoforms Chromatography Coupling Online Weak Cation Exchange-HILIC to Reversed Phase LC UVPD-HRMS. *Journal of proteome research* **2018**, *17*, 3791–3800.

45. Ito, T.; Nakahara, M.; Masuda, Y.; Ono, S.; Yamada, S.; Ishikura, H.; Imaizumi, H.; Kamikokuryo, C.; Kakihana, Y.; Maruyama, I. Circulating Histone H3 Levels Are Increased in Septic Mice in a Neutrophil-Dependent Manner: Preclinical Evaluation of a Novel Sandwich ELISA for Histone H3. *Journal of Intensive Care* **2018**, *6*, 1–6.

46. Xu, Z.; Huang, Y.; Mao, P.; Zhang, J.; Li, Y. Sepsis and ARDS: The Dark Side of Histones. *Mediators of inflammation* **2015**, *2015*.

47. Ekaney, M.L.; Otto, G.P.; Sossdorf, M.; Sponholz, C.; Boehringer, M.; Loesche, W.; Rittirsch, D.; Wilharm, A.; Kurzai, O.; Bauer, M. Impact of Plasma Histones in Human Sepsis and Their Contribution to Cellular Injury and Inflammation. *Critical care* **2014**, *18*, 1–9.

48. Lu, N.-F.; Jiang, L.; Zhu, B.; Yang, D.-G.; Zheng, R.-Q.; Shao, J.; Xi, X.-M. Elevated Plasma Histone H4 Level Predicts Increased Risk of Mortality in Patients with Sepsis. *Ann. Palliat. Med* **2020**, *9*, 1084–1091.

49. Yokoyama, Y.; Ito, T.; Yasuda, T.; Furubeppu, H.; Kamikokuryo, C.; Yamada, S.; Maruyama, I.; Kakihana, Y. Circulating Histone H3 Levels in Septic Patients Are Associated with Coagulopathy, Multiple Organ Failure, and Death: A Single-Center Observational Study. *Thrombosis journal* **2019**, *17*, 1–7.

50. Zhan, X.; Liu, D.; Dong, Y.; Gao, Y.; Xu, X.; Xie, T.; Zhou, H.; Wang, G.; Zhang, H.; Wu, P. Early Changes and Predictive Value of Serum Histone H3 Concentration in Urosepsis: A Prospective Observational Study. *Advances in Therapy* **2022**, *39*, 1310–1323.

51. Faustino, V.; Catarino, S.O.; Lima, R.; Minas, G. Biomedical Microfluidic Devices by Using Low-Cost Fabrication Techniques: A Review. *Journal of biomechanics* **2016**, *49*, 2280–2292.

52. Kojic, S.P.; Stojanovic, G.M.; Radonic, V. Novel Cost-Effective Microfluidic Chip Based on Hybrid Fabrication and Its Comprehensive Characterization. *Sensors* **2019**, *19*, 1719.

53. Cai, G.; Xue, L.; Zhang, H.; Lin, J. A Review on Micromixers. *Micromachines* **2017**, *8*, 274.

54. Hessel, V.; Löwe, H.; Schönfeld, F. Micromixers—a Review on Passive and Active Mixing Principles. *Chemical engineering science* **2005**, *60*, 2479–2501.

55. Nam-Trung, N.; Zhigang, W. Micromixers—a Review. *J Micromech Microeng* **2005**, *15*, R1.

56. Suh, Y.K.; Kang, S. A Review on Mixing in Microfluidics. *Micromachines* **2010**, *1*, 82–111.

57. Au, A.K.; Lai, H.; Utela, B.R.; Folch, A. Microvalves and Micropumps for BioMEMS. *Micromachines* **2011**, *2*, 179–220.

58. Laser, D.J.; Santiago, J.G. A Review of Micropumps. *Journal of micromechanics and microengineering* **2004**, *14*, R35.

59. Wang, Y.-N.; Fu, L.-M. Micropumps and Biomedical Applications–A Review. *Microelectronic Engineering* **2018**, *195*, 121–138.

60. Woias, P. Micropumps—Past, Progress and Future Prospects. *Sensors and Actuators B: Chemical* **2005**, *105*, 28–38.

61. Oh, K.W.; Ahn, C.H. A Review of Microvalves. *Journal of micromechanics and microengineering* **2006**, *16*, R13.

62. Choi, S.; Goryll, M.; Sin, L.Y.M.; Wong, P.K.; Chae, J. Microfluidic-Based Biosensors toward Point-of-Care Detection of Nucleic Acids and Proteins. *Microfluidics and Nanofluidics* **2011**, *10*, 231–247.

63. Luka, G.; Ahmadi, A.; Najjaran, H.; Alocilja, E.; DeRosa, M.; Wolthers, K.; Malki, A.; Aziz, H.; Althani, A.; Hoorfar, M. Microfluidics Integrated Biosensors: A Leading Technology towards Lab-on-a-Chip and Sensing Applications. *Sensors* **2015**, *15*, 30011–30031.

64. Chong, Z.Z.; Tan, S.H.; Gañán-Calvo, A.M.; Tor, S.B.; Loh, N.H.; Nguyen, N.-T. Active Droplet Generation in Microfluidics. *Lab on a Chip* **2016**, *16*, 35–58.

65. Seemann, R.; Brinkmann, M.; Pfohl, T.; Herminghaus, S. Droplet Based Microfluidics. *Reports on progress in physics* **2011**, *75*, 016601.

66. Zhu, P.; Wang, L. Passive and Active Droplet Generation with Microfluidics: A Review. *Lab on a Chip* **2017**, *17*, 34–75.

67. Lenshof, A.; Laurell, T. Continuous Separation of Cells and Particles in Microfluidic Systems. *Chemical Society Reviews* **2010**, *39*, 1203–1217.

68. Sajeesh, P.; Sen, A.K. Particle Separation and Sorting in Microfluidic Devices: A Review. *Microfluidics and nanofluidics* **2014**, *17*, 1–52.

69. Sonker, M.; Sahore, V.; Woolley, A.T. Recent Advances in Microfluidic Sample Preparation and Separation Techniques for Molecular Biomarker Analysis: A Critical Review. *Analytica chimica acta* **2017**, *986*, 1–11.

70. Scott, S.M.; Ali, Z. Fabrication Methods for Microfluidic Devices: An Overview. *Micromachines* **2021**, *12*, 319.

71. Cui, F.; Rhee, M.; Singh, A.; Tripathi, A. Microfluidic Sample Preparation for Medical Diagnostics. *Annual review of biomedical engineering* **2015**, *17*, 267–286.

72. Giordano, B.C.; Burgi, D.S.; Hart, S.J.; Terray, A. On-Line Sample Pre-Concentration in Microfluidic Devices: A Review. *Analytica chimica acta* **2012**, *718*, 11–24.

73. Shallan, A.I.; Guijt, R.M.; Breadmore, M.C. Electrokinetics for Sample Preparation of Biological Molecules in Biological Samples Using Microfluidic Systems. *Bioanalysis* **2014**, *6*, 1961–1974.

74. Salafi, T.; Zeming, K.K.; Zhang, Y. Advancements in Microfluidics for Nanoparticle Separation. *Lab on a Chip* **2017**, *17*, 11–33.

75. Mai, J.; Sommer, G.J.; Hatch, A.V. Microfluidic Digital Isoelectric Fractionation for Rapid Multidimensional Glycoprotein Analysis. *Analytical chemistry* **2012**, *84*, 3538–3545.

76. Lim, P.; North, R.; Vigh, G. Rapid Isoelectric Trapping in a Micropreparative-scale Multicompartment Electrolyzer. *Electrophoresis* **2007**, *28*, 1851–1859.

77. de Mello, A.J.; Beard, N. Focus. Dealing with 'Real'Samples: Sample Pre-Treatment in Microfluidic Systems. *Lab on a Chip* **2003**, *3*, 11N-20N.

78. Kumar, S.; Sahore, V.; Rogers, C.I.; Woolley, A.T. Development of an Integrated Microfluidic Solid-Phase Extraction and Electrophoresis Device. *Analyst* **2016**, *141*, 1660–1668.

79. Wen, J.; Legendre, L.A.; Bienvenue, J.M.; Landers, J.P. Purification of Nucleic Acids in Microfluidic Devices. *Analytical chemistry* **2008**, *80*, 6472–6479.

80. Kim, J.; Johnson, M.; Hill, P.; Gale, B.K. Microfluidic Sample Preparation: Cell Lysis and Nucleic Acid Purification. *Integrative Biology* **2009**, *1*, 574–586.

81. Wujcik, E.; Wei, H.; Zhang, X.; Guo, J.; Yan, X.; Sutrave, N.; Wei, S.; Guo, Z. Antibody Nanosensors: A Detailed Review. *Rsc Advances* **2014**, *4*, 43725–43745.

82. Cox, J.C.; Hayhurst, A.; Hesselberth, J.; Bayer, T.S.; Georgiou, G.; Ellington, A.D. Automated Selection of Aptamers against Protein Targets Translated in Vitro: From Gene to Aptamer. *Nucleic acids research* **2002**, *30*, e108–e108.

83. Betancourt, T.; Brannon-Peppas, L. Micro-and Nanofabrication Methods in Nanotechnological Medical and Pharmaceutical Devices. *International journal of nanomedicine* **2006**, *1*, 483–495.

84. Damodara, S.; Shahriari, S.; Wu, W.-I.; Rezai, P.; Hsu, H.-H.; Selvaganapathy, R. Materials and Methods for Microfabrication of Microfluidic Devices. In *Microfluidic Devices for Biomedical Applications*; Elsevier, 2021; pp. 1–78.

85. Pinto, E.; Faustino, V.; Rodrigues, R.O.; Pinho, D.; Garcia, V.; Miranda, J.M.; Lima, R. A Rapid and Low-Cost Nonlithographic Method to Fabricate Biomedical Microdevices for Blood Flow Analysis. *Micromachines* **2014**, *6*, 121–135.

86. Taylor, A.W.; Harris, D.M. Optimized Commercial Desktop Cutter Technique for Rapid-Prototyping of Microfluidic Devices and Application to Taylor Dispersion. *Review of Scientific Instruments* **2019**, *90*, 116102, doi:10.1063/1.5123130.

87. Walsh III, D.I.; Kong, D.S.; Murthy, S.K.; Carr, P.A. Enabling Microfluidics: From Clean Rooms to Makerspaces. *Trends in biotechnology* **2017**, *35*, 383–392.

88. Bartholomeusz, D.A.; Boutte, R.W.; Andrade, J.D. Xurography: Rapid Prototyping of Microstructures Using a Cutting Plotter. *J. Microelectromech. Syst.* **2005**, *14*, 1364–1374, doi:10.1109/JMEMS.2005.859087.

89. Gale, B.K.; Jafek, A.R.; Lambert, C.J.; Goenner, B.L.; Moghimifam, H.; Nze, U.C.; Kamarapu, S.K. A Review of Current Methods in Microfluidic Device Fabrication and Future Commercialization Prospects. *Inventions* **2018**, *3*, 60.

90. Martínez-López, J.I.; Mojica, M.; Rodríguez, C.A.; Siller, H.R. Xurography as a Rapid Fabrication Alternative for Point-of-Care Devices: Assessment of Passive Micromixers. *Sensors* **2016**, *16*, 705.

91. Martínez-López, J.I.; Betancourt, H.; García-López, E.; Rodriguez, C.A.; Siller, H.R. Rapid Fabrication of Disposable Micromixing Arrays Using Xurography and Laser Ablation. *Micromachines* **2017**, *8*, 144.

92. Greer, J.; Sundberg, S.O.; Wittwer, C.T.; Gale, B.K. Comparison of Glass Etching to Xurography Prototyping of Microfluidic Channels for DNA Melting Analysis. *Journal of Micromechanics and Microengineering* **2007**, *17*, 2407.

93. Phan, D.-T.; Shaegh, S.A.M.; Yang, C.; Nguyen, N.-T. Sample Concentration in a Microfluidic Paper-Based Analytical Device Using Ion Concentration Polarization. *Sensors and Actuators B: Chemical* **2016**, *222*, 735–740, doi:10.1016/j.snb.2015.08.127.

94. Yuan, X.; Renaud, L.; Audry, M.-C.; Kleimann, P. Electrokinetic Biomolecule Preconcentration Using Xurography-Based Micro-Nano-Micro Fluidic Devices. *Anal. Chem.* **2015**, *87*, 8695–8701, doi:10.1021/acs.analchem.5b01352.

95. Zhang, J.; Mahalanabis, M.; Liu, L.; Chang, J.; Pollock, N.; Klapperich, C. A Disposable Microfluidic Virus Concentration Device Based on Evaporation and Interfacial Tension. *Diagnostics* **2013**, *3*, 155–169, doi:10.3390/diagnostics3010155.

96. Damodara, S.; Dwivedi, D.J.; Liaw, P.C.; Fox-Robichaud, A.E.; Selvaganapathy, P.R.; Canadian Critical Care Translational Biology Group Single Step Separation and Concentration of Biomarker Proteins Using Agarose Based Miniaturized Isoelectric Gates for Point of Care Diagnostics. *Sensors and Actuators B: Chemical* **2021**, *330*, 129265.

97. Damodara, S.; Arora, J.; Dwivedi, D.J.; Liaw, P.C.; Fox-Robichaud, A.E.; Selvaganapathy, P.R.; Canadian Critical Care Translational Biology Group Microfluidic Device for Single Step Measurement of Protein C in Plasma Samples for Sepsis Prognosis. *Lab on a Chip* **2022**, *22*, 2566–2577.

98. Goy, C.B.; Chaile, R.E.; Madrid, R.E. Microfluidics and Hydrogel: A Powerful Combination. *Reactive and Functional Polymers* **2019**, *145*, 104314.

99. Zhang, X.; Li, L.; Luo, C. Gel Integration for Microfluidic Applications. *Lab on a Chip* **2016**, *16*, 1757–1776.

100. Gerver, R.E.; Herr, A.E. Microfluidic Western Blotting of Low-Molecular-Mass Proteins. *Analytical chemistry* **2014**, *86*, 10625–10632.

101. Mohamadi, R.M.; Svobodova, Z.; Bilkova, Z.; Otto, M.; Taverna, M.; Descroix, S.; Viovy, J.-L. An Integrated Microfluidic Chip for Immunocapture, Preconcentration and Separation of β-Amyloid Peptides. *Biomicrofluidics* **2015**, *9*, 054117.

102. Herzog, C.; Poehler, E.; Peretzki, A.J.; Borisov, S.M.; Aigner, D.; Mayr, T.; Nagl, S. Continuous On-Chip Fluorescence Labelling, Free-Flow Isoelectric Focusing and Marker-Free Isoelectric Point Determination of Proteins and Peptides. *Lab on a Chip* **2016**, *16*, 1565–1572.

103. Poehler, E.; Herzog, C.; Lotter, C.; Pfeiffer, S.A.; Aigner, D.; Mayr, T.; Nagl, S. Label-Free Microfluidic Free-Flow Isoelectric Focusing, pH Gradient Sensing and near Real-Time Isoelectric Point Determination of Biomolecules and Blood Plasma Fractions. *Analyst* **2015**, *140*, 7496–7502.

104. Chung, S.; Sudo, R.; Mack, P.J.; Wan, C.-R.; Vickerman, V.; Kamm, R.D. Cell Migration into Scaffolds under Co-Culture Conditions in a Microfluidic Platform. *Lab on a Chip* **2009**, *9*, 269–275.

105. Kim, M.; Kim, T. Diffusion-Based and Long-Range Concentration Gradients of Multiple Chemicals for Bacterial Chemotaxis Assays. *Analytical Chemistry* **2010**, *82*, 9401–9409.

106. Beebe, D.J.; Moore, J.S.; Bauer, J.M.; Yu, Q.; Liu, R.H.; Devadoss, C.; Jo, B.-H. Functional Hydrogel Structures for Autonomous Flow Control inside Microfluidic Channels. *Nature* **2000**, *404*, 588–590.

107. Chen, L.; Wang, K.X.; Doyle, P.S. Effect of Internal Architecture on Microgel Deformation in Microfluidic Constrictions. *Soft Matter* **2017**, *13*, 1920–1928.

108. Garcia-Schwarz, G.; Santiago, J.G. Integration of On-Chip Isotachophoresis and Functionalized Hydrogels for Enhanced-Sensitivity Nucleic Acid Detection. *Analytical chemistry* **2012**, *84*, 6366–6369.

109. Koh, W.-G.; Pishko, M. Immobilization of Multi-Enzyme Microreactors inside Microfluidic Devices. *Sensors and Actuators B: Chemical* **2005**, *106*, 335–342.

110. Eker, B.; Temiz, Y.; Delamarche, E. Heterogeneous Integration of Gels into Microfluidics Using a Mesh Carrier. *Biomedical microdevices* **2014**, *16*, 829–835.

111. Sommer, G.J.; Mai, J.; Singh, A.K.; Hatch, A.V. Microscale Isoelectric Fractionation Using Photopolymerized Membranes. *Analytical chemistry* **2011**, *83*, 3120–3125.

2 Chapter 2 Integration of hydrogels into microfluidic devices using porous membranes

Full Citation: Shahriari S, Selvaganapathy PR. Integration of hydrogels into microfluidic devices with porous membranes as scaffolds enables their drying and reconstitution. Biomicrofluidics. 2022 Sep 1;16(5).

Integration of hydrogels into microfluidic devices with porous membranes as scaffolds enables their drying and reconstitution

*Shadi Shahriari[1], P. Ravi Selvaganapathy[1,2]**

[1]Department of Mechanical Engineering, McMaster University, Hamilton, ON, Canada

[2] School of Biomedical Engineering, McMaster University, Hamilton, ON, Canada

** Corresponding author. E-mail address: selvaga@mcmaster.ca*

Abstract

Hydrogels are a critical component of many microfluidic devices. They have been used in cell culture applications, biosensors, gradient generators, separation microdevices, micro actuators, and microvalves. Various techniques have been utilized to integrate hydrogels into microfluidic devices such as flow confinement and gel photopolymerization. However, in these methods hydrogels are typically introduced in post processing steps which adds complexity, cost and extensive fabrication steps to the integration process and can be prone to user induced variations. Here, we introduce an inexpensive method to locally integrate hydrogels into microfluidic devices during the fabrication process without the need for post processing. In this method, porous and fibrous membranes such as electrospun membranes are used as scaffolds to hold gels and they are patterned using xurography. Hydrogels in various shapes as small as 200 μm can be patterned using this method in a scalable manner. The electrospun scaffold facilitate drying and reconstitution of these gels without loss of shape or leakage that is beneficial in a number of applications. Such reconstitution is not feasible using other hydrogel integration techniques. Therefore, this method is suitable for long time storage of hydrogel in devices which is useful in

point of care (POC) devices. This hydrogel integration method was used to demonstrate gel electrophoretic concentration and quantification of short DNA (150 bp) with different concentrations in rehydrated agarose embedded in electrospun polycaprolactone (PCL) membrane. This can be developed further to create a point of care device to quantify cell-free DNA which is a prognostic biomarker for severe sepsis patients.

Keywords : Microfluidics, hydrogel, porous membranes, DNA quantification, sepsis

2.1 Introduction

Microfluidic technology provides the tools and techniques to handle and manipulate small volumes of fluids [1]. Its advantages such as low reagent use, low response time, and high accuracy make microfluidic devices promising tools for the developing of point-of-care technologies [2]. In addition, microfluidic techniques have found applications in patterning of cells and extracellular matrix (ECM) for applications in drug discovery and biomedicine [3]. There are multiple methods for fabrication of microfluidic devices; among those xurography is a low-cost and rapid fabrication technique which does not require clean room facilities. Xurography as a microfabrication method, was first introduced by Bartholomeusz et al. in 2005 [4]. In xurography, a physical blade is used to cut the materials based on a desirable design. Each layer of the device is individually cut. Then the layers are aligned and laminated one after another to create a multilayer stack which forms the microfluidic device [5]. Various materials including pressure sensitive adhesives (PSA) [5–7] , polymer films [5,8], thin metal films [9,10], paper [11,12], and membranes [13] can be used as constituent layers in this fabrication method.

Hydrogels are extensively used in the biomedical field as they are biocompatible, high permeable for small molecules, and optically clear. Also, some of the hydrogels can resemble biological

tissues and extracellular matrix properties [3,14,15]. Hydrogels have been used as barriers for increasing fluid resistance and creating a free diffusion environment in microfluidic devices [15]. They have been incorporated into microfluidic devices used for various applications including cell culture, biosensors, gradient generator, as well as in creation of active elements such as valves, and separation devices. Hydrogels are a vital part of cell culture and cell patterning microdevices [16,17]. Furthermore, they are able to keep biomolecules inside and form a 3D environment for optical [18,19] or electrochemical [20,21] biosensors. Hydrogel permeability to diffusion has been exploited in gradient generator microdevices [22–24]. Some classes of hydrogels can undergo volume transition in response to external stimuli -such as temperature, pH, and light [25]. These types of hydrogels have been used to create active elements such as valves and actuators inside a microchannel [26,27]. Most importantly, hydrogels have been an essential part of many separation microfluidic devices, such as cell separation [28], electrophoretic concentration and separation of biomolecules [29,30], and isoelectric focusing separation microdevices [31,32].

Multiple methods have been used for integration hydrogels into microfluidic devices; such as gel photopolymerization for creating micro-structures, and flow-solidification based integration [33]. In these methods hydrogel is mostly integrated in-plane and in the same level of the microfluidic channels, not as a separate layer. In flow-solidification based method, [34–36] the gel solidification is controlled by surface tension. For instance, hydrophilic patterns on a hydrophobic surface was used to control the localize where the gel was introduced [15]. However, this method is not always straightforward and can add complexity to the fabrication.

Photopolymerization of the UV-curable gels can be used for embedding hydrogel in the microfluidic devices as well [26,37–46]. Uniform exposure, using a mask, or direct writing are the methods used for photopolymerization. Some UV-curable hydrogels that have been incorporated

into microfluidic devices, include polyethylene glycol diacrylate (PEG-DA), poly-N-isopropyl acrylamide (pNIPAAM), and polyacrylamide (PAAM) . This technique provides desired features with high resolution; however, UV-curable hydrogels are limited, and they are difficult to integrate in post processing as they require the unpolymerized gel to be removed from the channels. In a typical fabrication process using this technique, the microchannels are first filled with precursor. In the next step, the desired regions are photopolymerized and uncrosslinked gel precursor is removed. These post-polymerization steps make this technique relatively complicated [47,48]. Eker et al. used mesh carriers to transfer and embed small volumes of biomolecule loaded poly(ethylene)glycol-based acrylamide (PEGACA) hydrogel in the desired locations of microfluidic devices to serve as reagent reservoirs. The mesh was used as a transfer substrate instead of a scaffold and was not integrated into the device. Furthermore, the gel was photopolymerized in the form of drops and transferred to the microfluidic chip without any functional assessment such as its ability to seal or retain shape upon drying and reconstitution [47]. In summary, most of the methods in literature require integration of gels as a post-processing step that will add extra cost to the fabrication of the device. They are also more suited to in-plane fabrication of gels in microfluidic channels such as in DNA or protein separation devices. Very few methods exist that can integrate gels as part of the fabrication process flow. None of these methods are suited in applications where the gel needs to be integrated in-between two channel layers either as a diffusion barrier in diagnostic applications or to hold cells exposed to different analytes on either side in organ on chip type applications. Finally, drying and rehydration of the gels and the consequent effect on their integrity and leakage have not been studied in the literature but is crucial for devices that are to be stored for up to 6-12 month prior to use in the field.

Here, a low-cost and easy to implement method to integrate hydrogels into microfluidic devices during the fabrication process is introduced to overcome these limitations. It is shown that thin porous and fibrous membranes, such as electrospun PCL membrane can be used as scaffold for hydrogel embedding within microfluidic devices. In this method hydrogel is integrated as a separate layer, sandwiched between other layers of the device. Xurography is used to expose regions of the membrane onto which the hydrogels can be loaded. The same technique has been used to integrate the gel loaded membranes into microfluidic channels. It is also shown that PCL membrane can prevent complete collapse of the gel upon dehydration and retain the macrostructure of hydrogel after rehydration. It also maintains intimate contact between the gel and the sidewalls of the channels which is important in preventing leakages and convective flows. These features make this hybrid approach suitable for long term dried storage of hydrogels inside microfluidic devices possible for the first time, thereby avoiding loading of gels at the point of use. A demonstration of its usefulness was performed by fabricating a point of care microfluidic device containing dried agarose loaded membrane for accumulation and quantification of 150 bp DNA which is useful for developing a tool for sepsis prognostics.

2.2 Experimental

2.2.1 Materials

Transfer adhesive tape (7952MP-3M™, 50 µm thickness) was obtained from 3M™, Maplewood, MN. One-sided hydrophilic adhesive tape (polyester film with acrylic adhesive (93049-AR), 100 µm thickness) was obtained from adhesive research (AR), Glen Rock, PA. Polyvinyl chloride (PVC) films (Clear-Lay, 127 µm thickness) were from Grafix, Maple Heights, OH. Polyimide (Kapton) tape with silicone adhesive (double-sided and double Liner, 100 µm) was from Caplinq. The copper-polyimide composite foil (9 µm-Cu and 12 µm-PI thickness, Pyralux®) was acquired

from DuPont, USA. The dicing tape (UV curable acrylic adhesive on PVC film, 95 µm thickness) was obtained from Ultron Systems, US. Whatman cellulose chromatography paper (1 Chr, 180 µm thickness) was from Sigma Aldrich. Agarose powder and 50x TAE buffer concentrate were from BioShop Canada Inc, Burlington, ON. Polycaprolactone average M_n 80,000, dichloromethane and methylene blue were from Sigma Aldrich. Quant-iT PicoGreen® dsDNA kit was from Life Technologies. 150 bp DNA sample was provided by Thrombosis & Atherosclerosis Research Institute (TaARI).

2.2.2 Fabrication process

2.2.2.1 Electrospinning and membrane fabrication

Non-woven porous polycaprolactone (PCL) membrane was prepared by electrospinning. Briefly, a 10 wt/v% PCL solution in a mixture of dichloromethane (DCM) and ethanol with a 4:1 volume ratio was prepared. The electrospinning was performed at an optimized parameters of 13 kV applied voltage, 8 cm distance between the needle (blunt needle gauge 18) and the aluminium collector (a flat stationary surface), and flow rate of 0.3 mL/h to produce uniform and narrow distribution of fiber diameter and bead free fibers. The process was performed under ambient conditions at room temperature. Electrospinning was performed for 25 minutes which resulted in 250 ± 39.8 µm thick membrane (number of measurements (n)=20). SEM image of electrospun PCL membrane is presented in figure 2.1a. Fiber size was measured from the SEM images of over 100 fibers using ImageJ. Figure 2.1b demonstrates the fiber diameter distribution. Fibers diameter average size was 1.05 ± 0.27µm.

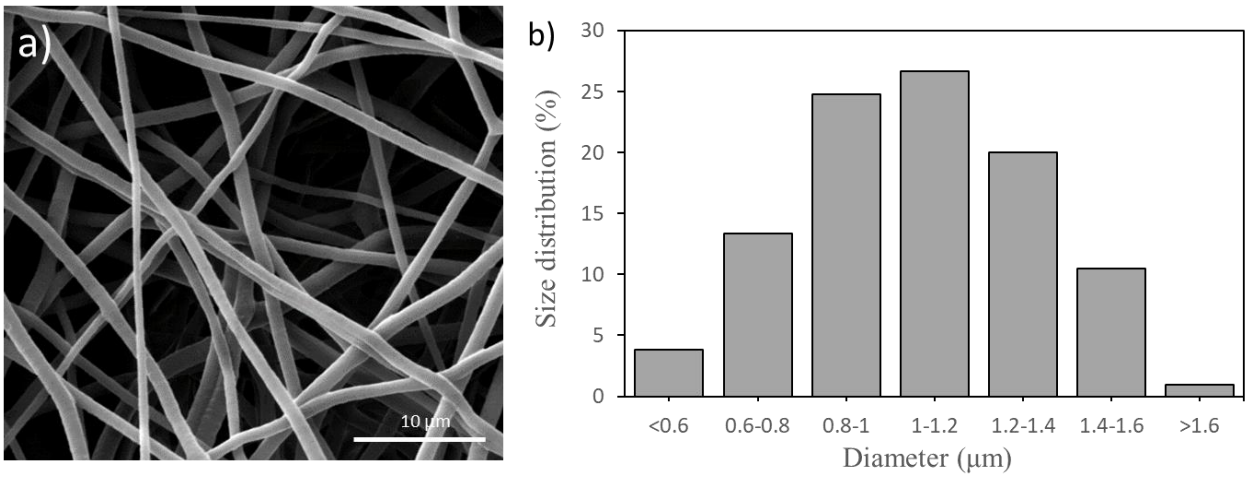

Figure 2.1 Electrospun PCL membrane. a) SEM image of membrane b) Size distribution of the electrospun fibers.

2.2.2.2 Hydrogel embedding into the membrane

The electrospun PCL membrane is hydrophobic and has a contact angle of 112 ± 3 (n=3), measured using an optical goniometer (OCA 35). Therefore, embedding hydrogels into it is a challenge. The hydrophilicity of the regions of PCL membrane intended for integration of the hydrogel was increased selectively by plasma treatment using the process shown in figure 2.2 Two layers of double-sided Kapton tape were cut using a cutter plotter (FC8600, Graphtec America, US) based on the desired designs for embedded hydrogel in the device (figure 2.2a). Layers were assembled in a layer-by-layer manner with proper alignment on either side of the PCL layer in the center. Next, this sandwiched layer was exposed to oxygen plasma for 80 seconds (figure 2.2b) which selectively makes the exposed regions of the PCL membrane hydrophilic (contact angle ~0°) while the rest of the membrane remains hydrophobic. Then, the hydrogel (2 wt% agarose in TAE buffer, prepared by microwaving the solution) was pipetted in the open hydrophilic regions on the membrane and its excess amount was removed from the surface after gelation (figure 2.2c).

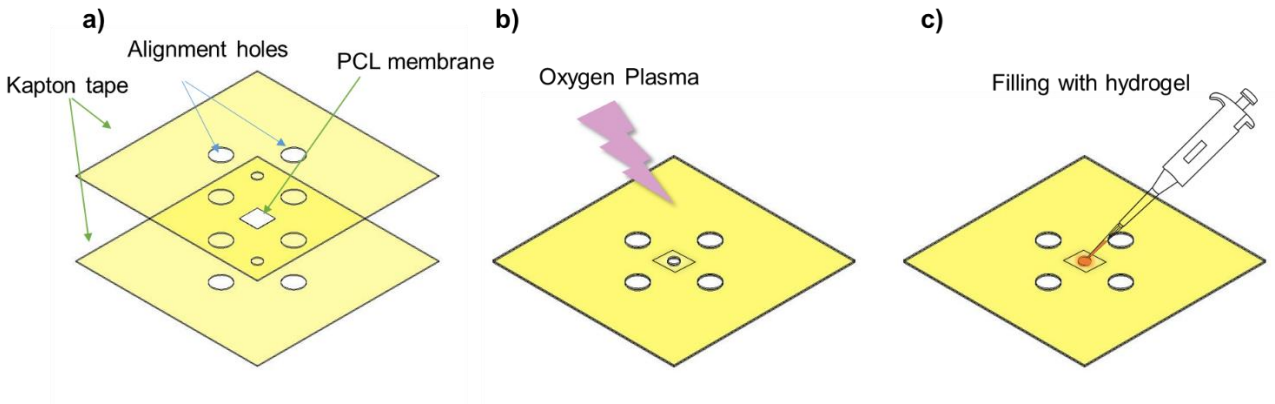

Figure 2.2 Hydrogel embedding into the PCL membrane process. a) Sandwiching the membrane between two layers of Kapton tape b) Oxygen plasma c) Filling the open hydrophilic region with hydrogel.

2.2.2.3 Drying and rehydration of embedded hydrogel

Agarose loaded electrospun PCL membrane was dried overnight at room temperature. The next day, one droplet of 1X TAE buffer was used for rehydration of agarose in the membrane for 1 minute. A camera (Infinity3, Lumenera, US) mounted on a stereo microscope (SZ61, Olympus, Japan) was used to take images of cross section of the membrane before and after rehydration. SEM microscopy was also used to further evaluate the microstructure of dried agarose embedded membrane.

2.2.2.4 Evaluation of the sealing of the hydrogel by transport of colorimetric dye

A device containing two cross channels was fabricated using xurography method. The schematic of the layers of the device and the exploded view of the layers are shown in figure 2.3a and b respectively. Cutter plotter was used to cut different layers of the final device in predefined patterns. Circular openings with 1.1 mm diameter for hydrogel section were cut in two layers of Kapton tape. Assembly of the layers and hydrogel integration process was similar as before (in case of two and three layers of PCL, more membrane layers were stacked on each other between two Kapton tapes and plasma exposure and hydrogel loading were performed from both sides of

membrane layer). Two channels with 1.6 mm width and 10 mm length were cut out of 127 µm thick PVC film and were attached to the top and bottom of the Kapton tapes. Finally, a hydrophilic adhesive (93049-AR) with openings for inlets and outlets was attached to the top channel. Another layer of hydrophilic adhesive was used to seal the bottom channel. A cross-sectional view of the device with dimensions with respect to the scale of the different layers is demonstrated in figure 2.3c. All the layers were aligned one after the other using alignment marks. At the end, the device passed through a laminator.

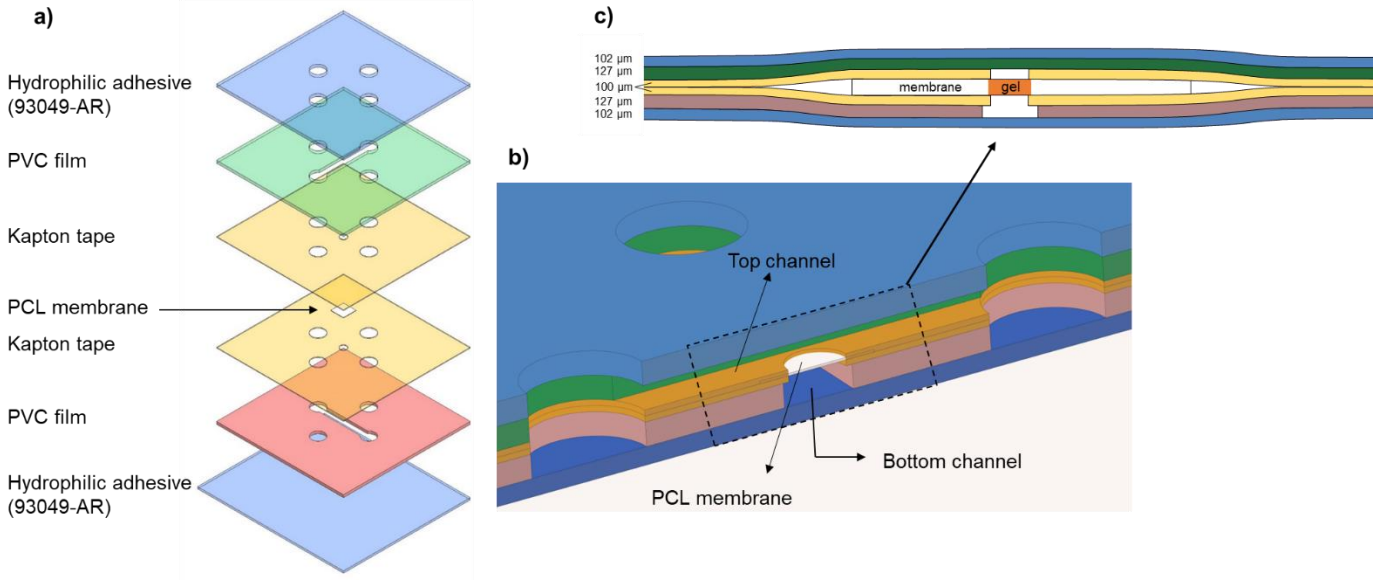

Figure 2.3 Fabricated device for evaluation the sealing of the hydrogel by transport of methylene blue. a) Configuration and layers of the device b) Schematic of the device c) Cross-sectional view of the device with loaded hydrogel.

The fabricated device with intersecting channels was used to study the sealing of the hydrated and rehydrated agarose in the membrane. Top and bottom channels were filled with 1X TAE buffer and methylene blue solution, respectively. The diffusion of methylene blue from bottom to top channel was tracked using a camera (Infinity3, Lumenera, US) mounted on a stereo microscope (SZ61, Olympus, Japan). Images were taken every 4 minutes and were analyzed using ImageJ. The original RGB images were transferred to grey scale format ranging from 0 to 255 and the

intensity in the circular agarose region was calculated as an aggregate grey scale value. The brighter color gives a higher grey scale value. The intensity was normalized by subtracting the obtained grey scale value from the starting grey value (background) for each image before the dye was added.

The effect of electric field on the transport of methylene blue was studied by incorporating electrodes in the fabricated device using xurography. Electrodes were made from thin copper film (21 µm thickness) and dicing tape was used as the support for electrode patterns. Copper foil was sandwiched between two layers of dicing tape. Then, the top layer and metal film were cut using the cutter plotter (top dicing tape prevents the metal from being torn in the process of cutting). Then, the top and bottom sides were exposed to UV light to make the dicing tape non-sticky and help with peeling the unwanted regions of metal foil. On top of the electrode layer, a transfer adhesive tape was used to attach the electrodes to the other layers of the device (figure 2.4a). The channel containing methylene blue and the buffer channel were connected to anode and cathode, respectively. A 10 V was applied using a DC power supply (Keithley 2636) for 6 minutes between the two microchannels and images of the hydrogel region were taken to analyze the mass transfer. The sealing efficiency of the dried (air-dried overnight) and rehydrated agarose in the membrane was studied similarly. First, the hydrogel was rehydrated using TAE buffer in the top channel for 1 minute. Then, the bottom channel was filled with methylene blue and the transport of that in the absence and presence of electric field was observed.

2.2.2.5 Concentration and quantification of DNA in agarose loaded membrane

A cross channel microfluidic device (figure 2.4b) was fabricated to concentrate and quantify DNA from its initial solution. The devices used for the DNA concentration experiments were fabricated similar to those in the previous section. The hydrogel region was defined using PCL membrane

which had been sandwiched between two Kapton tapes with circular openings of 350 µm radius in one layer and 700 µm in the other. The sample channel was fabricated with dimensions of 800 µm (w), 127 µm (H), and 8 mm (L) and buffer channel with dimensions of 1.6 mm (W), 127 µm (H), and 8 mm (L). The open region was filled with 2% agarose after exposure to oxygen plasma. The agarose embedded layer dried overnight at room temperature. Device was sealed with a hydrophilic tape (93049-AR) containing the inlets and outlets of the channels.

DNA samples were prepared by diluting the 150 bp DNA stock solution in 1X TE (200 mM Tris-HCl and 20 mM EDTA) buffer to the desired concentrations (1 and 5 µg/mL). Then, 200 times diluted PicoGreen was added to the DNA sample with a 1:1 volume ratio. The tube containing prepared sample was kept in dark for 10 minutes for the DNA and dye to completely intercalated. A fluorescent microscope (Etaluma, Model 500) was used for imaging purposes. After connecting the sample channel and buffer channel inlets to cathode and anode respectively, the buffer channel was filled with 4 µl of 1X TAE buffer to rehydrate the agarose embedded in the membrane. One minute later, the sample channel was filled with 2 µl DNA sample. Cross section of the channels is presented in figure 2.4c. The electrodes were connected to a DC power supply (Keithley 2636) and a 5 V voltage was applied to the device to initiate the DNA transfer.

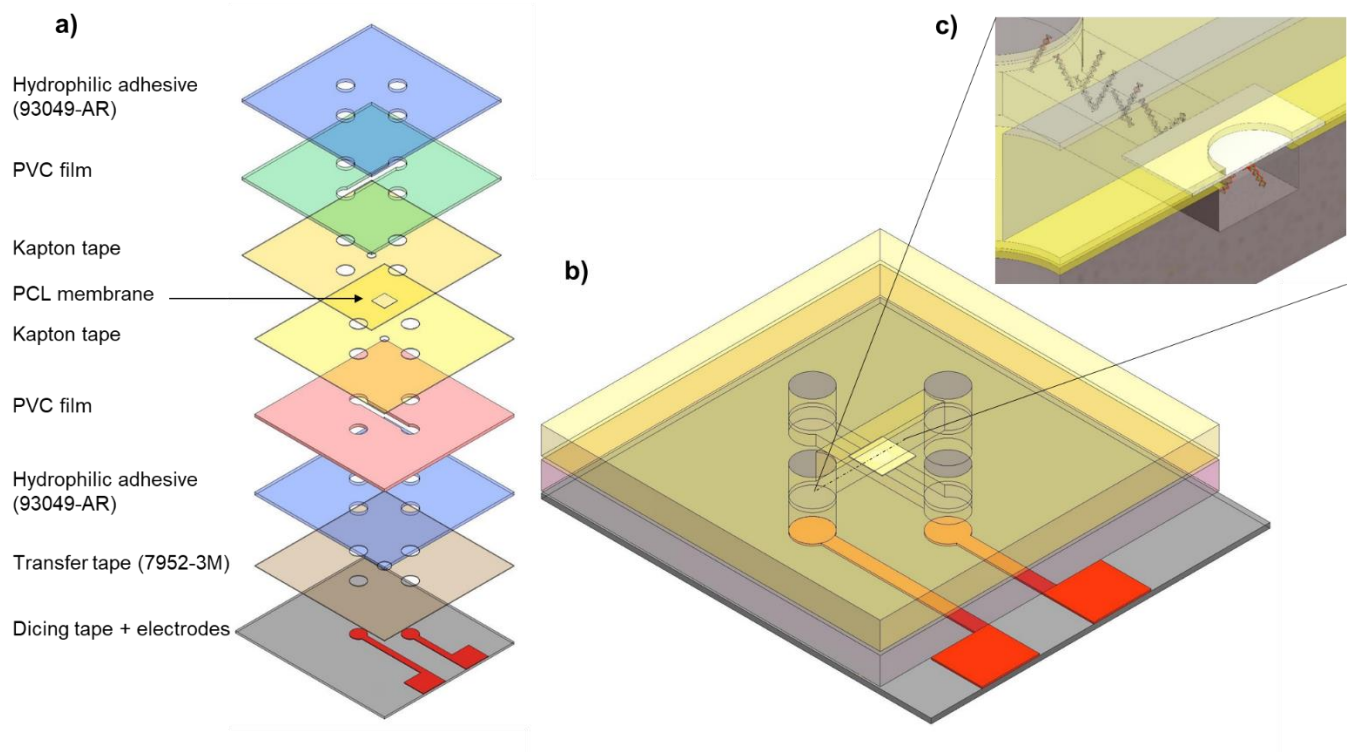

Figure 2.4 Fabricated device with incorporated electrodes and agarose loaded PCL membrane. a) Configuration and layers of the device b) Microfluidic device for concentration and quantification DNA c) Cross-section view of the channels.

2.3 Results and discussion

2.3.1 Hydrogel integration, resolution characterization, and patterning

Electrospinning has been used here to create a non-woven fibrous membrane with large pores and high porosity to serve as a scaffold to embed a small volume of hydrogel. The use of the scaffold is beneficial in maintaining the macrostructure of the hydrogel even when it is dried and reconstituted which is important for many point-of-care applications.

The electrospun membrane was made from 10 wt/v% PCL solution in a mixture of DCM and ethanol. Various applied voltage and distance between the needle and collector were used to arrive at the final optimized conditions for electrospinning. An applied voltage was 13 kV and the distance between the needle and the collector of 8 cm with a solution flow rate of 0.3 mL/h was

found to be optimal to produce uniform fiber diameter, pore size, and bead free membranes. Electrospinning was performed for 25 minutes in order to achieve a 250 ± 39.8 μm thick membrane with average 1.05 ± 0.27 μm fiber diameter size. The fabricated membrane was suitable for embedding enough amount of hydrogel while the structure of hydrogel is maintained by fibers. Thinner membranes proved to be more fragile and less mechanically stable when loaded with hydrogel.

The as spun PCL membrane is hydrophobic (contact angle of 112 ± 3) which is suitable to prevent the spread of the imbibed gel further from the patterned regions. However, it also prevents complete and robust imbibition of the gel within the patterned regions. Therefore, a self aligned hydrophilization process was developed that can convert the patterned regions of the membrane for robust imbibition of the gel. It has been shown that surface plasma treatment enhances the hydrophilicity of the PCL membrane by forming oxygen-containing groups [49]. Therefore, PCL membrane was sandwiched between two Kapton tape layers with opening sections for hydrogel loading. These Kapton tape layers protect PCL membrane from exposure to plasma and consequent hydrophilization in all the regions except in the openings where hydrogel is to be loaded. Upon dropping a small bolus of hydrogel, the plasma treated region also imbibes the gel while the surrounding regions do not due to their hydrophobic nature. The excess gel on top of the membrane was wiped away leaving behind a precisely defined volume of hydrogel that was loaded on to the membrane. For demonstrations we use agarose as the hydrogel, but this method should be applicable to any other hydrogels as well. Hydrophilic regions of the membrane were filled with agarose colored with food dye.

Using this technique, hydrogel microstructures in different shapes and sizes can be obtained. Thickness of the hydrogel layer is controlled by thickness of the membrane. By making the

membrane thicker or stacking several membranes on top of each other thicker gel layer can be obtained. In order to determine the lateral resolution of this method a series of circular and square regions with different sizes were cut and filled with hydrogel. Circular and square patterns (ranging from 100 μm to 1 mm with 100 μm increments) were fabricated and filled with 2% agarose colored with food dye. It is shown that different patterns of hydrogel with dimensions as small as 300 μm can be created (figure 2.5). This resolution corresponds to ~ 20 nL of hydrogel inside the membrane (considering thickness of the membrane be 250 μm and ignoring the volume of the fibers). Xurography was not able to create reliable patterns smaller than 300 μm in Kapton tape and the patterns did not resemble the designed shapes below that limit. Although this resolution is less than the resolution associated with photopolymerization method for creating gel microstructures (25 μm) [26], it is still sufficient for many point of care applications where hydrogel integration is desired. This hydrogel integration technique resolution can be improved by using a better cutter plotter machine with higher resolution. Moreover, using a thinner double-sided tape (Kapton tape thickness is 250 μm) should be helpful for getting better cuts and greater resolution. Alternatively, laser micromachining can be used to cut Kapton tape with a much higher resolution.

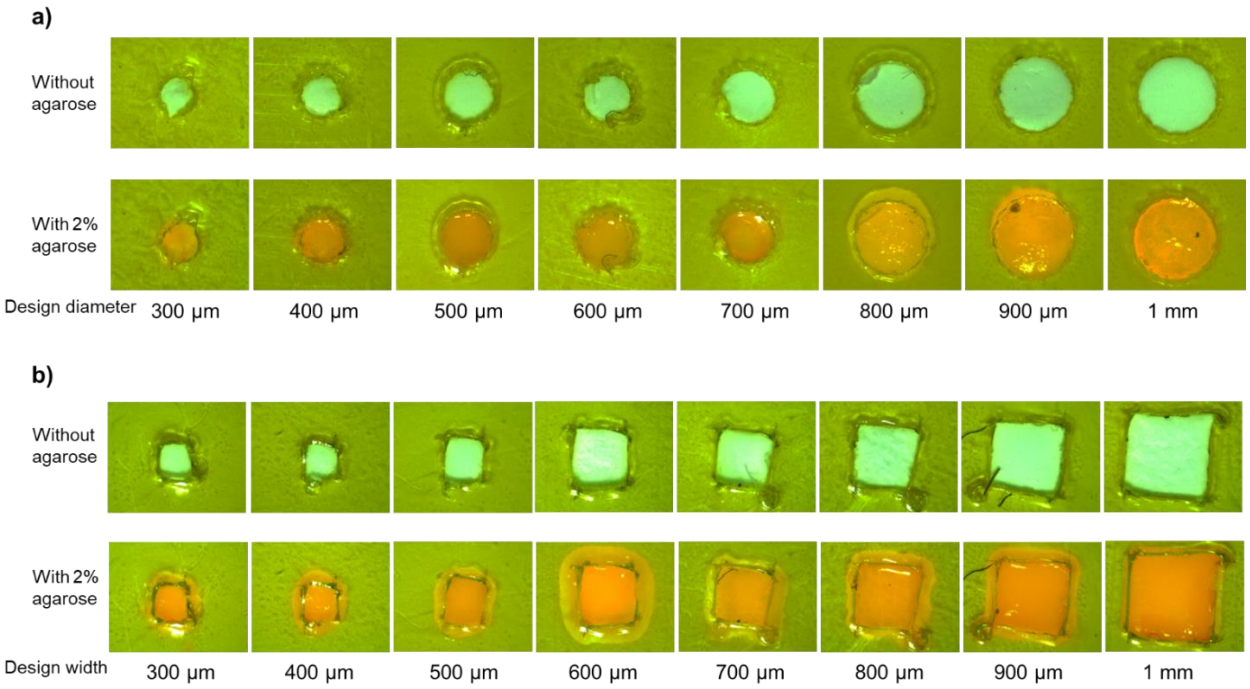

Figure 2.5 Characterization of fabrication and hydrogel integration. a) Circular patterns with different sizes before and after filling with 2% agarose b) Square patterns with different sizes before and after filling with 2% agarose.

The xurographic process is flexible and can create a wide range of patterns. Long line type patterns are important for creating separation columns from gels and can also be patterned using the xurographic gel integration process. As shown in figure 2.6a long hydrogel lines with width as small as 200 µm can be created. Xurography did not provide a good cut for 150 µm wide line. It is also demonstrated that by using this technique more complex patterns such as alphabets shown in figure 2.6b can be obtained. Another benefit of this technique is its scalability. The xurographic process can be used to create multiple gel locations on the same device. These locations can be imbibed with different gel compositions that can be used to create a microarray as shown in figure 2.6c. This capability is especially advantageous when multiple conditions, concentrations and analytes need to be detected or analyzed using the same sample. The layer containing hydrogel patterns can be attached by adhesive to the other layers of microfluidic devices fabricated using xurography technique. This method allows for integration of gels into microfluidic devices in an

out-of-plane manner. It also allows integration of gels in-between two microfluidic channels where it could be used as a convection barrier to separate the fluid and particle interaction between the contents of those channels. It can also be used as a mean to expose a layer of cells to analytes on both sides such as in a transwell membrane. Other methods such as photopolymerization typically integrate gels in-plane with the channels and are more suitable for biomolecule separation type devices such as for DNA electrophoresis.

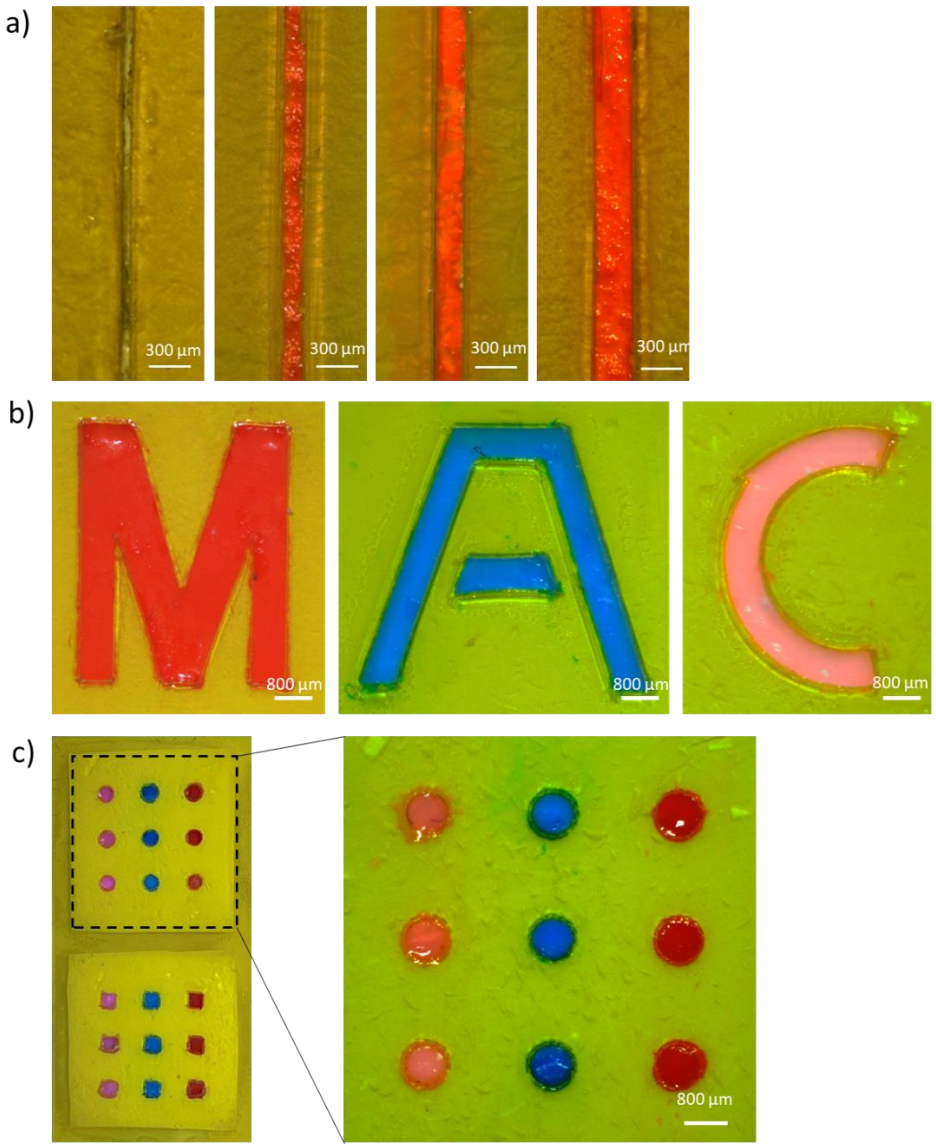

Figure 2.6 Demonstration different hydrogel patterns and the technique scalability. a) Long line patterns with 150, 200, 250, and 300 µm designed width (from left to right) b) Patterning the hydrogel in alphabets c) Creating multiple colored hydrogel spots to show the scalability of the method.

Other porous materials with a fibrous texture such as paper can also be used in this process for integrating hydrogels. Unlike PCL that is hydrophobic and provides an automatic confinement of the imbibed gel from spreading, paper is hydrophilic. Therefore, to accurately maintain the pattern of hydrogel, wax printing was used. Compared to PCL membrane, paper did not provide an effective scaffold for hydrogel, and this was confirmed by transport study of methylene blue

(Supplementary information figure S.6). In addition, paper exhibits high autofluorescence which is not desirable is fluorescent based studies [50].

2.3.2 Drying and rehydration of the hydrogel

For many microfluidic applications such as in point of care devices, it is beneficial to store the hydrogel inside the microfluidic device and rehydrate that when is required. Therefore, drying and rehydrating the hydrogel loaded into the hydrophilic section of the membrane was studied. 10µl of agarose solution was pipetted in the open region of membrane and after diffusion of the gel inside the membrane and its gelation, excess amount of gel was wiped from top of the tape and leaving the gel only in the hydrophilic section of membrane layer. Gel embedded membrane was air dried overnight and rehydrated the following day. Membrane sandwiched between two Kapton tape was weighted in each step. For instance, alphabet “M” hydrogel pattern shown in previous section was weighted before and after agarose loading and 2.375 ± 0.25 mg (n=4) increase was observed. After one day drying, membrane layer weight was almost the same as membrane only, which shows all the hydrogel water was evaporated. After rehydration with buffer, weight increased again for 2.5 ± 0.07 mg, which is slightly higher than the value for hydrated agarose in the membrane. Part of that can be because of excess absorbed buffer by the membrane.

The cross section of a sandwiched PCL membrane between two Kapton tapes with circular openings is shown in figure 2.7a. Agarose loaded membrane is compared before and after air-drying and rehydration with TAE buffer. From images, very few changes were detectable between hydrated and rehydrated agarose in the PCL membrane. From SEM image of electrospun PCL membrane after filling with agarose (figure 2.7b), it was noted that the pores between the PCL fibers were filled completely with gel and fibers were able to keep the structure of dried agarose.

Therefore, using this method to integrate hydrogels into microfluidic devices, it is possible to store the hydrogel in dried state in the device and rehydrate it once is required.

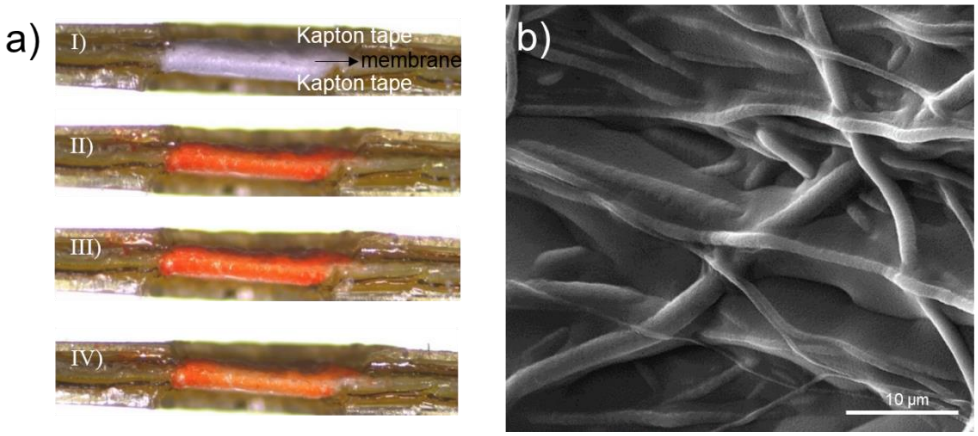

Figure 2.7 Drying and rehydrating agarose loaded membrane. a) Cross-sectional view of the PCL membrane sandwiched between two Kapton tape layers; I) One PCL membrane layer between two layers of Kapton tape II) After filling with 2% agarose III) After air-drying agarose overnight IV) After rehydration agarose by adding TAE buffer b) SEM image of electrospun PCL membrane loaded with 2% agarose.

2.3.3 Evaluation of the sealing of the hydrogel by transport of colorimetric dye

It is important to determine if both hydrated and rehydrated hydrogel in the membrane create a leak free barrier and effective sealing. Therefore, transport of small molecules such as methylene blue through hydrated as well as the dried and then rehydrated agarose loaded membrane with different thicknesses in presence and absence of electric field was studied. By increasing the number of the membrane layers, the thickness of embedded hydrogel can be increased. A microfluidic device containing two channels was fabricated by xurography as described previously.

2.3.3.1 Diffusional transport through integrated gel layers

In order to investigate the integrity of the gel membrane as a leakage free separator, diffusional experiments were performed. Methylene blue solution as a colorimetric dye was used in one of the channels of the cross channel device and diffusion of the dye to the other side was measured by

taking images of the other channel every 4 minutes (figure 2.8a). The intensity of the circular region in each image was quantified using ImageJ and results for different numbers of layers were compared in figure 2.8b. The results show that a single layer of gel loaded electrospun membrane acted as a poor separator and was quickly saturated (within 8 min) with the dye due to diffusional transport. On the other hand, 2 and 3 layers of membrane were able to withstand significant saturation over a longer duration of time. Moreover, in all the cases it was clear that the gel formed a tight seal against the sidewalls of the device and did not allow any convective flow between the two channels indicating formation of a highly reliable seal.

We also compared the observed kinetics of the mass transfer with the characteristic time scale $\tau_D = h^2/D$; (h the thickness of the hydrogel and D the diffusion coefficient of methylene blue) of methylene blue diffusion in agarose layer. Assuming a diffusion constant of 5.74×10^{-6} cm^2s^{-1} [51] for methylene blue, τ_D of 1.8, 7.3, and 16.4 minutes was calculated for 1, 2, and 3 layers of agarose loaded membrane respectively. These values are in the same range as the observations made in our experiments. As an example, in case of one layer of PCL membrane, the intensity of the color reaches ~ 90% of the saturation value in ~ 3 min which is close to the calculated value.

Similar transport study was performed on dried and subsequently rehydrated gel layers. These layers (two layers of PCL membrane loaded with agarose) were dried overnight followed by hydration. The transport of the dye was compared with freshly hydrated agarose in figure 2.8c.

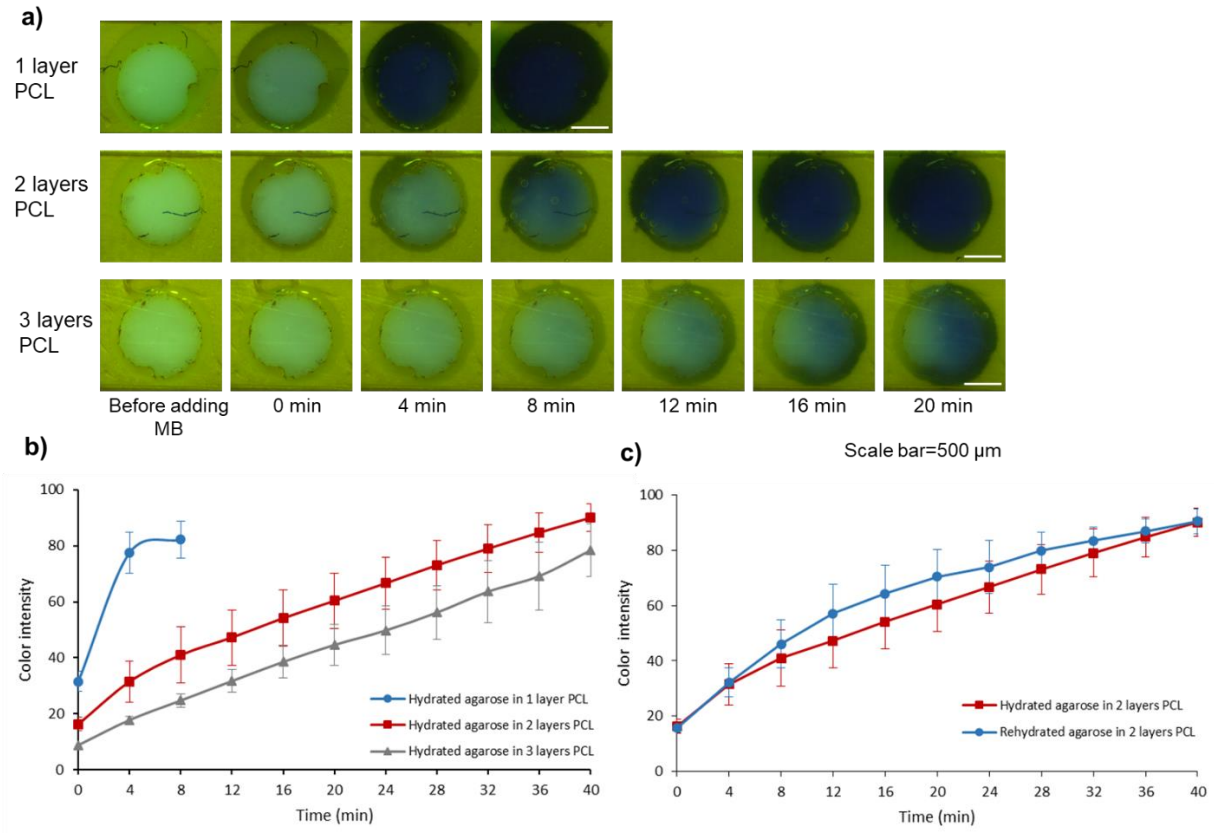

Figure 2.8 Diffusion of methylene blue through agarose loaded electrospun PCL membrane. a) Diffusion of methylene blue through hydrated 2% agarose gel in 1, 2, and 3 layers of membrane b) Comparison of the diffusion of methylene blue between 1, 2, and 3 layers of agarose loaded membrane over time c) Comparison of methylene blue diffusion between hydrated and rehydrated agarose embedded in 2 layers of PCL membrane.

The diffusional behaviour of methylene blue through rehydrated agarose was almost similar to the freshly hydrated (undehydrated) gel indicating that the drying and reconstitution of the gel did not affect its integrity and its capacity to serve as a convective barrier. This is in contrast with the gel loaded into channels without scaffolds that often leads to gap formation between the rehydrated gel and the sidewalls allowing convective flow. This phenomenon is demonstrated in figure 2.9 where agarose was directly (without any scaffold) loaded into the circular region. Initially, the gel was trapped in the circular region between the two microchannels and formed a barrier (figure 2.9a). However, when it was dried (8 mins) it considerably shrunk due to loss of water and detached from the sides of the circular region leaving a large gap (figure 2.9b). Subsequent

rehydration of this gel swelled it to fill most of the volume in the circular region but not completely (figure 2.9c). The formed gaps allowed considerable convective flow of the colorimetric dye from bottom channel into the top channel (figure 2.9d).

We also performed tests on the integrity of the membrane when it is dried and rehydrated multiple times. We noted that the membrane and the gel integrity was preserved and visually there were no large gaps or holes in the intersection region. Nevertheless, diffusion of the dye through the gel layer was faster after the second drying and rehydration compared with the first one (figure S.7). This indicates that there may be some microscopic degradation of the gel layer and loss of material.

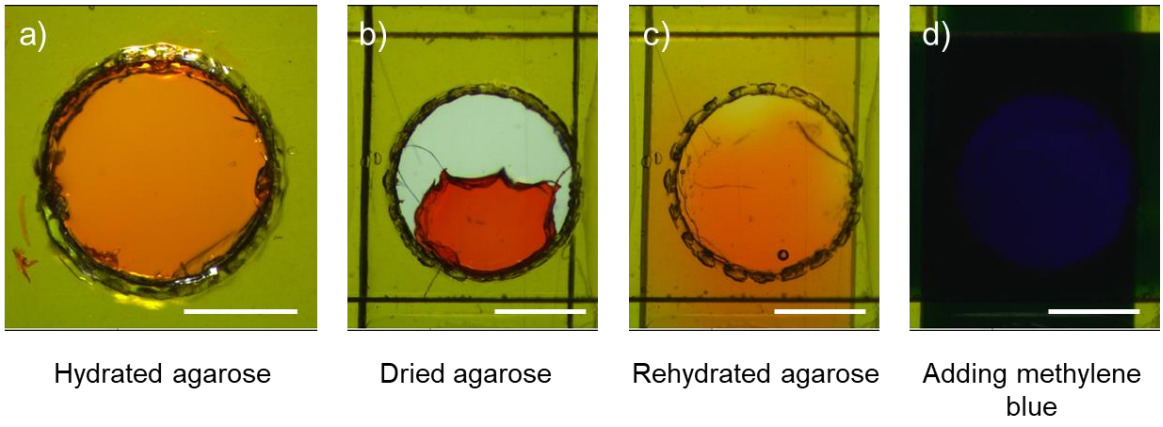

Figure 2.9 Loading agarose into the device without scaffold and evaluating the sealing by transport of methylene blue. a) Hydrated agarose b) Dried agarose c) Rehydrated agarose d) After filling the bottom channel with methylene blue. (scale bar = 700µm)

We also tested the mechanical integrity of the gel layers formed when a transmembrane pressure was imposed. It was shown that for 1, 2, and 3 layers of PCL membrane filled with agarose the systems remained robust under about 245, 385, and 524 mbar respectively (supplementary information).

2.3.3.2 Enhanced transport under electric field

Electric field can enhance the transport of methylene blue through the hydrogel membrane due to electrophoresis. Electrophoretic transport of methylene blue was used to identify if small pinholes exist in the gel membrane. To this end, same device with electrodes added to its reservoirs and containing two layers of agarose embedded PCL membrane was used. Electrodes were fabricated using xurography based on the process that was previously developed [9]. The top channel was filled with buffer solution and bottom channel was loaded with methylene blue. An electric potential of 10 V was applied for 6 minutes between the two microchannels. The application of electric field caused enhanced electrokinetic transport of methylene blue molecules through the agarose loaded membrane to the top channel (figure 2.10a). When an electric field is applied between two channels, the electric field lines are routed through agarose loaded membrane and transport of methylene blue occur along the electric field lines [52]. Comparison between transport of methylene blue through agarose embedded membrane in absence and presence of electric field showed an increase in mass transfer rate when electric field is applied (figure 2.10b). The electrokinetic transport was much greater than the diffusional transport as expected and can be used to dose small amount of reagents between one channel to the next through the gel barriers. It is notable that the transport of the molecules is much higher in the bottom right end as compared with the top left as this region is closer to the electrode and has a higher density of electric field lines. Interestingly, there were no point locations where the methylene blue leaked through indicating the good barrier property of the membrane. Similar to the solely diffusion case, a comparison between electrokinetic transport of methylene blue through hydrated and rehydrated agarose in membrane was performed and evaluated under electrokinetic transport. No significant difference (figure 2.10c) was observed between the two cases which confirms that PCL membrane

has been able to keep the structure of agarose layer in the device and the sealing remained good after rehydration.

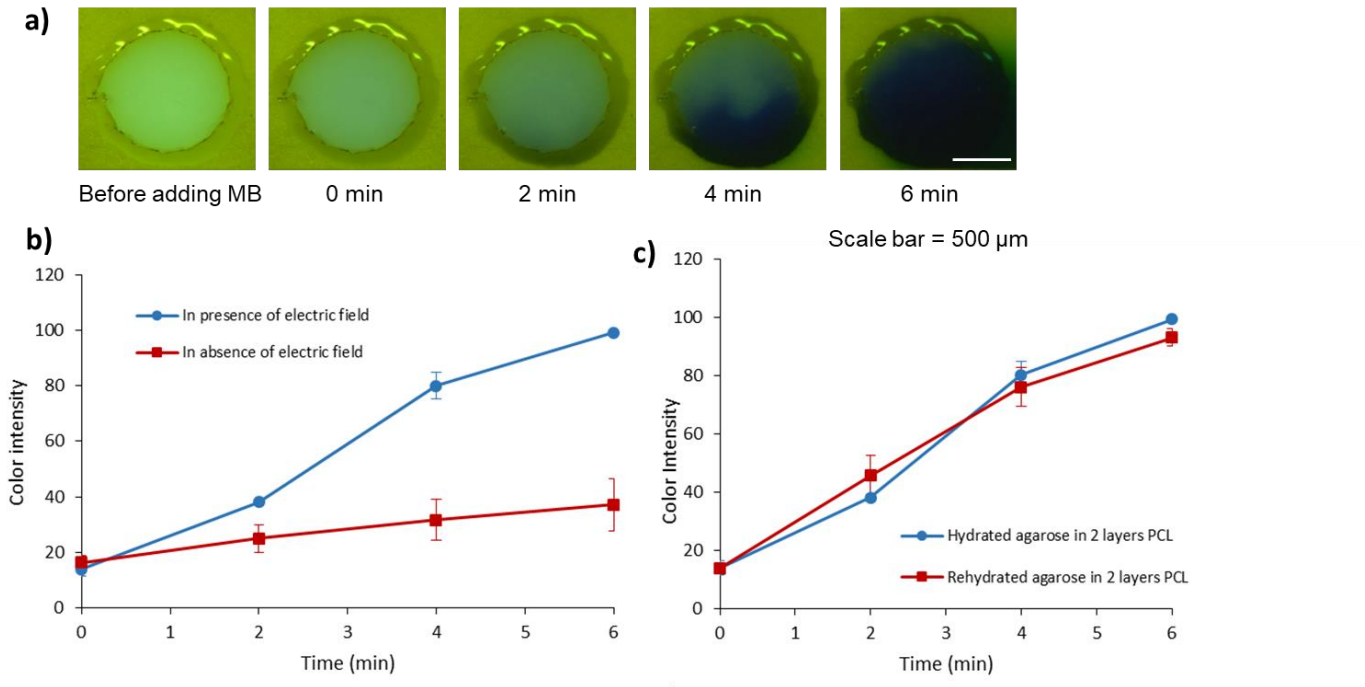

Figure 2.10 Transport of methylene blue through agarose loaded membrane in presence of electric field. a) Transport of methylene blue through hydrated 2% agarose gel in two layers of membrane in presence of electric field (10 volts) b) Comparison of methylene blue transfer in presence and absence of electric field c) Comparison between transport of methylene blue in hydrated and rehydrated agarose.

2.3.4 Application in concentration and quantification of DNA from samples

Hydrogel integrated microfluidic devices can be used to concentrate DNA from a solution for applications such as sepsis prognostics by concentrating and quantifying cell-free DNA (cfDNA) from a sample such as blood [53]. Yang et al. performed electrophoretic concentration and quantification of cfDNA in agarose gel in a microfluidic device. One of the challenges encountered in point of care use of this device was the need to load agarose gel immediately prior to the detection with the sample which made the sample preparation complex and not user friendly. The ability to store the gel and its constituents in a dried form that can be reconstituted by a buffer

solution or simply the sample itself can greatly simplify the sample preparation process and facilitate the use of this method for point of care sepsis prognostics.

Sepsis is the leading cause of death and a critical illness in the Western world [54]. One challenge in this area is to predict mortality in ICU patients. Several biomarkers have been discovered to be a great tool for diagnosis and prognosis of sepsis. CfDNA which is comprised of short-lived fragments of DNA and released due to cell necrosis and apoptosis has been found to be a biomarker for prediction of mortality in ICU sepsis patients. Based on a study on 80 patients with severe sepsis, the mean cfDNA level in survivors was 1.16±0.13μg/mL which was similar to healthy volunteers (0.93±0.76μg/mL); however, for non-survivors was 4.65±0.48μg/mL. Thus, measuring cfDNA level and other sepsis biomarkers (e.g. Protein C and Procalcitonin) in combination with current scoring systems (e.g. MODS) yields a stronger predictive power and assists physicians in prediction the severity of sepsis for each patient and provide more aggressive care plan [55].
The microfluidic device designed for this purpose consisted of two channels perpendicular to each other and separated using an agarose loaded PCL membrane. The agarose membrane was used as a low mobility environment for electrophoretic concentration of DNA. Agarose was dried at room temperature overnight prior to the experiment. The sample solution was prepared using 150 bp DNA which is similar to actual cfDNA size. Sample was fluorescently labeled with PicoGreen. 1 and 5 μg/mL of DNA solutions, similar to the cfDNA concentration for survivors and non-survivor patients, respectively, were studied. A device that had the gel layer dried was used in these experiments to simulate the situation where such devices are used in the field. The top channel was first filled with the buffer solution to rehydrate the gel and the DNA sample was loaded into the bottom channel after some time. The rehydration of the gel can also be accomplished by the sample itself. A 5V DC electric field was applied between channels and fluorescent images of the gel were

taken every minute for a total of 4 minutes to measure the fluorescent intensity (figure 2.11a). DNA moved towards anode due to its negative charge and accumulated in agarose gel as the mobility is lower. The DNA concentration of both the 1 and 5 µg/mL of DNA samples increased over time (figure 2.11b). This is because the gel serves as a trap to hold the DNA for a longer duration of time as it is electrophoretically transported into it from the surrounding solution. The rate of increase was higher in the case of 5 µg/mL of DNA as expected as the surrounding concentration was higher. There was a clear difference in the intensities of the gel region between 1 and 5 µg/mL indicating that the rehydrated device can potentially be used as a low-cost and easy to fabricate tool that can differentiate between 1 and 5 µg/mL of 150 bp DNA with high accuracy in a rapid way.

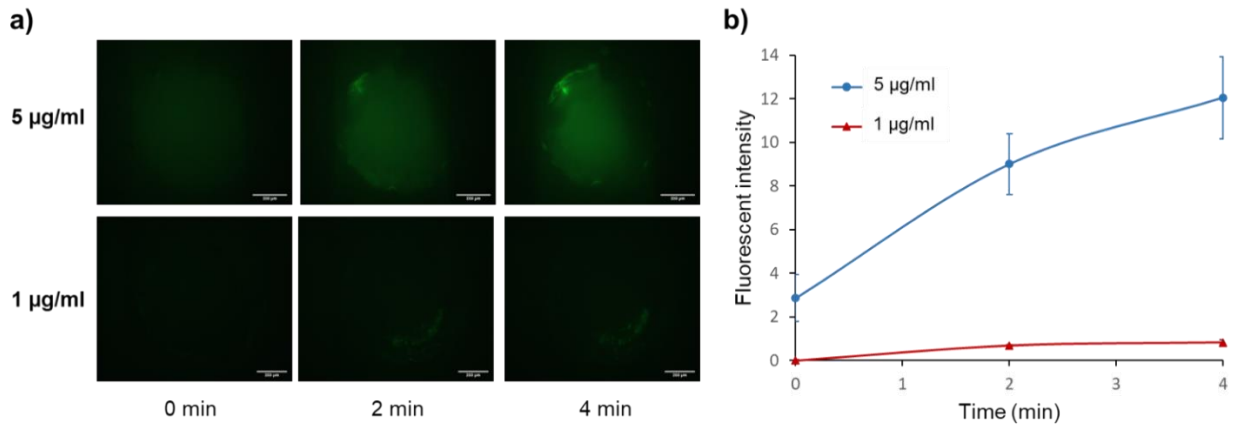

Figure 2.11 Concentration and quantification 150 bp DNA in the microfluidic device containing agarose loaded membrane. a) Images of agarose loaded membrane region where DNA concentrate b) Comparison of the fluorescent intensity between 1 and 5 µg/mL. (n=3, scale bar=200 µm)

2.4 Conclusion

In summary, this paper introduces a simple and low-cost technique to integrate hydrogels such as agarose into microfluidic devices within the fabrication process using PCL electrospun membrane and xurography. Multiple hydrogel spots in different shapes and sizes as small as 200 µm can be patterned in the membrane. Furthermore, the thickness and amount of hydrogel can be controlled

by the number of the membrane layers. This technique is especially beneficial in applications where longer storage of hydrogels is required in the devices as hydrogel can be rehydrated around and inside the fibers of the membrane while the sealing is kept. Electrophoretic accumulation and quantification of 150 bp DNA with different concentrations was demonstrated in rehydrated agarose in a microfluidic device. This microfluidic device can be developed as a point of care device for quantification of cell-free DNA in blood sample of sepsis patients as cfDNA is a prognosis indicator for sepsis ICU mortality.

Supplementary Material

The supplementary information contains the results related to using chromatography paper as the scaffold for integration of hydrogels.

References

1. Whitesides, G.M. The Origins and the Future of Microfluidics. *nature* **2006**, *442*, 368–373.
2. Pandey, C.M.; Augustine, S.; Kumar, S.; Kumar, S.; Nara, S.; Srivastava, S.; Malhotra, B.D. Microfluidics Based Point-of-care Diagnostics. *Biotechnology journal* **2018**, *13*, 1700047.
3. Nie, J.; Fu, J.; He, Y. Hydrogels: The Next Generation Body Materials for Microfluidic Chips? *Small* **2020**, *16*, 2003797.
4. Bartholomeusz, D.A.; Boutté, R.W.; Andrade, J.D. Xurography: Rapid Prototyping of Microstructures Using a Cutting Plotter. *Journal of Microelectromechanical systems* **2005**, *14*, 1364–1374.
5. Mohammadzadeh, A.; Fox-Robichaud, A.E.; Selvaganapathy, P.R. Rapid and Inexpensive Method for Fabrication of Multi-Material Multi-Layer Microfluidic Devices. *Journal of Micromechanics and Microengineering* **2018**, *29*, 015013.

6. Islam, M.; Natu, R.; Martinez-Duarte, R. A Study on the Limits and Advantages of Using a Desktop Cutter Plotter to Fabricate Microfluidic Networks. *Microfluidics and nanofluidics* **2015**, *19*, 973–985.
7. Yuen, P.K.; Goral, V.N. Low-Cost Rapid Prototyping of Flexible Microfluidic Devices Using a Desktop Digital Craft Cutter. *Lab on a Chip* **2010**, *10*, 384–387.
8. Cassano, C.L.; Simon, A.J.; Liu, W.; Fredrickson, C.; Fan, Z.H. Use of Vacuum Bagging for Fabricating Thermoplastic Microfluidic Devices. *Lab on a Chip* **2015**, *15*, 62–66.
9. Mohammadzadeh, A.; Robichaud, A.E.F.; Selvaganapathy, P.R. Rapid and Inexpensive Method for Fabrication and Integration of Electrodes in Microfluidic Devices. *Journal of Microelectromechanical Systems* **2019**, *28*, 597–605.
10. Stojanović, G.; Paroški, M.; Samardžić, N.; Radovanović, M.; Krstić, D. Microfluidics-Based Four Fundamental Electronic Circuit Elements Resistor, Inductor, Capacitor and Memristor. *Electronics* **2019**, *8*, 960.
11. Glavan, A.C.; Martinez, R.V.; Maxwell, E.J.; Subramaniam, A.B.; Nunes, R.M.; Soh, S.; Whitesides, G.M. Rapid Fabrication of Pressure-Driven Open-Channel Microfluidic Devices in Omniphobic RF Paper. *Lab on a Chip* **2013**, *13*, 2922–2930.
12. Samae, M.; Ritmetee, P.; Chirasatitsin, S.; Kojić, S.; Kojić, T.; Jevremov, J.; Stojanović, G.; Al Salami, H. Precise Manufacturing and Performance Validation of Paper-Based Passive Microfluidic Micromixers. *International Journal of Precision Engineering and Manufacturing* **2020**, *21*, 499–508.
13. Fang, X.; Wei, S.; Kong, J. Based Microfluidics with High Resolution, Cut on a Glass Fiber Membrane for Bioassays. *Lab on a Chip* **2014**, *14*, 911–915.

14. Goy, C.B.; Chaile, R.E.; Madrid, R.E. Microfluidics and Hydrogel: A Powerful Combination. *Reactive and Functional Polymers* **2019**, *145*, 104314.
15. Zhang, X.; Li, L.; Luo, C. Gel Integration for Microfluidic Applications. *Lab on a Chip* **2016**, *16*, 1757–1776.
16. Gao, D.; Liu, J.; Wei, H.-B.; Li, H.-F.; Guo, G.-S.; Lin, J.-M. A Microfluidic Approach for Anticancer Drug Analysis Based on Hydrogel Encapsulated Tumor Cells. *Analytica chimica acta* **2010**, *665*, 7–14.
17. Koh, W.-G.; Itle, L.J.; Pishko, M.V. Molding of Hydrogel Microstructures to Create Multiphenotype Cell Microarrays. *Analytical chemistry* **2003**, *75*, 5783–5789.
18. Duan, K.; Ghosh, G.; Lo, J.F. Optimizing Multiplexed Detections of Diabetes Antibodies via Quantitative Microfluidic Droplet Array. *Small* **2017**, *13*, 1702323.
19. Jung, Y.K.; Kim, J.; Mathies, R.A. Microfluidic Linear Hydrogel Array for Multiplexed Single Nucleotide Polymorphism (SNP) Detection. *Analytical chemistry* **2015**, *87*, 3165–3170.
20. Aymerich, J.; Márquez, A.; Terés, L.; Muñoz-Berbel, X.; Jiménez, C.; Domínguez, C.; Serra-Graells, F.; Dei, M. Cost-Effective Smartphone-Based Reconfigurable Electrochemical Instrument for Alcohol Determination in Whole Blood Samples. *Biosensors and Bioelectronics* **2018**, *117*, 736–742.
21. Matharu, Z.; Enomoto, J.; Revzin, A. Miniature Enzyme-Based Electrodes for Detection of Hydrogen Peroxide Release from Alcohol-Injured Hepatocytes. *Analytical chemistry* **2013**, *85*, 932–939.
22. Bachmann, B.; Spitz, S.; Rothbauer, M.; Jordan, C.; Purtscher, M.; Zirath, H.; Schuller, P.; Eilenberger, C.; Ali, S.F.; Mühleder, S. Engineering of Three-Dimensional Pre-Vascular

Networks within Fibrin Hydrogel Constructs by Microfluidic Control over Reciprocal Cell Signaling. *Biomicrofluidics* **2018**, *12*, 042216.

23. Wu, X.; Newbold, M.A.; Haynes, C.L. Recapitulation of in Vivo-like Neutrophil Transendothelial Migration Using a Microfluidic Platform. *Analyst* **2015**, *140*, 5055–5064.
24. Yoon, D.; Kim, H.; Lee, E.; Park, M.H.; Chung, S.; Jeon, H.; Ahn, C.-H.; Lee, K. Study on Chemotaxis and Chemokinesis of Bone Marrow-Derived Mesenchymal Stem Cells in Hydrogel-Based 3D Microfluidic Devices. *Biomaterials research* **2016**, *20*, 1–8.
25. Ahmed, E.M. Hydrogel: Preparation, Characterization, and Applications: A Review. *Journal of advanced research* **2015**, *6*, 105–121.
26. Beebe, D.J.; Moore, J.S.; Bauer, J.M.; Yu, Q.; Liu, R.H.; Devadoss, C.; Jo, B.-H. Functional Hydrogel Structures for Autonomous Flow Control inside Microfluidic Channels. *Nature* **2000**, *404*, 588–590.
27. Harmon, M.E.; Tang, M.; Frank, C.W. A Microfluidic Actuator Based on Thermoresponsive Hydrogels. *Polymer* **2003**, *44*, 4547–4556.
28. Lin, R.-Z.; Hatch, A.; Antontsev, V.G.; Murthy, S.K.; Melero-Martin, J.M. Microfluidic Capture of Endothelial Colony-Forming Cells from Human Adult Peripheral Blood: Phenotypic and Functional Validation in Vivo. *Tissue Engineering Part C: Methods* **2015**, *21*, 274–283.
29. Gerver, R.E.; Herr, A.E. Microfluidic Western Blotting of Low-Molecular-Mass Proteins. *Analytical chemistry* **2014**, *86*, 10625–10632.
30. Mohamadi, R.M.; Svobodova, Z.; Bilkova, Z.; Otto, M.; Taverna, M.; Descroix, S.; Viovy, J.-L. An Integrated Microfluidic Chip for Immunocapture, Preconcentration and Separation of β-Amyloid Peptides. *Biomicrofluidics* **2015**, *9*, 054117.

31. Herzog, C.; Poehler, E.; Peretzki, A.J.; Borisov, S.M.; Aigner, D.; Mayr, T.; Nagl, S. Continuous On-Chip Fluorescence Labelling, Free-Flow Isoelectric Focusing and Marker-Free Isoelectric Point Determination of Proteins and Peptides. *Lab on a Chip* **2016**, *16*, 1565–1572.

32. Poehler, E.; Herzog, C.; Lotter, C.; Pfeiffer, S.A.; Aigner, D.; Mayr, T.; Nagl, S. Label-Free Microfluidic Free-Flow Isoelectric Focusing, pH Gradient Sensing and near Real-Time Isoelectric Point Determination of Biomolecules and Blood Plasma Fractions. *Analyst* **2015**, *140*, 7496–7502.

33. Zhang, X.; Li, L.; Luo, C. Gel Integration for Microfluidic Applications. *Lab on a Chip* **2016**, *16*, 1757–1776.

34. Chung, S.; Sudo, R.; Mack, P.J.; Wan, C.-R.; Vickerman, V.; Kamm, R.D. Cell Migration into Scaffolds under Co-Culture Conditions in a Microfluidic Platform. *Lab on a Chip* **2009**, *9*, 269–275.

35. Luo, X.; Shen, K.; Luo, C.; Ji, H.; Ouyang, Q.; Chen, Y. An Automatic Microturbidostat for Bacterial Culture at Constant Density. *Biomedical microdevices* **2010**, *12*, 499–503.

36. Puchberger-Enengl, D.; Krutzler, C.; Keplinger, F.; Vellekoop, M.J. Single-Step Design of Hydrogel-Based Microfluidic Assays for Rapid Diagnostics. *Lab on a Chip* **2014**, *14*, 378–383.

37. Beck, A.; Obst, F.; Busek, M.; Grünzner, S.; Mehner, P.J.; Paschew, G.; Appelhans, D.; Voit, B.; Richter, A. Hydrogel Patterns in Microfluidic Devices by Do-It-Yourself UV-Photolithography Suitable for Very Large-Scale Integration. *Micromachines* **2020**, *11*, 479.

38. Chen, L.; Wang, K.X.; Doyle, P.S. Effect of Internal Architecture on Microgel Deformation in Microfluidic Constrictions. *Soft Matter* **2017**, *13*, 1920–1928.

39. Garcia-Schwarz, G.; Santiago, J.G. Integration of On-Chip Isotachophoresis and Functionalized Hydrogels for Enhanced-Sensitivity Nucleic Acid Detection. *Analytical chemistry* **2012**, *84*, 6366–6369.

40. Jung, Y.K.; Kim, J.; Mathies, R.A. Microfluidic Hydrogel Arrays for Direct Genotyping of Clinical Samples. *Biosensors and Bioelectronics* **2016**, *79*, 371–378.

41. Koh, W.-G.; Pishko, M. Immobilization of Multi-Enzyme Microreactors inside Microfluidic Devices. *Sensors and Actuators B: Chemical* **2005**, *106*, 335–342.

42. Liu, J.; Gao, D.; Li, H.-F.; Lin, J.-M. Controlled Photopolymerization of Hydrogel Microstructures inside Microchannels for Bioassays. *Lab on a chip* **2009**, *9*, 1301–1305.

43. Liu, Z.-B.; Zhang, Y.; Yu, J.-J.; Mak, A.F.-T.; Li, Y.; Yang, M. A Microfluidic Chip with Poly (Ethylene Glycol) Hydrogel Microarray on Nanoporous Alumina Membrane for Cell Patterning and Drug Testing. *Sensors and Actuators B: Chemical* **2010**, *143*, 776–783.

44. Nash, A.T.; Foster, D.A.; Thompson, S.I.; Han, S.; Fernandez, M.K.; Hwang, D.K. A New Rapid Microfluidic Detection Platform Utilizing Hydrogel-Membrane under Cross-Flow. *Advanced Materials Technologies* **2022**, 2101396.

45. Nguyen, H.-T.; Massino, M.; Keita, C.; Salmon, J.-B. Microfluidic Dialysis Using Photo-Patterned Hydrogel Membranes in PDMS Chips. *Lab on a Chip* **2020**, *20*, 2383–2393.

46. Paustian, J.S.; Azevedo, R.N.; Lundin, S.-T.B.; Gilkey, M.J.; Squires, T.M. Microfluidic Microdialysis: Spatiotemporal Control over Solution Microenvironments Using Integrated Hydrogel Membrane Microwindows. *Physical Review X* **2013**, *3*, 041010.

47. Eker, B.; Temiz, Y.; Delamarche, E. Heterogeneous Integration of Gels into Microfluidics Using a Mesh Carrier. *Biomedical microdevices* **2014**, *16*, 829–835.

48. Heo, J.; Crooks, R.M. Microfluidic Biosensor Based on an Array of Hydrogel-Entrapped Enzymes. *Analytical chemistry* **2005**, *77*, 6843–6851.

49. Mochane, M.J.; Motsoeneng, T.S.; Sadiku, E.R.; Mokhena, T.C.; Sefadi, J.S. Morphology and Properties of Electrospun PCL and Its Composites for Medical Applications: A Mini Review. *Applied Sciences* **2019**, *9*, 2205.

50. Shah, K.G.; Yager, P. Wavelengths and Lifetimes of Paper Autofluorescence: A Simple Substrate Screening Process to Enhance the Sensitivity of Fluorescence-Based Assays in Paper. *Analytical chemistry* **2017**, *89*, 12023–12029.

51. Samprovalaki, K.; Robbins, P.; Fryer, P. Investigation of the Diffusion of Dyes in Agar Gels. *Journal of food engineering* **2012**, *111*, 537–545.

52. Upadhyaya, S.; Selvaganapathy, P.R. Microfluidic Devices for Cell Based High Throughput Screening. *Lab on a Chip* **2010**, *10*, 341–348.

53. Yang, J.; Selvaganapathy, P.R.; Gould, T.J.; Dwivedi, D.J.; Liu, D.; Fox-Robichaud, A.E.; Liaw, P.C. A Microfluidic Device for Rapid Quantification of Cell-Free DNA in Patients with Severe Sepsis. *Lab on a Chip* **2015**, *15*, 3925–3933.

54. Angus, D.C.; Linde-Zwirble, W.T.; Lidicker, J.; Clermont, G.; Carcillo, J.; Pinsky, M.R. Epidemiology of Severe Sepsis in the United States: Analysis of Incidence, Outcome, and Associated Costs of Care. *Read Online: Critical Care Medicine| Society of Critical Care Medicine* **2001**, *29*, 1303–1310.

55. Dwivedi, D.J.; Toltl, L.J.; Swystun, L.L.; Pogue, J.; Liaw, K.-L.; Weitz, J.I.; Cook, D.J.; Fox-Robichaud, A.E.; Liaw, P.C.; Canadian Critical Care Translational Biology Group Prognostic Utility and Characterization of Cell-Free DNA in Patients with Severe Sepsis. *Critical care* **2012**, *16*, R151.

S1 Supplementary information

Fabrication and gel integration process

Chromatography paper was another fibrous and porous membrane selected to be used as scaffold for hydrogel. Wax printing was used to pattern the paper and define the hydrogel regions. In wax patterning, hydrophobic walls of wax are printed using a wax printer on the surface of paper and a hot plate or oven is used to melt the wax into the paper for creating hydrophobic wax walls. The wax-patterned features for embedding hydrogel (squares and circles with width and diameters ranging from 700 µm to 2 mm with increments of 100 µm) were characterized and compared before and after the fabrication process (heating the wax at about 120 °C in oven for 1 minute). Figure S.1a demonstrates the features after heating the paper. The patterns shrunk as the result of heating process. Dimensions of the features were compared before and after the baking process (figure S.1b). Patterns smaller than 900 µm were almost filled with the wax after heating.

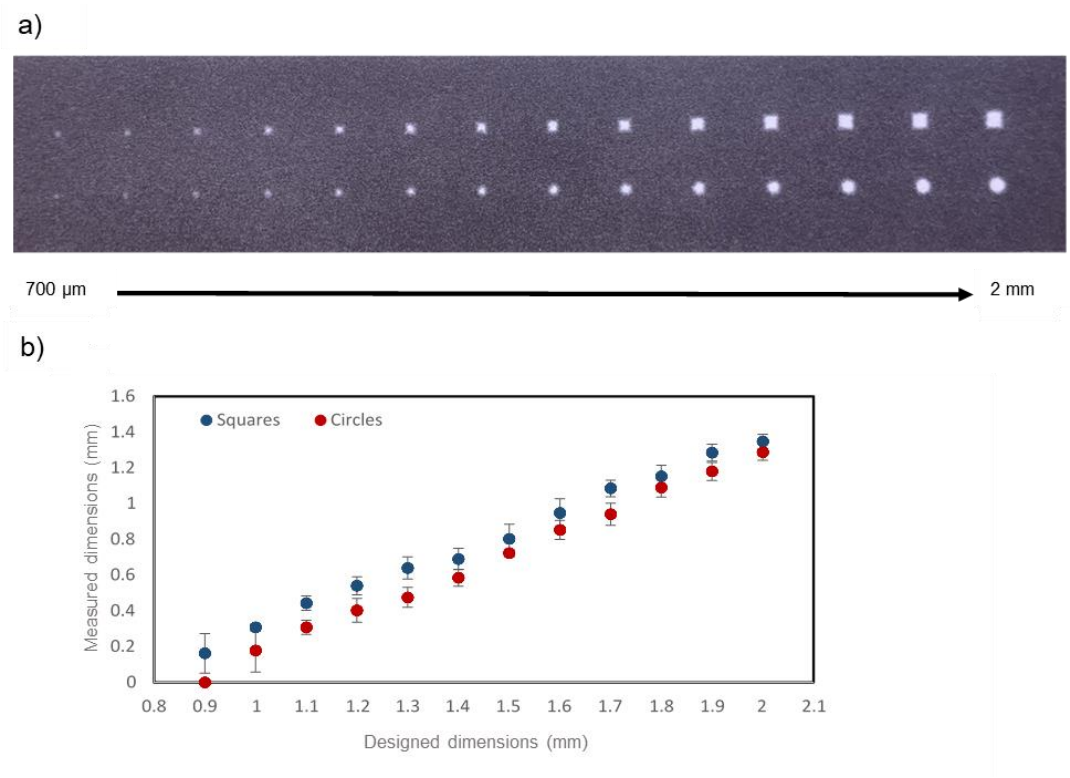

Figure S.1 Wax printing the patterns for embedding hydrogel and characterization of dimensions before and after heating. a) Wax-printed paper after baking (series of squares and circles with width and diameters ranging from 700 µm to 2 mm with increments of 100 µm) b) Characterization of the patterns before and after heating.

To fill the open patterns with hydrogel, 2% agarose was used. 10 µl of hot agarose solution containing food dye was pipetted in the openings of paper. After gelation of agarose, excess amount was wiped away from the surface of the paper (figure S.2).

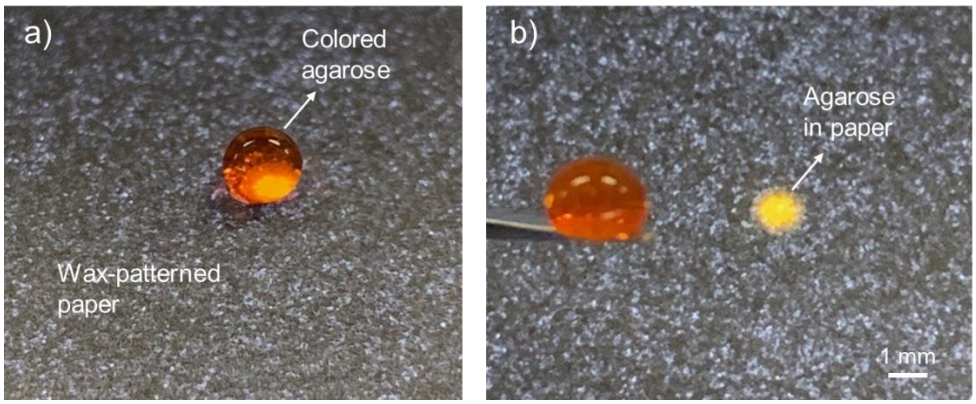

Figure S.2 Filling process of the membrane with agarose. a) Pipetting 10 µl of 2 % agarose b) Removing the excess amount.

Resolution characterization

Characterization of resolution for embedded hydrogel into wax-patterned paper is presented in figure S.3. Squares and circles with dimensions ranging from 1 mm to 2 mm with increments of 100 µm were printed. They were filled with agarose using the technique previously described. The smallest possible pattern for hydrogel was about 1 mm which shrunk to 200-300 µm after heating the paper.

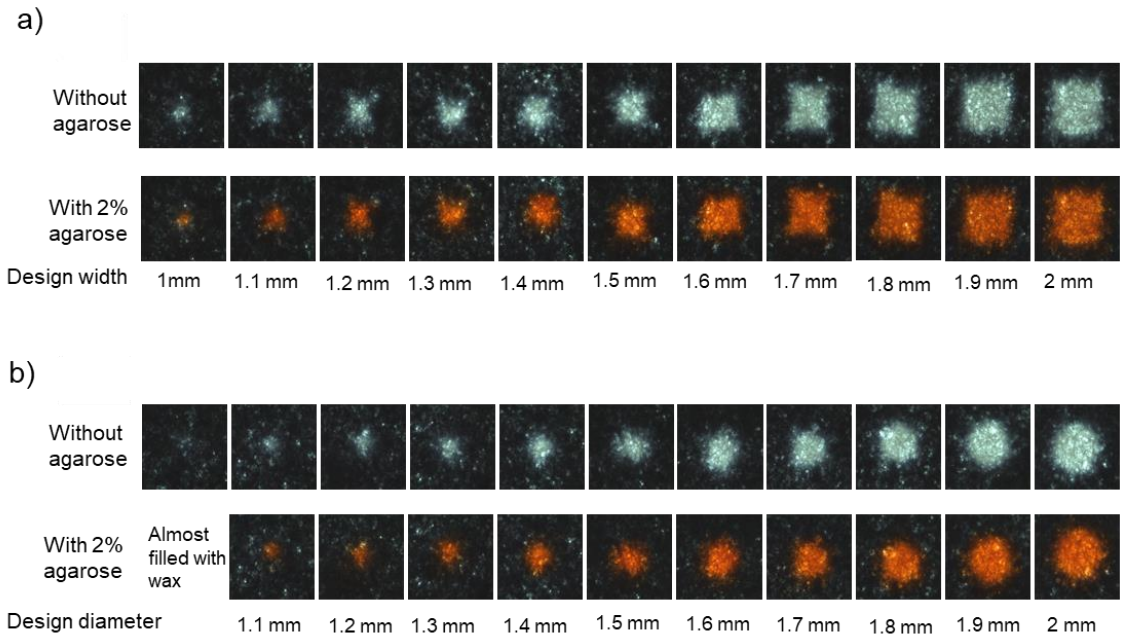

Figure S.3 Characterization of resolution for hydrogel integration into the wax-patterned paper. a) Square patterns with different sizes before and after filling with 2% agarose b) Circular patterns with different sizes before and after filling with 2% agarose.

Drying and rehydration of agarose in chromatography paper

Cross section images of 2% agarose loaded into wax-patterned paper before and after drying overnight and rehydration using 1X TAE buffer are demonstrated in figure S.4. From images, no significant difference is detectable between hydrated and rehydrated agarose in paper.

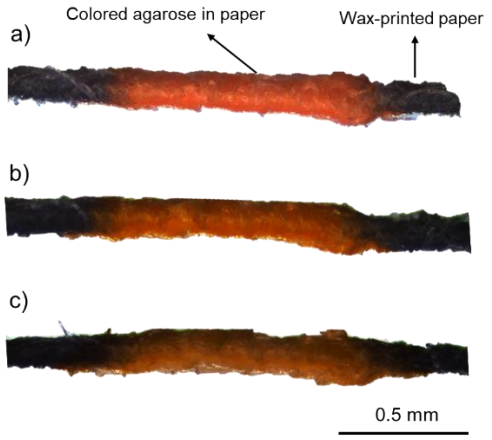

Figure S.4 Cross-sectional view of the agarose loaded wax patterned paper. a) After filling with 2% agarose and removing the excess amount of that from the surface b) After drying agarose in the paper over-night c) After rehydration of the agarose.

Figure S.5 presents SEM images of wax-patterned paper before and after filling with agarose. However, unlike the PCL membrane, dried agarose in paper was not detectable and looked like agarose has been absorbed by the fibers of paper.

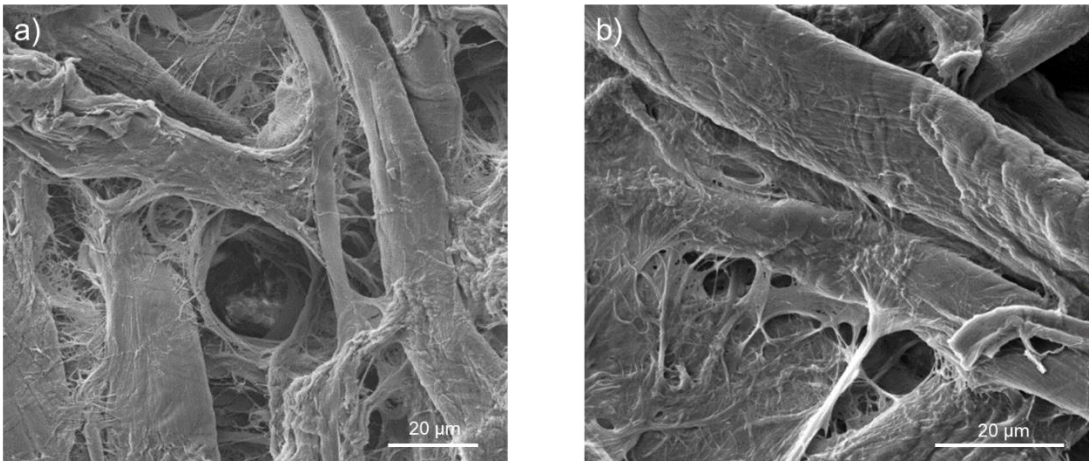

Figure S.5 SEM images of 1chr chromatography paper. a) Chromatography paper b) Paper loaded with 2% agarose.

Evaluation of the sealing of the hydrogel by transport of colorimetric dye

A device containing two cross channels was fabricated using xurography method (figure S.6a). First, a circular pattern with 2 mm diameter was wax printed and baked. Then, a 2 mm wide and 10 mm long channel was cut out of double-sided Kapton tape using a cutting plotter. Kapton tape

showed good adhesion to the wax printed paper. The channel layer was attached to the back of the paper below the circular part. Another channel layer with the same dimensions was attached to the top of the paper, perpendicular to the bottom channel. To increase the thickness of the agarose layer, more wax-patterned paper with circular openings were stacked by folding the wax paper with multiple openings exactly on top of each other. Next, circular openings were filled with 2% agarose from both sides of the paper layer. Then, the device was sealed from the bottom and top using hydrophilic adhesive (93049-AR) containing inlets and outlets for the channels. All the layers were aligned one after the other using alignment marks. Finally, the device passed through a laminator.

To evaluate the barrier efficiency of agarose loaded paper, transport of methylene blue through hydrated agarose was studied. In order to do that, immediately after filling the openings with agarose and fabrication of the device, the top channel was filled with 1X TAE buffer, and the bottom channel was filled with methylene blue solution. Figure S.6b shows the diffusion of methylene blue through agarose loaded paper to the other channel. Figure S.6c compares the changing of color intensity of circular agarose region over time for different number of gel layers. By increasing the number of agarose loaded paper layers diffusion rate was decreasing, however, compared to PCL membrane methylene blue was diffusing much faster to the top channel and agarose in paper was not able to withstand saturation over a long duration of time. This could happen because paper could not maintain the agarose structure compared to electrospun PCL membrane. This was confirmed by SEM images as well.

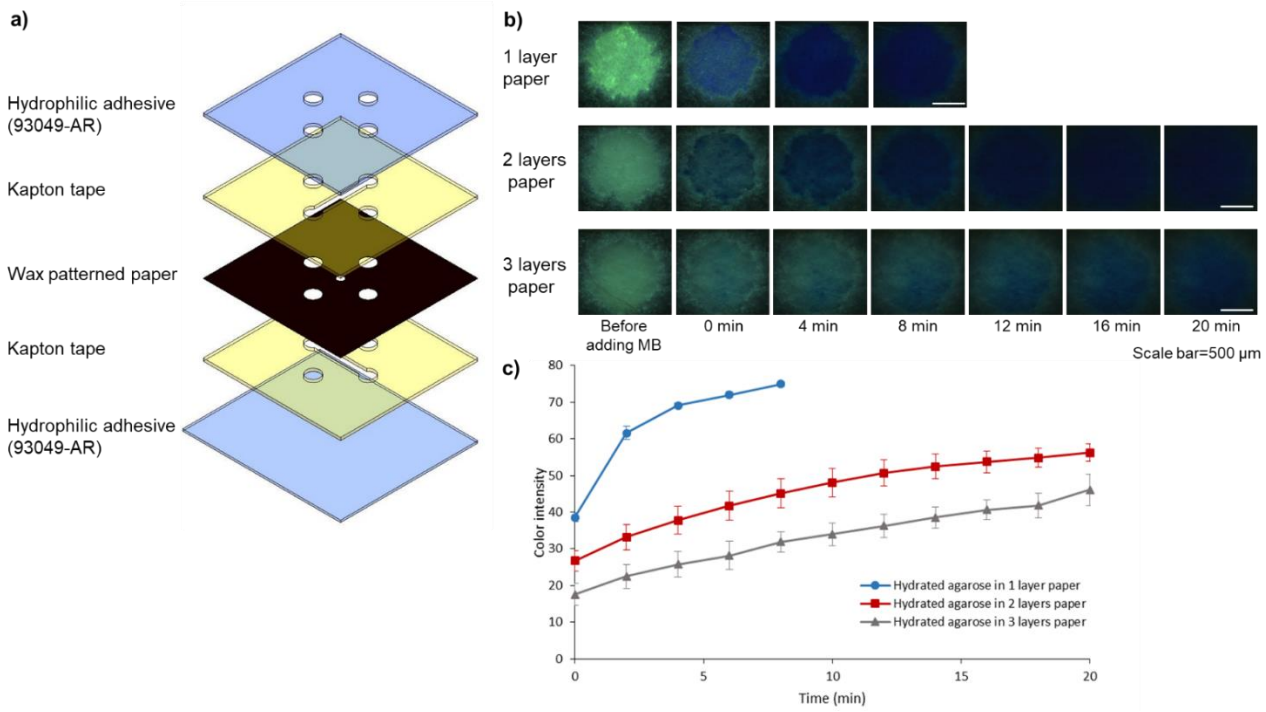

Figure S.6 Diffusion of methylene blue through agarose loaded wax-patterned paper. a) Configuration and layers of the device for study the transport of methylene blue b) Diffusion of methylene blue through hydrated 2% agarose gel in 1, 2 and 3 layers of paper c) Comparison of the methylene blue diffusion between 1, 2 and 3 layers of agarose loaded paper over time.

Evaluation of the sealing of the hydrogel in PCL membrane after multiple drying and rehydration

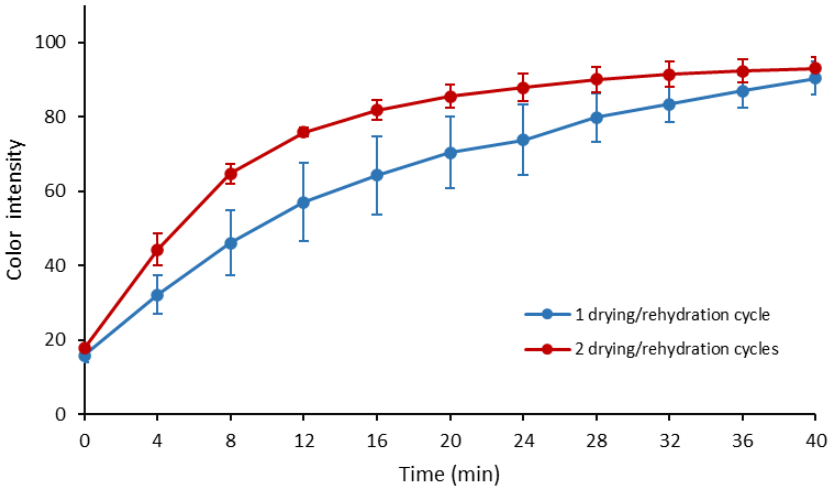

Figure S.7 Comparison of methylene blue diffusion between one and two cycles of drying and rehydration of agarose embedded in two layers of PCL membrane.

Evaluation of the sealing of the hydrogel embedded PCL membrane under pressure

In order to test the robustness of the agarose loaded PCL membrane in the presence of imposed flow, the transmembrane pressure for different number of the membrane layers was measured. The same cross channel device was used here as well. A syringe pump with a 10 mL syringe was connected via Tygon® tubing to a pressure transducer (OMEGA, PXM409-001BGUSBH) connected to the inlet of bottom channel of the cross channel device. The outlet of the bottom channel was completely closed with a tape. The top channel with open reservoirs was filled with TAE buffer. Methylene blue was pumped at a rate of 200 µl/min. The pressure was read to the maximum value after which it started to drop. The maximum obtained pressure versus number of gel layers is plotted in figure S.8.

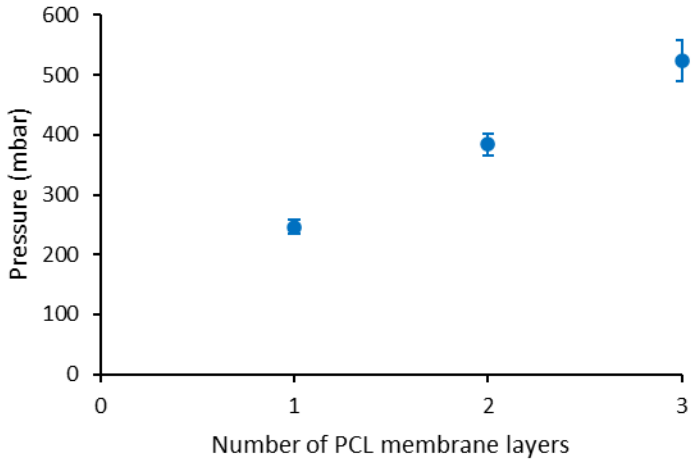

Figure 0.8 Transmembrane pressure for different number of agarose loaded membrane layers

3 Chapter 3 Isoelectric trapping and discrimination of histones from plasma in a microfluidic device using dehydrated isoelectric gate

Full Citation: Shahriari S, Damodara S, Selvaganapathy PR. Isoelectric trapping and discrimination of histones from plasma in a microfluidic device using dehydrated isoelectric gate. Microchimica Acta. 2024 Mar;191(3):131.

Isoelectric trapping and discrimination of histones from plasma in a microfluidic device using dehydrated isoelectric gate

*Shadi Shahriari[1], Sreekant Damodara[1], and P. Ravi Selvaganapathy[1,2] **

[1] *Department of Mechanical Engineering, McMaster University, Hamilton, ON, Canada*

[2] *School of Biomedical Engineering, McMaster University, Hamilton, ON, Canada*

** Corresponding author. E-mail address: selvaga@mcmaster.ca*

Abstract

Histones are basic proteins with isoelectric point around 11. It has been shown that the level of plasma circulating histones increases significantly during sepsis and circulating free histones are associated with sepsis severity and mortality. It was found that median plasma total free histone concentration of sepsis ICU non-survivors is higher compared to survivors. Therefore, histone concentration can serve as a prognostic indicator and there is a need for a simple, low-cost, and rapid method for measuring histone levels. In this work, we have developed a microfluidic device containing an isoelectric membrane made of dehydrated agarose gel of a specific pH embedded in a porous membrane for isoelectric trapping of histones rapidly. Although isoelectric gates have been used for trapping proteins before, they have to be introduced at the time of experiment. Here we show that isoelectric gates formed by gels loaded in a scaffold can be integrated directly into the fabrication process flow, dehydrated for storage, and rehydrated during experiment and still function effectively to achieve isoelectric trapping. A low-cost and rapid microfabrication technique, xurography, was used for agarose integration and device fabrication. The integrated device was tested with samples containing buffered histone, histone in the presence of high concentration bovine serum albumin (BSA), and histone spiked in blood plasma. The results show

that the device can be used to distinguish between survivors and non-survivors of sepsis in less than 10 minutes, making it suitable as a point of care device for sepsis prognosis.

Keywords: Isoelectric trapping, Histones, Sepsis, Agarose gate, Microfluidics, Xurography, Fluorescence detection

3.1 Introduction

Histones are basic, intra-nuclear proteins that support the structure of chromatin [1,2]. Chromatin is made of nucleosomes. A nucleosome consists of two copies of histones H2A, H2B, H3 and H4 and a 146 bp DNA which is wrapped around histones [2,3]. Histones have N-terminal tail rich in lysine and arginine, which forms the basic nature of the histone proteins [4]. Histones have an isoelectric point close to 11 and a molecular weight of 10−22 kDa depending on the fraction [5]. Histones can be released into the blood circulation during apoptosis, necrosis, and NETosis [2,4,6]. Histones can also act as damage-associated molecular pattern (DAMP) molecules and increase inflammation and mediates organ injury [4,7,8]. These extracellular histones, especially histones H3 and H4 are toxic towards host cells and cause endothelial dysfunction and may ultimately lead to organ failure during sepsis [2,7,9]. Sepsis is life-threatening organ dysfunction caused by a dysregulated host response to infection [10]. Sepsis is the main cause of death from infection. There are about 20 millions sepsis cases per year with approximately 26% mortality rate [11]. There is a 7.6 % decrease in chance of survival for each hour delay till the treatment is initiated [12].

Recently, there has been an ongoing emphasis on identifying novel prognostic biomarkers for sepsis to achieve a better health care plan for septic patients. Extracellular histones have been identified as prognostic biomarkers for sepsis and other inflammatory diseases. Studies have shown that high concentrations of circulating histones are considerably associated with sepsis

severity and mortality and there is a direct correlation between circulating histone level (either total or subtypes) and sepsis severity [2,4,13–19]. Extracellular histones have not been detected in healthy donors or detected in very low concentrations [2,13]. The focus of some studies has been on introducing a specific histone subtype such as histone H3 and H4 in ICU sepsis patients as prognosis biomarker [2,17]. In another group of studies, the relation between total free histone level in plasma and mortality has been reported. Cheng et al. showed that total circulating histone level was higher in septic patients who died within 28 days of ICU admission (32.7 μg/mL) compared to patients who survived (20.1 μg/mL) ($P < 0.0001$). Total circulating histone concentration for healthy donors was much less (1.3 μg/mL) [13]. Therefore, circulating histone can be a prognostic biomarker for sepsis and enable physicians to identify patients require a more aggressive care plan. Thus, there is a need for a rapid and convenient method for measuring histone levels.

Semiquantitative western blot (immunoblot) analysis and enzyme-linked immunosorbent assay (ELISA) are two major methods currently available for analysis of histone levels [3,7,16,18]. There are some limitations associated with semiquantitative analysis such as differences in reproducibility and variable cross-reactivity [16]. Also, with immunoblot methods, free circulating histones, histones bound to DNA, or histones that are part of a nucleosome can not be distinguished. Likewise, ELISAs have been developed for quantification some specific histone subtypes. Polyclonal antibodies against histones are usually used in these assays, so, it is not likely that these antibodies only detect free histones [3]. Also, as these assays are specific to only exact histone type, the total level is usually estimated by theoretical molecular ratio [13,20,21]. Roche Cell Death Detection ELISAPLUS has been frequently employed for histone level measurement. This assay incorporates a monoclonal anti-histone antibody as the catching antibody along with a

monoclonal anti-DNA antibody for the detection process. Therefore, it detects the amount of cleaved DNA/histone complexes [3]. Furthermore, ELISA assays are expensive and require multiple steps and 3-4 hours for each run. Thus, to our knowledge there is no direct method that can detect and measure total circulating free histones. Therefore, an alternative method can be beneficial for development a device for distinguishing between total circulating histones concentration of survivors (20.1 μg/mL) and non survivors (32.7 μg/mL) of sepsis.

One method used for protein separation is isoelectric trapping (IET) which is categorized under isoelectric focusing technique for separation of proteins based on their isoelectric point (pI). In IET, a step wise pH gradient is produced using a series of buffering membranes, instead of a continuous pH gradient. Using discrete pH gates allows targeted separation of proteins and it offers some advantages such as pH inherent consistency [22]. IET has been performed using different types of membranes such as PVA, agarose, and poly(acryloylaminoethoxyethanol) [23]. Microscale IET devices for isolation of molecular species have been introduced [22,24]. This type of microfluidic chips with integrated isoelectric gates (pH-specific membranes) can be used to isolate and trap analyte of interest from other species in the sample for different applications. They used photopolymerization for making the pH specific membranes. In-situ photopolymerization is the main method for integrating the pH specific gates into microfluidic chips. pH specific membranes were made with Immobilines which are nonamphoteric buffering compounds that are integrated into the polyacrylamide matrix backbone during polymerization. Photopolymerization increases the cost and complexity of the device, as additional post processing steps are needed to incorporate pH specific membrane and rinse the unpolymerized solution from the device [24]. In a recent study, agarose which is much cheaper than Immobilines, has been used for making the isoelectric membranes [25]. Membranes with specific pHs were fabricated from agarose made in

different buffers with certain pHs, depending on the targeted protein isoelectric point. In another study, protein C in blood plasma was detected by combining agarose isoelectric gates with barium-immobilized metal affinity trapping [26]. In these studies, agarose solution was loaded directly in the desired regions of the microfluidic device at the time of experiment. In this method, polymerization and post polymerization steps were avoided. However, this method is not suitable for a point of care device where long-term storage of agarose in the device is needed. Alternatively, a method for integrating hydrogels like agarose into the microfluidic devices was introduced in which porous membranes were used as scaffolds for maintaining the dehydrated structure of the gels inside the microfluidic devices and rehydrating them at the time of detection [27]. It has been shown that porous membrane enables drying and rehydration of the gels without the loss of shape or leakage. In this technique, hydrogels are introduced in the devices during the fabrication process without any post-processing step. This hydrogel integration method was employed to demonstrate gel electrophoretic concentration of DNA in rehydrated agarose embedded in electrospun polycaprolactone (PCL) membrane. However, protein concentration and separation in dehydrated/rehydrated gels embedded in membranes has not been demonstrated before. Xurography has been used for both gel integration and device fabrication. Xurography is a low cost and simple technique for fabrication of microfluidics out of adhesive and polymer films [28,29].

Here we fabricate isoelectric traps in a xurographically made microfluidic device with dehydrated agarose pH-specific membrane for separating and discriminating histones for differentiating between survivors and non-survivors of sepsis. Since histones are very basic proteins with an isoelectric point around 11, a single gate device can be used to separate them from other proteins in the plasma. We show that dehydrated and rehydrated agarose membrane gate still function

effectively to achieve isoelectric trapping. To the best of our knowledge, there is no available method for discriminating total free histones without using a histone specific tag while operating rapidly with a low voltage. Here, we demonstrate the separation and accumulation of histones tagged with a non-specific fluorescent dye in a dehydrated agarose membrane with pH 11, using 30 Volts in less than 10 minutes. This device can be developed further as a point of care device for measurement of histones as a prognostic biomarker in blood plasma of sepsis patients.

3.2 Device design and working principle

The device is designed to discriminate the total circulating histone in plasma of sepsis patients for a quick differentiation between survivors (~ 20 μg/mL) and non-survivors (~ 33 μg/mL). This selective trapping of histones was achieved by isolating them in a pH specific agarose membrane matching the isoelectric point of histones. The pH gate was a dehydrated agarose gel with pH 11 loaded in PTFE membrane. As mentioned, porous membranes are beneficial for integrating the hydrogels during the fabrication process in the device and maintaining dehydrated hydrogels structure and rehydrating when it is needed. The device consists of 6 layers of adhesives and films which were cut to form two channels positioned perpendicular to each other with the agarose loaded membrane as the isoelectric gate in between (figure 3.1). Porous PTFE membrane with 36 μm thickness was used as the support for agarose loading. To get a reasonably thick enough agarose layer gate, four layers of PTFE membrane were stacked and sandwiched between two double sided adhesives, Kapton tape and a silicone-based adhesive (AR-94119), with openings for loading agarose in the PTFE membranes. A wide variety of adhesive tapes were tested for sample channel layers. The combination of AR-94119 tape (silicone-based double-sided adhesive) and hydrophilic PET, proved to have the best performance for this application as they both demonstrated low auto-fluorescence with minimal non-specific binding of dye or conjugated

proteins to their surfaces. Agarose solution (3% w/v) made in CAPS buffer with pH 11 was loaded in the open circular region of the PTFE membrane. Top channel which was cut out of PVC film was attached to the gel containing layer from the Kapton tape side and it was sealed with a hydrophilic one-sided adhesive (AR-93049) with the inlets. The bottom channel cut from Kapton tape was attached to the gel layer from silicone-based adhesive (AR-94119) side. After positioning the copper electrodes in the two ends of this channel and one end for the top channel, it was sealed with a hydrophilic PET film (3M-9984). The cross-section view of the agarose loaded membrane section and other layers of the device is presented in figure 3.1a. At the time of experiments the top channel which was connected to cathode was filled with CAPS buffer with the same pH of the agarose membrane (pH 11). After agarose rehydration, the bottom channel was filled with the sample containing histones. The positive electrodes were positioned in the reservoirs of the sample channel.

The device was designed to exclude most of the plasma proteins from entering the pH specific membrane (pH 11) and trap histones in the isoelectric membrane. Tris-HCl buffer with pH 8 was used as the sample and dye dilution buffer. This pH value is close to blood plasma pH (~7.4). Therefore, pH 8 was a cut-off point for proteins charge determination and their movement direction in sample channel. All the proteins were labeled with a non-specific fluorescent dye. Once electric field is applied, proteins with an isoelectric point less than pH of the sample gain negative charge and move towards the positive electrodes in the reservoirs of the sample channel, moving away from the gate region. While proteins with isoelectric points higher than sample buffer, including histones, obtain positive charge and migrate towards cathode in the top channel. The majority of the highly abundant proteins in blood have pI of less than 8. For instance, the 10 most abundant plasma proteins which make up about 90% of the total protein concentration [30] have following

isoelectric points (Albumin (pI; 5.2), IgG (pI; 7.5-7.8), Transferrin (pI; 5.6), Fibrinogen (pI; 5.6) [31], IgA (pI; 4.5-6.8) [32], alpha2-macroglobulin (pI; 5-5.2) [33], IgM (pI; 5.6-6.7) [34], Alpha1-Antitrypsin (pI; 5.4) [31], Complement C3 (pI; 5.7) [35], Haptoglobin (pI; 5.5-6.2) [36]). Therefore, most of proteins migrate towards the electrodes and others with pI higher than 8 which are much less abundant, move towards the gate. Therefore, a large fraction of proteins is excluded. The proteins with pI larger than 8, depending on their pI value, either pass through the gate or accumulate in the membrane. The rate of migration of the proteins through the agarose gel gate is dependent on the difference between the pH of the gate and their pI. Once histones enter the agarose gel membrane with pH 11, they have very little charge, slow down, and accumulate. Therefore, histones can be quantified based on the fluorescent intensity in the agarose membrane captured by a camera. Figure 3.1b demonstrates the schematic of the device with its dimensions, its working principle, and interaction of different proteins.

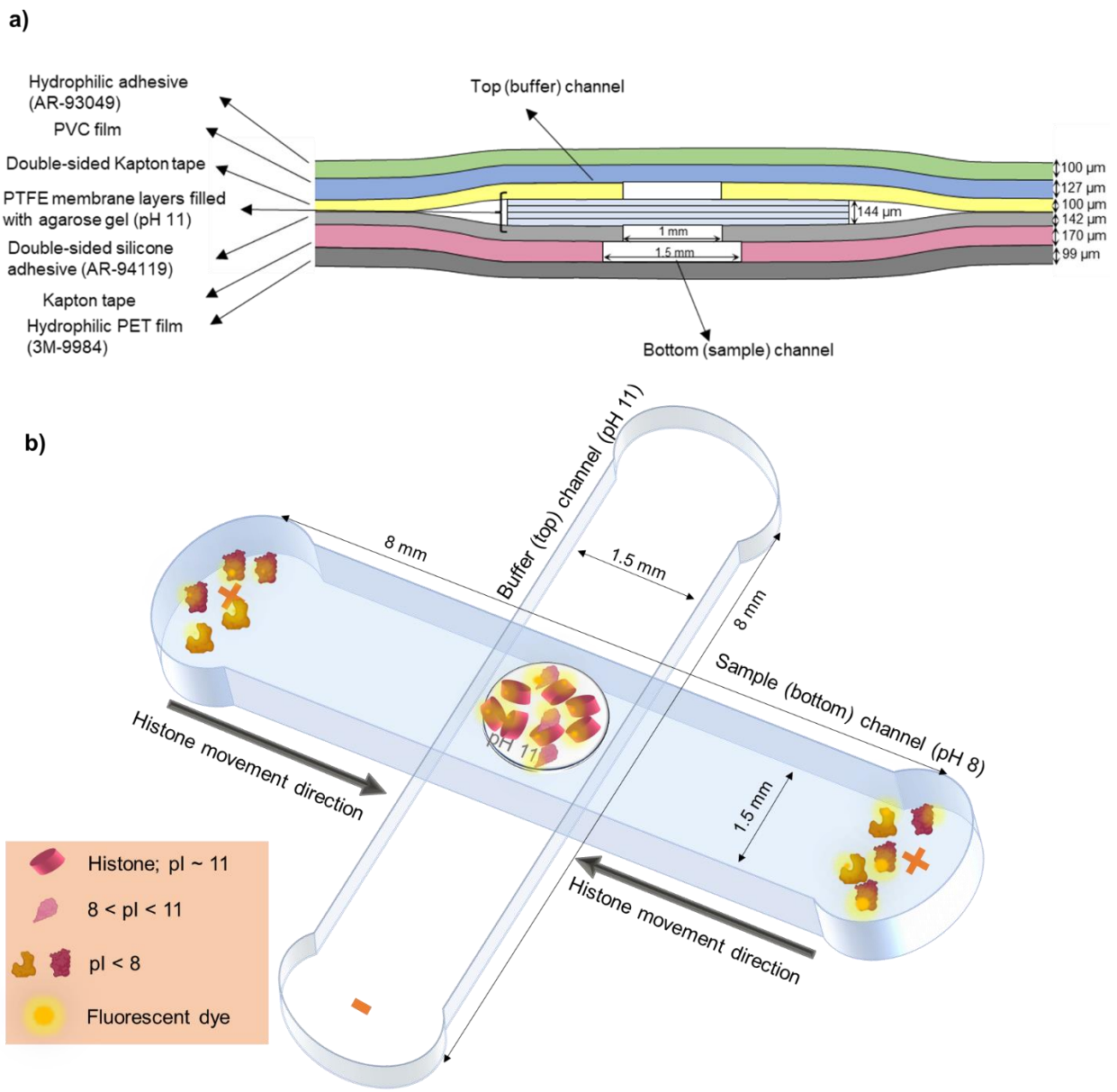

Figure 3.1 Illustration of a) Cross section of the device and different layers. b) Schematic of the complete device and its working principle.

3.3 Materials and methods

3.3.1 Materials

Histone from calf thymus type II-A, histone H3.1 human, and bovine serum albumin (BSA) were obtained from Millipore Sigma. Citrated pooled human plasma was obtained from Innovative research. Qubit protein assay kit and Tris- HCl (1M solution, pH 8.0, molecular biology grade)

was obtained from Thermo Fisher Scientific. CAPS buffer (0.2 M, pH 11) and (0.5 M, pH 11) were acquired from Bioworld and Thermo Fisher Scientific respectively. Agarose was purchased from BioShop Canada Inc, Burlington, ON. PTFE unlaminated membrane (hydrophilic with 1 micron pore size) was purchased from Sterlitech, Auburn, WA, USA. Surfactant free and hydrophilic polyester film (3M-9984, 99 μm thickness) was from 3M™, Maplewood, MN. A double-sided silicone-based pressure sensitive adhesive (ARcare-94119, 142 μm thickness) and one-sided hydrophilic acrylic adhesive tape (ARflow-93049, 100 μm thickness) were obtained from adhesive research, Glen Rock, PA. Polyvinyl chloride (PVC) film (Clear-Lay, 127 μm thickness) was from Grafix, Maple Heights, OH. Polyimide (Kapton) tape (double-sided and double Liner, 100 μm) was from Caplinq. Copper-polyimide composite foil (9 μm-Cu and 12 μm-PI thickness, Pyralux) was acquired from DuPont, USA.

3.3.2 Fabrication

The microfluidic device consists of two cross channels with an agarose loaded membrane in between. The fabrication process and final device are demonstrated in figure 3.2. Xurography was used for both gel integration and device fabrication. Cutter plotter (FC8600, Graphtec America, US) with CB09UB blade was used for cutting the layers. The device consists of six layers of different pressure sensitive adhesives and polymer films. First two layers of double-sided adhesives with 1 mm diameter circular openings for gel loading were cut out of Kapton tape (double sided polyimide tape with silicone adhesive) and AR-94119 (silicon based double sided adhesive). Then, four layers of PTFE membrane (36 μm thick each layer) were cut to squares with 2.5 mm width and they were stacked, sandwiched, and laminated between these two layers of double-sided tapes (figure 3.2a and b). An alignment tool with four pins was used for alignment of the layers. Then a 3% agarose made in 0.5 M CAPS buffer was heated in a microwave until the

solution became clear. One droplet of agarose solution was added to the open regions of the PTFE membranes (figure 3.2c). After wicking the agarose solution to the membrane and its gelation, the excess amount was wiped off from the surface of the sandwiched layer. This process was done from both sides of the sandwiched layer for at least two times to make sure that the membrane layer is completely filled with the agarose. Top channel with 1.5 mm width and 8 mm height was cut out 127 μm thick PVC film and it was aligned and attached to the sandwiched layer with agarose loaded PTFE membrane from the Kapton tape side. The bottom channel with the same dimension was cut out of double sided Kapton tape with one liner removed (170 μm thick) and it was adhered to the sandwiched layer from the AR-94119 double-sided adhesive side. The device was sealed from the top with a hydrophilic tape (AR-93049) containing the openings (1.2 mm radius) for inlets of the channels. The electrodes with 1.25 mm width were cut from copper film. They were positioned in bottom channel reservoirs and one of the top channel reservoirs, between the bottom channel and a layer of hydrophilic polyester film (3M-9984) for sealing the bottom channel. The layers of the device and their arrangement is shown in figure 3.2d. After assembly and alignment of all the layers, the device was laminated to get a leak free sealing. The schematic of the final device is presented in figure 3.2e.

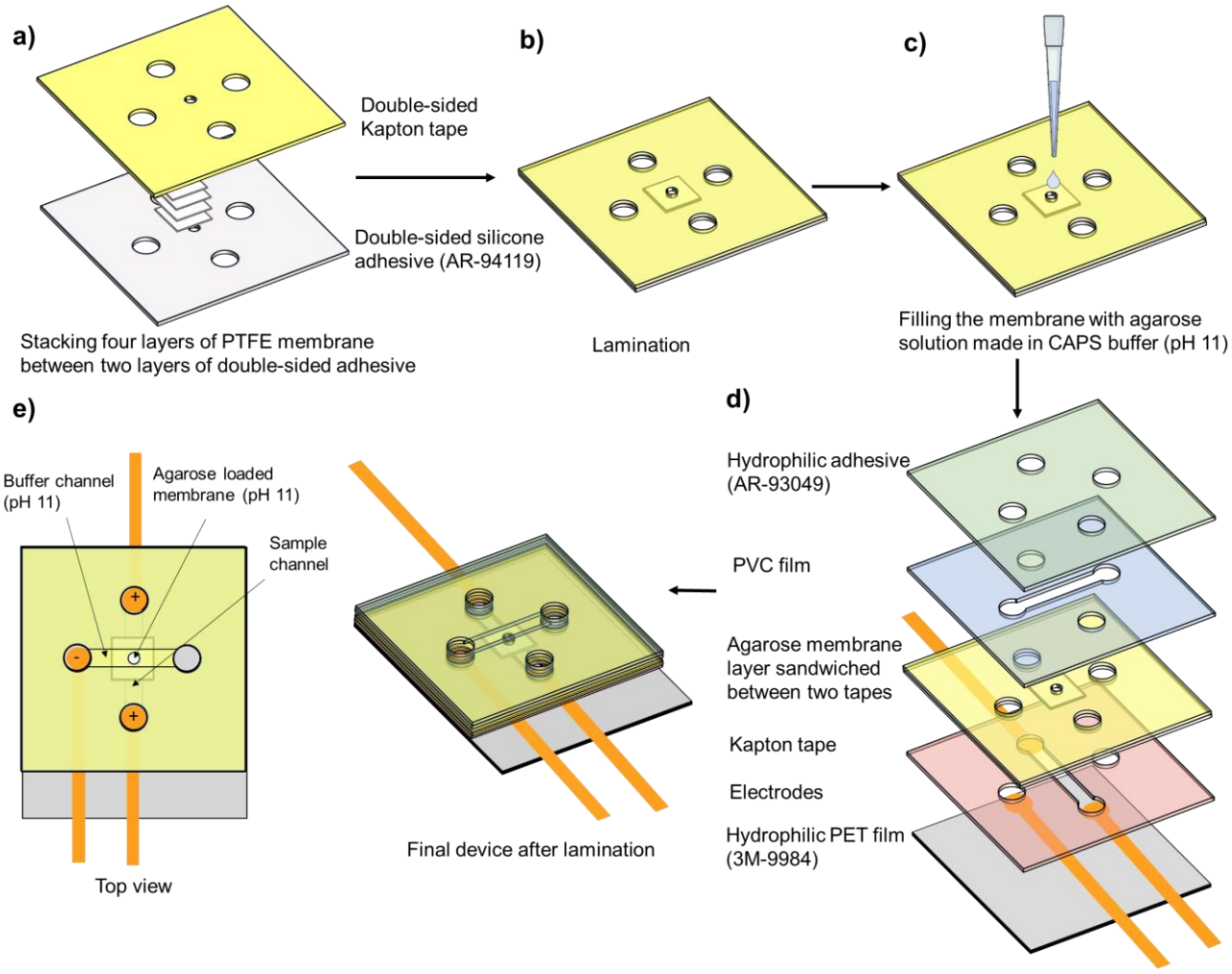

Figure 3.2 Fabrication steps of the device. a) Stacking and sandwiching four layers of PTFE membrane between Kapton tape and silicone-based adhesive. b) Alignment and lamination of the sandwiched layer. c) Loading agarose gel (pH 11) in the membranes. d) Layer by layer assembly and alignment of the other cut layers of the device. e) Top and side view of the final device after lamination.

3.3.3 Experimental method

Histone from calf thymus and human histone H3.1 were used to test the device for accumulating histones. A 2 mg/mL histone from calf thymus sample was prepared by dissolving the lyophilized histone powder in Milli-Q water. Then, the sample was mixed with Qubit protein dye by following the protocol for Qubit Protein Assay. The dye was diluted 200 times in 50 mM Tris-HCl pH 8 buffer and was mixed with sample with 1:9 (sample: diluted dye) volume ratio. The mixture was allowed to intercalate for 15 minutes at room temperature in a dark place before pipetting into the

device. This sample was used for histone concentration in dehydrated/hydrated agarose study. Human histone H3.1 was used for testing the device with histone in buffer, histone in the presence of BSA, and human plasma spiked with histone samples. Histone in Tris-HCl buffer sample was prepared by diluting the 1 mg/mL stock histone H3.1 solution to 20 and 33 µg/mL and mix that with 200 times diluted dye in 50 mM Tris-HCl buffer pH 8 with the 1:9 volume ratio. The second type of sample (histone mixed with BSA) was made similarly by adding 40 mg/mL BSA (equivalent to average HSA concentration in plasma) to histone sample. The final sample composed of 40 mg/mL BSA and 20 and 33 µg/mL histone H3.1 in Tris-HCl buffer. The dye dilution ratio was decreased to 50 times as more protein was present in this sample. The sample and diluted dye were mixed with the same ratio. The third sample type (histone spiked in plasma) was prepared by spiking histone H3.1 in plasma from healthy donor to get final concentrations of 20 and 33 µg/mL. The dye was diluted 25 times, as the total plasma protein concentration is about 60-80 mg/mL [37] (almost doubled the BSA concentration in previous sample). Similarly, sample and dye were mixed for 15 minutes before the experiment. For each device, 10 µl of sample was pipetted into the sample channel.

3.3.4 Experimental setup

The device was placed on a fluorescence microscope (Nikon Eclipse TE2000-S). The excitation window of 455 ± 25 nm and an emission window of 600 ± 30 nm, matching the excitation and emission of Qubit dye was used. X-Cite 120LED was used as the light source for the microscope with 30% of the maximum exposure. The microscope was connected to a raspberry pi camera and was programmed to switch on the light source 1 second before image capture and capture images every 30 seconds with an exposure time of 4 seconds and an ISO of 400. During the imaging the device was covered with a black cloth to reduce background light interference from outside. The

microscope was centered on the 0.5 mm radius agarose gate of the device. The device electrodes were connected to a power supply (Keithley 2410). First, the top channel was filled with 10 µl of 0.2 M CAPS buffer, pH 11. About two minutes was needed for rehydration of agarose loaded in the membrane. Once, agarose loaded membrane turned to a clear layer due to the absorbance of buffer (PTFE membrane is optically clear when is wet), the bottom channel was filled with sample. Then, 30 V was applied between the channels. The electric field was applied when the first image was captured. Images were taken every 30 seconds.

3.3.5 Image analysis

The images captured by raspberry pi camera were analyzed using ImageJ to characterize the fluorescence intensity. The original images were transferred to a grey scale format. A region of interest (ROI) was placed around the agarose gel membrane. The ROI was a slightly bigger circle enclosing the original gate circle to cover all the accumulation in case of any misalignment of the adhesive layers. The intensity was normalized by subtracting the obtained grey scale value for each image from the starting grey value (background). The background value was selected as the average value of the ROI for at least fifteen devices at the time point when the agarose gel was rehydrated, and a clear gel section was obtained.

3.4 Results and discussion

3.4.1 Histone trapping in hydrated and dehydrated/rehydrated IET membrane

In order to demonstrate that histones can be efficiently accumulated in the IET loaded membrane even after dehydrating and rehydrating of the agarose, a series of experiment with three states of agarose gel was performed. Devices containing agarose integrated on the same day, 1 day before, and 10 days before were tested. For each experiment a new device was used as all the devices are made for single use. A 2 mg/mL calf thymus histone in 50 mM Tris-HCl buffer, pH 8 sample

prepared as mentioned before was used in these experiments. For all the agarose states, the experimental method was the same and only difference was the storage time of the agarose in the device.

At the time of experiment, for all three groups of devices, at least about 2 minutes was needed for agarose rehydration (the devices made on the same day were rehydrated faster as the agarose may not have been completely dried compared to the other two cases). This rehydration was performed by loading the top channel with CAPS buffer with the same pH as the agarose isoelectric gate (pH 11). Agarose membrane was considered rehydrated when it turned clear as the result of absorbing buffer. An image was taken from the agarose membrane after the rehydration (Figure 3.3a, first column). Then, bottom channel was filled with the 2 mg/mL histone sample tagged with fluorescent dye and electric field was applied between the channels. Upon applying electric field histones due to their positive charge in the sample solution with pH 8, start to migrate towards cathode and the agarose membrane. Once, they reach the agarose membrane with pH 11 which is close to their isoelectric point, they almost lose their charge, slow down, and get trapped. Images were taken from the agarose gate every 30 seconds. Figure 3.3a shows the change in fluorescence intensity in the membrane every 5 minutes over the duration of the experiment (15 minutes). At 0 minute, there is a slight fluorescence increase from filling the channel with sample and it starts to increase after applying the electric field (30 V) for all the three cases. Figure 3.3b demonstrates the change of fluorescent intensity by time for the three sets of devices with different storage time of agarose. During the first 10 minutes, for all three states the fluorescent intensity increases. However, there is a slight increase or decrease in the intensity after that as the red channel of the RGB images was saturated in the areas of concentration, and no further increase could be measured in the greyscale intensity of the images. Therefore, the fluorescent intensity after 10 minutes

applying voltage was selected as the point for measurement. Figure 3.3c shows the comparison between the final histone accumulation for these three states of agarose. It is shown that for the same day made device, the fluorescent intensity is higher compared to the other two cases at all the points during the experiment. However, there is not a significant difference between 1 day and 10 days old device. Although the device made on the same day could trap and accumulate more of the histones, the other two types of devices with dehydrated and rehydrated agarose still demonstrated good trapping and the agarose membrane was still efficient for trapping proteins. Also, as the 1 and 10 days old devices showed very similar results and there was no sign of agarose deterioration over time, the device with the current agarose integration method can be potentially stored for an even longer time.

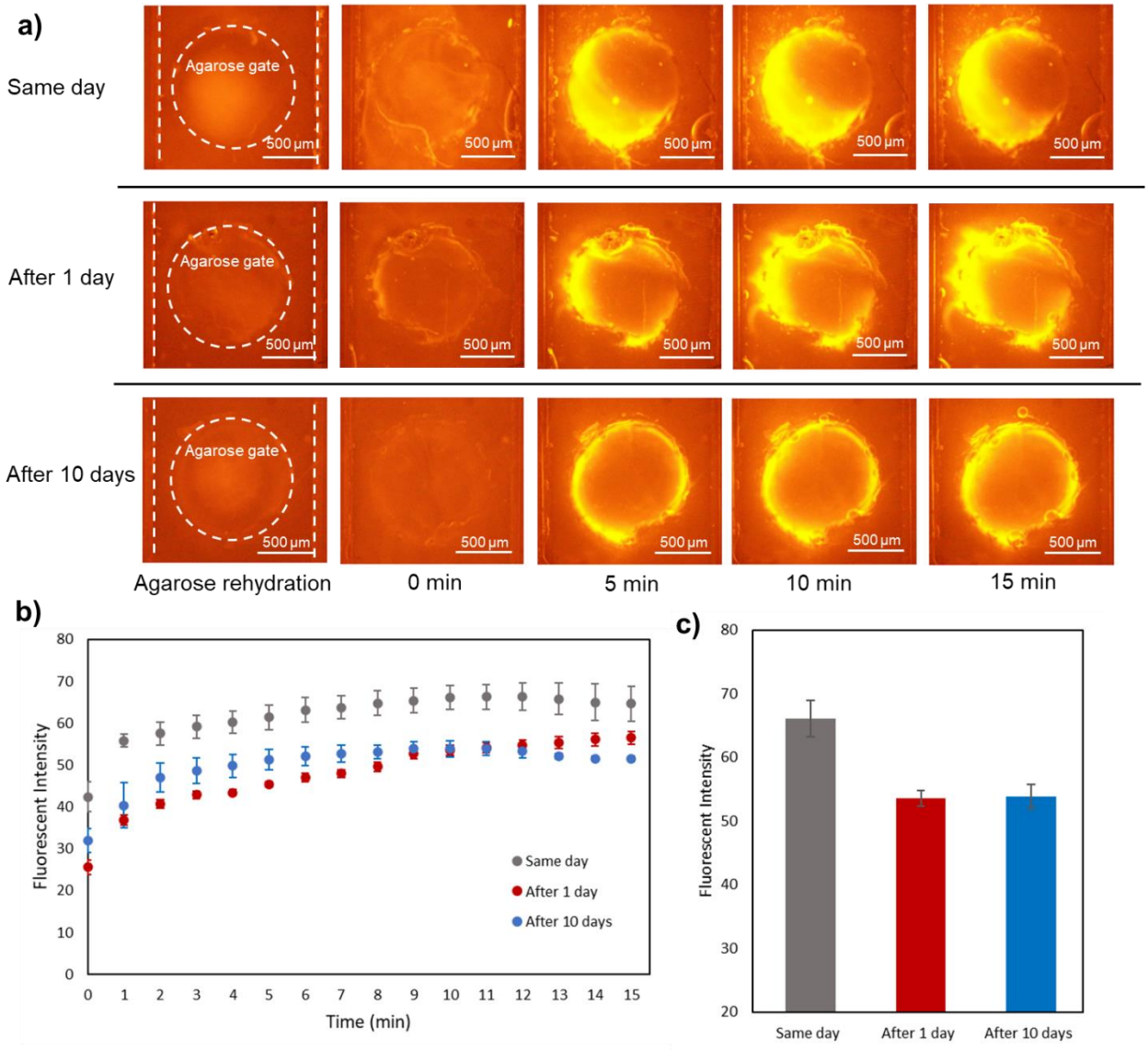

Figure 3.3 Trapping of histones in hydrated and dehydrated/rehydrated agarose membrane. a) Images captured from pH 11 agarose membrane every 5 minutes. b) Plot showing change in measured fluorescent intensity with time for each agarose state. c) Fluorescence intensity values at 10 minutes for the device made on the same day, 1 day and 10 days old (N=4).

3.4.2 Simulation of electric field distribution

To better understand the accumulation profile of histones in the IET membrane, the electric field distribution in the device was simulated using COMSOL Multiphysics in electric currents module. The geometry of the device was replicated, and the agarose loaded membrane was approximated by a cylinder with a radius of 0.5 mm. The simulation was run with the electrodes in the sample

channel set at 30 V, and the electrode in buffer channel set to ground potential. All the other channel surfaces were set to insulating boundary condition. The conductivity of 50 mM Tris-HCl, and 0.2 M CAPS was approximated to be 2 mS/cm [38] and 0.7 mS/cm [39] respectively. The simulation shows that the electric field gradient reaches its maximum at the intersection edge towards the cathode end side. The complete distribution is shown in figure 3.4. The electric field in the isoelectric gate was calculated to be ~ 2500 V m^{-1}. The sample channel had an electric field of ~ 1100 V m^{-1}. The higher electric field in the gel section where the mobility of the histones is the least while a lower electric field in the sample channel where the mobility is higher will improve the separation time. To better understand the concentration mechanism, the simulation results were compared with the experiments. For most of the experimental results a similar accumulation profile as the simulation (a non-symmetrical distribution) was obtained and the histones accumulated faster and more in the side of the circular region gate close to cathode. For example, in figure 3.3a, the asymmetry in fluorescent intensity at 10 minutes is because of the distribution of the electric field lines in the isoelectric agarose gate. Most of the histones are accumulated in the section of agarose gate close to cathode as the electric field is stronger in that part.

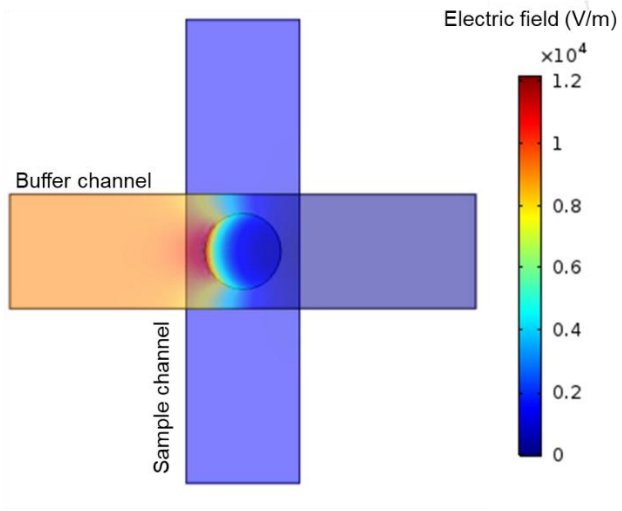

Figure 3.4 Distribution of electric field in the device.

3.4.3 Trapping of histones from a buffered sample

The ability of the device to trap lower concentration of histones in the physiological range in sepsis, was tested with samples containing 20 and 33 µg/mL histone H3.1 as the representative of all histone subtypes. Samples of histone H3.1 in 50 mM Tris-HCl pH 8 buffer with 0, 20, and 33 µg/mL concentration correlates to total free histone concentration in plasma of healthy persons, sepsis survivors, and non-survivors were made by following the protocol mentioned earlier. The experiments were performed with the devices made a day before with dehydrated agarose in 0.5 M CAPS buffer pH 11 loaded in PTFE membranes. As described earlier, CAPS buffer with pH 11 was introduced in the top channel for hydrogel rehydration. After about 2 minutes the sample was loaded in bottom channel and 30 Volt was applied between the channels. Based on the results in the previous section, 10 minutes was chosen as the final measurement point. Figure 3.5a demonstrates the images from agarose isoelectric membrane after agarose rehydration and at 0, 5, and 10 minutes after applying voltage for 0 and 33 µg/mL of histone sample. The average intensity at 10 minutes after applying voltage for each concentration after image analysis is shown in figure 3.5b. The control sample with the Qubit dye and no proteins in the solution had an intensity of 7.42 ± 0.96 after 10 minutes which is a very slight increase. Therefore, the Qubit dye with the

current dilution ratio did not cause any significant fluorescence. For all the samples, at 0 minute when the channel is filled with the sample there is only a slight intensity increase. For both 20 and 33 µg/mL of histone samples, they started to accumulate after applying electric field and fluorescent intensities increased by time. Here, as histone concentration is lower compared to previous section (figure 3.3), the fluorescent intensities after 10 minutes are smaller. A two-tailed t-test showed a p value of 0.06 between 20 and 33 µg/mL. Despite the low confidence with measuring buffered samples at 20 µg/mL compared with 33 µg/mL, the device provides a sufficient differentiation between 20 and 33 µg/mL of histones and blank sample ($p < 0.001$ and $p < 0.01$ respectively).

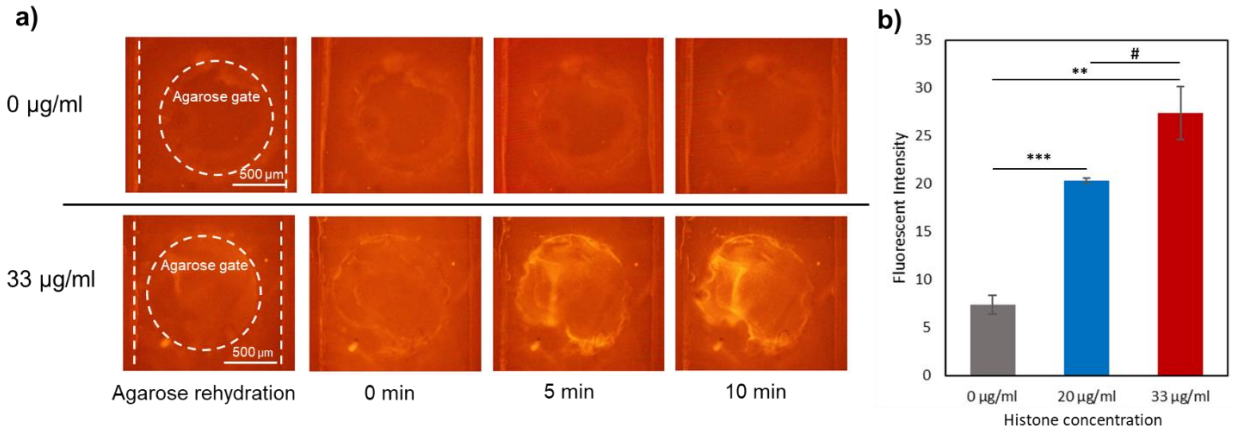

Figure 3.5 Trapping histones from buffer sample. a) Images captured every 5 minutes from agarose membrane. b) Fluorescence intensity values for each histone in buffer sample (N=3) Statistical significance for samples calculated by two-tailed t-test (** $p < 0.01$, * $p < 0.05$, # $p < 0.1$).

3.4.4 Trapping histones in the presence of high concentration of other background proteins (BSA)

The ability of the device for separation of histones in the presence of other proteins was tested. The sample was made by mixing 40 mg/mL of BSA with histone with different concentrations. BSA which has similar properties such as isoelectric point and weight to human serum albumin (HSA) was selected. Albumin is one of the major proteins of blood plasma with 35-50 mg/mL

concentration and isoelectric point ~ 5 [40]. Hence, BSA with concentration of 40 mg/mL was selected to represent albumin in plasma. Considering BSA isoelectric point and pH of the sample solution (pH 8), BSA gains negative charge, opposite of histone charge in the solution. Therefore, in the presence of electric field they migrate in different direction.

The device was prepared as previously described and 10 µl of the sample containing 40 mg/mL BSA and 0, 20, and 33 µg/mL of histone was added to sample channel followed by application of the electric field. Images are shown in figure 3.6a for both control sample (which contains only BSA) and BSA mixed with 33 µg/mL of histone at 0 and 6 minutes. When the bottom channel is filled with sample (0 minute), the channel and the gate show a high fluorescence due to the high concentration of BSA (40 mg/mL) for all the samples. Upon application of electric field, BSA due to its negative charge in pH 8 moves away from the gate towards the positive electrodes at the two ends of the sample channel, while histones migrate to the gate and get trapped. Similar to the buffered histone sample, electric field was applied for 10 minutes and change of fluorescent intensity in the membrane by time is shown in figure 3.6b. As it is presented in the plot, the difference between control sample and 20 and 33 µg/mL of histone sample is the most after around 6 minutes. Therefore, the average intensity at 6 minutes for samples with 0, 20, and 33 µg/mL of histone is plotted in figure 3.6c. As it is demonstrated in the images as well, at 6 minutes the fluorescence intensity is higher in the circular gate for 33 µg/mL sample compared to control sample. For control sample (0 µg/mL of histone) almost all the BSA migrated to electrodes and the membrane region got almost cleared from the BSA after 6 minutes applying electric field. However, there is still some background in the agarose gate which can be attributed to small amount of BSA which has not migrated away from the IET gate during the 10 minutes experiment or has been adsorbed on the surface of the device or due to the larger amount of the added dye.

This background fluorescent intensity level for control sample (40 mg/mL BSA in buffer) is much higher compared to that measured in the absence of any proteins in previous section. For 33 µg/mL histone mixed with BSA sample, histones were accumulated in the agarose gate with pH 11 and fluorescence intensity is higher. Also, at all concentrations of histone there is an increase in intensity compared to the respective measured intensities from only histone in previous section. This also can be due to the amount of BSA which is still in the vicinity of agarose isoelectric gate and less of histone being adsorbed on the surface of sample channel because of presence of high concentration of BSA. A two-tailed t-test gives $p < 0.01$ in differentiating any 2 samples in this device. This shows that the device can be used for differentiating between different concentrations of histones even in the presence of a high concentration albumin.

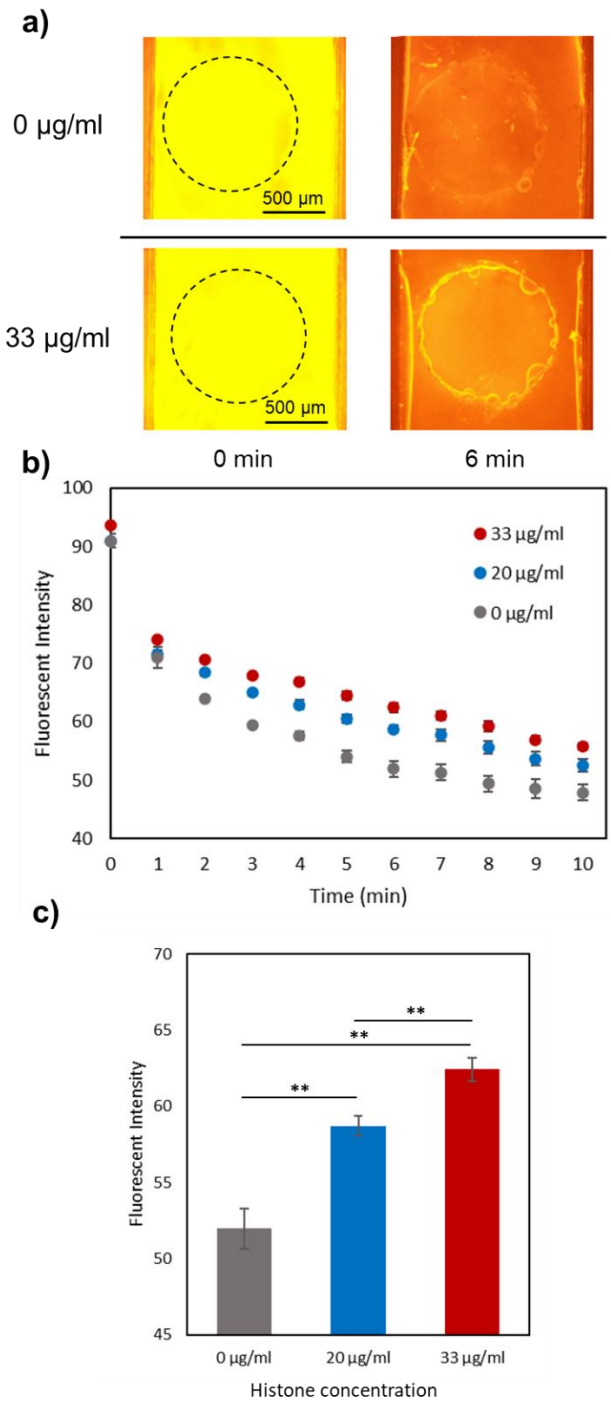

Figure 3.6 Trapping histones in the presence of 40 mg/mL BSA. a) Images captured at 0 minute (filling the sample channel) and after 6 minutes for samples containing 0 and 33 µg/mL of histone. b) Plot showing changes in measured fluorescent intensity with time for each sample after applying 30 V. c) Fluorescence intensity values for each concentration of histone in the sample containing BSA (N=3) Statistical significance for samples calculated by two-tailed t-test (** $p < 0.01$).

3.4.5 Histone quantification from human plasma samples

The device was used for quantification of defined quantities of histone that has been added to pooled human plasma to simulate the real patient sample under septic conditions. To prepare the samples similar protocol as previous section (histone mixed with BSA) was followed. Plasma was used instead of BSA in buffer and the amount of added dye was doubled as the total protein concentration in plasma can be up to 80 mg/mL. The experimental setup and condition were like before. Samples with 0, 10, 20, 33, and 45 µg/mL histones spiked in plasma were used. The experiment was repeated 3 times with a new device used in each repeat. The pH of the sample containing histone spiked in plasma mixed with dye diluted in Tris-HCl buffer measured to be 8. Upon applying electric field, the proteins with isoelectric point less than 8 that have a negative charge in plasma and migrate towards the positive electrodes in the reservoirs of sample channel, while the proteins with isoelectric point higher than 8, including histones, move towards cathode and they either accumulate in the vicinity of the gate or pass through the agarose gate (any protein with pI higher than 11 will pass through the gate). Images were taken every 30 seconds and images at 0 minute and 6 minutes for 0 and 33 µg/mL sample are shown in figure 3.7a. The intensity in the agarose membrane region is at maximum for all the samples at 0 minute, due to the high level of proteins in plasma sample. However, after application of electric field as most of plasma proteins with high concentration have pI less than 8 (at least more than 90% of total plasma protein concentration), they attain negative charge and move away from the gate. Therefore, the fluorescent intensity in the agarose membrane gate decreases by time for all the samples (figure 3.7b). Based on the results, after 6 minutes applying electric field, the difference between the measured intensities for different concentrations is the highest. Therefore, the average of measured intensities for each of the histone concentrations after 6 minutes is plotted in figure 3.7c. For

control sample, which is only plasma with no added histone, after 6 minutes most of the proteins are cleared from the gate area and only the protein portion of the plasma with isoelectric point between 8 and 11 may have been accumulated in the gel depends on their charge at that region. The background fluorescent intensity for plasma control sample is higher compared to the respective measured intensity from only BSA in buffer in previous section. This can be due to the higher concentration of proteins in the plasma especially with the pI between 8 and 11 and larger amount of added dye. Similarly, for all the samples the average intensity at all times during the experiment is higher compared to the same concentration of histone in buffer or histone mixed with BSA. This is due to the presence of other proteins than only albumin in plasma which can get accumulated in the vicinity of the gate because of their pI. Additionally, the higher concentration of plasma proteins can further reduce nonspecific binding of histones to the surface of the sample channel. Also, the amount of dye used for plasma samples was higher compared to previous samples. Another point that should also be mentioned here, is the background fluorescence from the plasma itself which can also affect the measured intensities. Based on figure 3.7c, the membrane fluorescent intensity increases by increasing the histone concentration, after 6 minutes applying voltage. However, a two-tailed t-test showed that the difference between control and 10 μg/mL histone in sample, and 10 μg/mL and 20 μg/mL histone sample is insignificant. Although, a two-tailed t-test gives $p < 0.05$ in differentiating between 0, 20, and 33 μg/mL histone spiked plasma samples using this device (figure 3.7d). The limit of detection (LOD) was calculated as $3\sigma/m$ where σ is the standard deviation of the blank (0 μg/mL spiked in plasma) and m is the slope of the calibration plot. LOD was found to be 17.92 μg/mL spiked in plasma. Therefore, this device can be used for differentiating between healthy persons, sepsis survivors and non-survivors using their plasma samples. This device can be developed further for a POC device for sepsis prognosis.

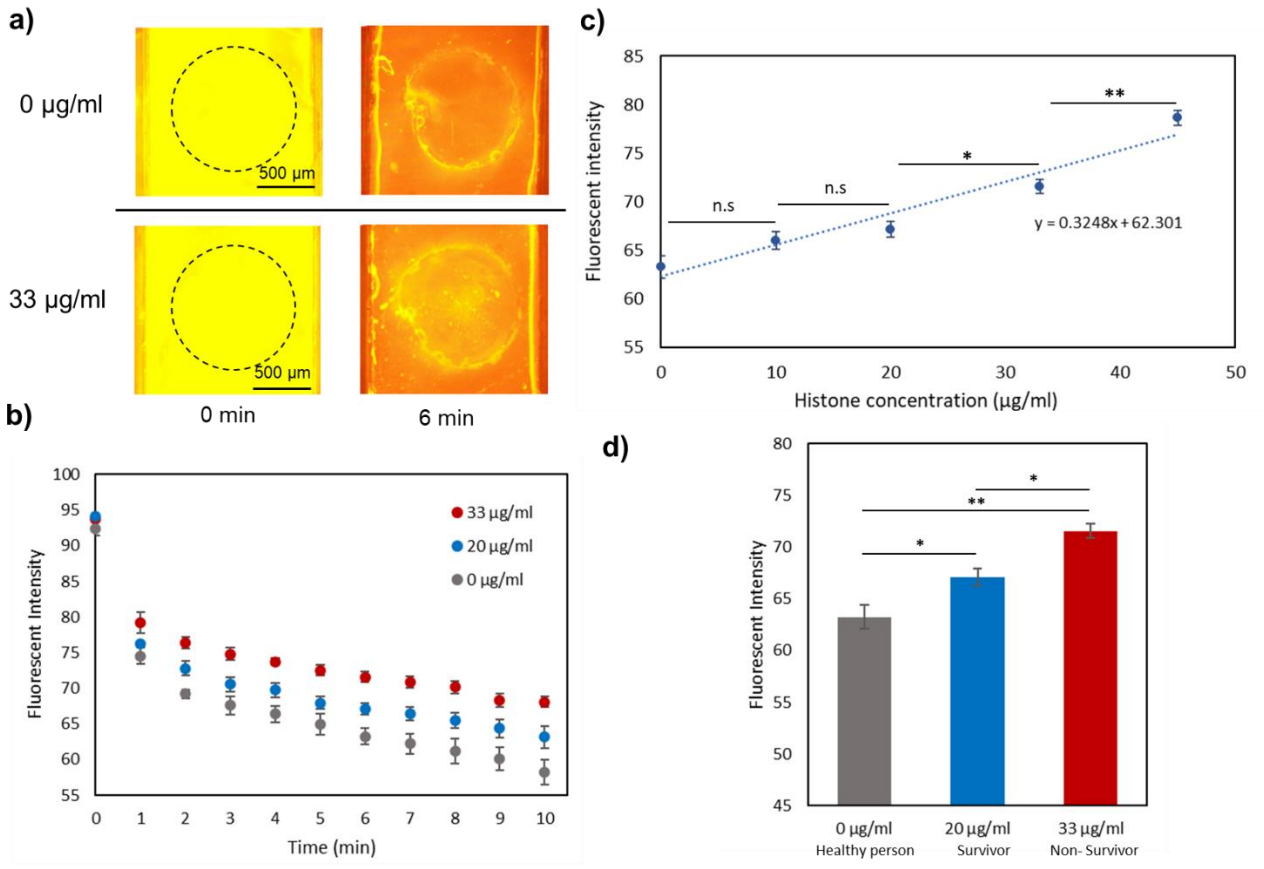

Figure 3.7 Trapping histones in the histone spiked plasma sample. a) Images captured at 0 minute (filling the sample channel) and after 6 minutes for plasma samples containing 0 and 33 µg/mL of histone. b) Plot showing changes in measured fluorescent intensity with time for each sample after applying 30 V. c) Plot showing changes in measured fluorescent intensity with histone concentration for various samples after 6 minutes. d) Fluorescence intensity values for histone concentrations corresponding to survivors and non-survivors (N=3). Statistical significance for samples calculated by two-tailed t-test (** $p < 0.01$, * $p < 0.05$).

3.5 Conclusion

A rapid, simple, and low-cost microfluidic device for detection and discrimination total circulating histones in plasma was developed. This device has the potential to be used as a bedside tool for stratifying severity of sepsis. Unlike conventional laboratory methods such as ELISA or western blot which are difficult to perform on the bedside, this approach of using isoelectric characteristics of the histones to concentrate them and measure using optical methods provides sufficient accuracy for discrimination of patients with high and low histone levels that can be used for patient stratification. The response from this device is fast (less than 10 min) and requires only 30 V which

can be generated by a bank of batteries. It also uses only 10 µl of the sample. It was shown that the device can be used for differentiating between healthy persons, survivors, and non-survivors of sepsis. Currently, due to manufacturing issues, there is some variability in the size and volume of gels that are integrated which restricts the resolution of this approach. With improved manufacturing, the resolution can be significantly improved to make fine discrimination and quantification possible. This device can be expanded by adding multiple isoelectric gates for separation and detection of other proteins from the sample as well. In future work, more characterization will be performed for using clinical patients blood samples and the device needs to be modified further for better sensitivity and resolution. Also, the experimental method and setup should be improved for a POC device. For instance, the fluorescent dye can be integrated inside the device for avoiding any sample preparation step. Furthermore, the device can be developed into a fully functionalized and compact system by replacing DC power supply with batteries and the fluorescent microscope can be simplified with a LED light source and optical filters.

References

1. Nofi, C.P.; Wang, P.; Aziz, M. Chromatin-Associated Molecular Patterns (CAMPs) in Sepsis. *Cell Death & Disease* **2022**, *13*, 700.
2. Wildhagen, K.C.; Wiewel, M.A.; Schultz, M.J.; Horn, J.; Schrijver, R.; Reutelingsperger, C.P.; van der Poll, T.; Nicolaes, G.A. Extracellular Histone H3 Levels Are Inversely Correlated with Antithrombin Levels and Platelet Counts and Are Associated with Mortality in Sepsis Patients. *Thrombosis research* **2015**, *136*, 542–547.

3. Marsman, G.; Zeerleder, S.; Luken, B.M. Extracellular Histones, Cell-Free DNA, or Nucleosomes: Differences in Immunostimulation. *Cell death & disease* **2016**, *7*, e2518–e2518.

4. Li, Y.; Wan, D.; Luo, X.; Song, T.; Wang, Y.; Yu, Q.; Jiang, L.; Liao, R.; Zhao, W.; Su, B. Circulating Histones in Sepsis: Potential Outcome Predictors and Therapeutic Targets. *Frontiers in Immunology* **2021**, *12*, 650184.

5. Gargano, A.F.; Shaw, J.B.; Zhou, M.; Wilkins, C.S.; Fillmore, T.L.; Moore, R.J.; Somsen, G.W.; Paša-Tolić, L. Increasing the Separation Capacity of Intact Histone Proteoforms Chromatography Coupling Online Weak Cation Exchange-HILIC to Reversed Phase LC UVPD-HRMS. *Journal of proteome research* **2018**, *17*, 3791–3800.

6. Xu, Z.; Huang, Y.; Mao, P.; Zhang, J.; Li, Y. Sepsis and ARDS: The Dark Side of Histones. *Mediators of inflammation* **2015**, *2015*.

7. Ito, T.; Nakahara, M.; Masuda, Y.; Ono, S.; Yamada, S.; Ishikura, H.; Imaizumi, H.; Kamikokuryo, C.; Kakihana, Y.; Maruyama, I. Circulating Histone H3 Levels Are Increased in Septic Mice in a Neutrophil-Dependent Manner: Preclinical Evaluation of a Novel Sandwich ELISA for Histone H3. *Journal of Intensive Care* **2018**, *6*, 1–6.

8. Xu, J.; Zhang, X.; Pelayo, R.; Monestier, M.; Ammollo, C.T.; Semeraro, F.; Taylor, F.B.; Esmon, N.L.; Lupu, F.; Esmon, C.T. Extracellular Histones Are Major Mediators of Death in Sepsis. *Nature medicine* **2009**, *15*, 1318–1321.

9. Han, Z.; Yuan, Z.; Shu, L.; Li, T.; Yang, F.; Chen, L. Extracellular Histone H3 Facilitates Ferroptosis in Sepsis through ROS/JNK Pathway. *Immunity, Inflammation and Disease* **2023**, *11*, e754.

10. Singer, M.; Deutschman, C.S.; Seymour, C.W.; Shankar-Hari, M.; Annane, D.; Bauer, M.; Bellomo, R.; Bernard, G.R.; Chiche, J.-D.; Coopersmith, C.M. The Third International Consensus Definitions for Sepsis and Septic Shock (Sepsis-3). *Jama* **2016**, *315*, 801–810.
11. Purcarea, A.; Sovaila, S. Sepsis, a 2020 Review for the Internist. *Romanian Journal of Internal Medicine* **2020**, *58*, 129–137.
12. Kumar, A.; Roberts, D.; Wood, K.E.; Light, B.; Parrillo, J.E.; Sharma, S.; Suppes, R.; Feinstein, D.; Zanotti, S.; Taiberg, L. Duration of Hypotension before Initiation of Effective Antimicrobial Therapy Is the Critical Determinant of Survival in Human Septic Shock. *Critical care medicine* **2006**, *34*, 1589–1596.
13. Cheng, Z.; Abrams, S.T.; Alhamdi, Y.; Toh, J.; Yu, W.; Wang, G.; Toh, C.-H. Circulating Histones Are Major Mediators of Multiple Organ Dysfunction Syndrome in Acute Critical Illnesses. *Critical care medicine* **2019**, *47*, e677–e684.
14. Eichhorn, T.; Linsberger, I.; Lauková, L.; Tripisciano, C.; Fendl, B.; Weiss, R.; König, F.; Valicek, G.; Miestinger, G.; Hörmann, C. Analysis of Inflammatory Mediator Profiles in Sepsis Patients Reveals That Extracellular Histones Are Strongly Elevated in Nonsurvivors. *Mediators of Inflammation* **2021**, *2021*.
15. Ekaney, M.L.; Otto, G.P.; Sossdorf, M.; Sponholz, C.; Boehringer, M.; Loesche, W.; Rittirsch, D.; Wilharm, A.; Kurzai, O.; Bauer, M. Impact of Plasma Histones in Human Sepsis and Their Contribution to Cellular Injury and Inflammation. *Critical care* **2014**, *18*, 1–9.
16. García-Giménez, J.; Romá-Mateo, C.; Carbonell, N.; Palacios, L.; Peiró-Chova, L.; García-López, E.; García-Simón, M.; Lahuerta, R.; Gimenez-Garzó, C.; Berenguer-Pascual, E. A New Mass Spectrometry-Based Method for the Quantification of Histones in Plasma from Septic Shock Patients. *Scientific reports* **2017**, *7*, 1–10.

17. Lu, N.-F.; Jiang, L.; Zhu, B.; Yang, D.-G.; Zheng, R.-Q.; Shao, J.; Xi, X.-M. Elevated Plasma Histone H4 Level Predicts Increased Risk of Mortality in Patients with Sepsis. *Ann. Palliat. Med* **2020**, *9*, 1084–1091.

18. Yokoyama, Y.; Ito, T.; Yasuda, T.; Furubeppu, H.; Kamikokuryo, C.; Yamada, S.; Maruyama, I.; Kakihana, Y. Circulating Histone H3 Levels in Septic Patients Are Associated with Coagulopathy, Multiple Organ Failure, and Death: A Single-Center Observational Study. *Thrombosis journal* **2019**, *17*, 1–7.

19. Zhan, X.; Liu, D.; Dong, Y.; Gao, Y.; Xu, X.; Xie, T.; Zhou, H.; Wang, G.; Zhang, H.; Wu, P. Early Changes and Predictive Value of Serum Histone H3 Concentration in Urosepsis: A Prospective Observational Study. *Advances in Therapy* **2022**, *39*, 1310–1323.

20. Abrams, S.T.; Zhang, N.; Manson, J.; Liu, T.; Dart, C.; Baluwa, F.; Wang, S.S.; Brohi, K.; Kipar, A.; Yu, W. Circulating Histones Are Mediators of Trauma-Associated Lung Injury. *American journal of respiratory and critical care medicine* **2013**, *187*, 160–169.

21. Alhamdi, Y.; Abrams, S.T.; Cheng, Z.; Jing, S.; Su, D.; Liu, Z.; Lane, S.; Welters, I.; Wang, G.; Toh, C.-H. Circulating Histones Are Major Mediators of Cardiac Injury in Patients with Sepsis. *Critical care medicine* **2015**, *43*, 2094–2103.

22. Mai, J.; Sommer, G.J.; Hatch, A.V. Microfluidic Digital Isoelectric Fractionation for Rapid Multidimensional Glycoprotein Analysis. *Analytical chemistry* **2012**, *84*, 3538–3545.

23. Pergande, M.R.; Cologna, S.M. Isoelectric Point Separations of Peptides and Proteins. *Proteomes* **2017**, *5*, 4.

24. Sommer, G.J.; Mai, J.; Singh, A.K.; Hatch, A.V. Microscale Isoelectric Fractionation Using Photopolymerized Membranes. *Analytical chemistry* **2011**, *83*, 3120–3125.

25. Damodara, S.; Dwivedi, D.J.; Liaw, P.C.; Fox-Robichaud, A.E.; Selvaganapathy, P.R.; Canadian Critical Care Translational Biology Group Single Step Separation and Concentration of Biomarker Proteins Using Agarose Based Miniaturized Isoelectric Gates for Point of Care Diagnostics. *Sensors and Actuators B: Chemical* **2021**, *330*, 129265.
26. Damodara, S.; Arora, J.; Dwivedi, D.J.; Liaw, P.C.; Fox-Robichaud, A.E.; Selvaganapathy, P.R.; Canadian Critical Care Translational Biology Group Microfluidic Device for Single Step Measurement of Protein C in Plasma Samples for Sepsis Prognosis. *Lab on a Chip* **2022**, *22*, 2566–2577.
27. Shahriari, S.; Selvaganapathy, P.R. Integration of Hydrogels into Microfluidic Devices with Porous Membranes as Scaffolds Enables Their Drying and Reconstitution. *Biomicrofluidics* **2022**, *16*, 054108.
28. Damodara, S.; Shahriari, S.; Wu, W.-I.; Rezai, P.; Hsu, H.-H.; Selvaganapathy, R. Materials and Methods for Microfabrication of Microfluidic Devices. In *Microfluidic Devices for Biomedical Applications*; Elsevier, 2021; pp. 1–78.
29. Shahriari, S.; Patel, V.; Selvaganapathy, P.R. Xurography as a Tool for the Fabrication of Microfluidic Devices. *Journal of Micromechanics and Microengineering* **2023**.
30. Paul, J.; Veenstra, T.D. Separation of Serum and Plasma Proteins for In-Depth Proteomic Analysis. *Separations* **2022**, *9*, 89.
31. De, M.; Rana, S.; Akpinar, H.; Miranda, O.R.; Arvizo, R.R.; Bunz, U.H.; Rotello, V.M. Sensing of Proteins in Human Serum Using Conjugates of Nanoparticles and Green Fluorescent Protein. *Nature chemistry* **2009**, *1*, 461–465.

32. Monteiro, R.C.; Halbwachs-Mecarelli, L.; Roque-Barreira, M.C.; Noel, L.-H.; Berger, J.; Lesavre, P. Charge and Size of Mesangial IgA in IgA Nephropathy. *Kidney international* **1985**, *28*, 666–671.

33. Barrett, A.J.; Brown, M.A.; Sayers, C.A. The Electrophoretically 'Slow'and 'Fast'Forms of the A2-Macroglobulin Molecule. *Biochemical Journal* **1979**, *181*, 401–418.

34. Prin, C.; Bene, M.C.; Gobert, B.; Montagne, P.; Faure, G.C. Isoelectric Restriction of Human Immunoglobulin Isotypes. *Biochimica et Biophysica Acta (BBA)-General Subjects* **1995**, *1243*, 287–289.

35. Adler, A.; Manivel, V.A.; Fromell, K.; Teramura, Y.; Ekdahl, K.N.; Nilsson, B. A Robust Method to Store Complement C3 With Superior Ability to Maintain the Native Structure and Function of the Protein. *Frontiers in Immunology* **2022**, *13*, 891994.

36. Ayyub, A.; Saleem, M.; Musharraf, S.G.; Naz, M.; Tariq, A.; Hashmi, N. Mass Spectrometric Identification, Characterization and Validation of the Haptoglobin β-Chain Protein as a Lung Cancer Serum Biomarker. *Molecular Medicine Reports* **2015**, *12*, 3755–3762.

37. Leeman, M.; Choi, J.; Hansson, S.; Storm, M.U.; Nilsson, L. Proteins and Antibodies in Serum, Plasma, and Whole Blood—Size Characterization Using Asymmetrical Flow Field-Flow Fractionation (AF4). *Analytical and bioanalytical chemistry* **2018**, *410*, 4867–4873.

38. Fullarton, J.; Kenny, A. A Rapid System for Preparative Electrophoresis Depending on Isoelectric Buffers of Low Conductivity. *Biochemical Journal* **1970**, *116*, 147.

39. Dötsch, V.; Withers, R.S. Low-Conductivity Buffers for Magnetic Resonance Measurements. **2005**.

40. Wiig, H.; Kolmannskog, O.; Tenstad, O.; Bert, J.L. Effect of Charge on Interstitial Distribution of Albumin in Rat Dermis in Vitro. *The Journal of Physiology* **2003**, *550*, 505–514.

4 Chapter 4 A fully integrated microfluidic device with immobilized dyes for simultaneous detection of cell-free DNA and histones from plasma using dehydrated agarose gates

Full Citation: Shahriari S, Selvaganapathy PR. A fully integrated microfluidic device with immobilized dyes for simultaneous detection of cell-free DNA and histones from plasma using dehydrated agarose gates. Gels. 2024 Mar 8;10(3):186.

A fully integrated microfluidic device with immobilized dyes for simultaneous detection of cell-free DNA and histones from plasma using dehydrated agarose gates

*Shadi Shahriari[1] and P. Ravi Selvaganapathy[1,2] **

[1] *Department of Mechanical Engineering, McMaster University, Hamilton, ON, Canada*

[2] *School of Biomedical Engineering, McMaster University, Hamilton, ON, Canada*

** Corresponding author. E-mail address: selvaga@mcmaster.ca*

Abstract

Sepsis, a life-threatening condition resulting from a failing host response to infection, causes millions of deaths annually, necessitating rapid and simple prognostic assessments. A variety of genomic and proteomic biomarkers have been developed for sepsis. For example, it has been shown that the level of plasma cell free DNA (cfDNA) and circulating histones increases considerably during sepsis and they are linked with sepsis severity and mortality. Developing a diagnostic tool that is capable of assessing such diverse biomarkers is challenging as the detection methodology is quite different for each. Here, a fully integrated microfluidic device capable of detecting a genomic biomarker (cfDNA) and a proteomic biomarker (total circulating histones) using a common detection platform has been demonstrated. The microfluidic device utilizes dehydrated agarose gates loaded with pH-specific agarose to electrophoretically trap cfDNA and histones at their respective isoelectric points. It also incorporates fluorescent dyes within the device, eliminating the need for off-chip sample preparation and allowing direct testing of plasma samples without the need for labeling DNA and histones with fluorescent dyes beforehand. Xurography which is a low-cost and rapid method for fabrication of microfluidics is used in all the fabrication steps. Experimental results demonstrate the effective accumulation and separation of

cfDNA and histones in the agarose gates in a total processing time of 20 minutes, employing 10 and 30 Volts for cfDNA and histone accumulation and detection, respectively. The device can potentially be used to distinguish between survivors and non-survivors of sepsis. The integration of both biomarkers detection into a single device and dye immobilization enhances its clinical utility for rapid point-of-care assessment of sepsis prognosis.

Keywords: Sepsis; Microfluidics; cfDNA; Histones; Xurography; Agarose

4.1 Introduction

Sepsis arises from abnormal host response to an infection which leads to critical organ dysfunction [1]. It is estimated that there are about 31.5 million sepsis cases with 5.3 million deaths worldwide each year [2]. In septic patients, the risk of mortality increases by 8% for every hour of delay in sepsis treatment [3]. Identifying severe sepsis early on could result in timely interventions that have the potential to decrease sepsis mortality. Therefore, the clinical utility of prognostic and diagnostic biomarkers in sepsis is significant [4]. Many biomarkers have been studied for their use in sepsis prognosis. Notably, procalcitonin (PCT) and C-reactive protein (CRP) have been extensively considered as biomarkers for diagnosis and prognosis of sepsis [5]. More recently, cell-free DNA (cfDNA) and histones have been introduced as two biomarkers for sepsis prognosis which both reflects cellular death activity [2,6–10]. Nucleosomes consist of 145 bp DNA wrapped around a core histone octamer, which contains two copies of histones H2A, H2B, H3, and H4. Widespread cell death during sepsis can contribute to extracellular release of DNA and histones. Circulating levels of nucleosomes, cfDNA, and histones are increased in sepsis [11–14]. Neutrophils are the major source of released cfDNA. High concentrations of cfDNA showed high discriminative power for prediction mortality among patients with severe sepsis [15]. A study

showed that, the mean cfDNA level in sepsis survivors was 1.16±0.13µg/mL which was similar to healthy persons (0.93±0.76µg/mL); however, for non-survivors was 4.65±0.48µg/mL [7].

Similarly, as the result of the rupture of the nuclear and plasma cell membrane which happens during organ injury, histones will be released into extracellular environment. Studies showed that high levels of circulating histones are significantly linked with sepsis severity and mortality. Free histones have not been found in healthy persons or detected in very low concentrations [6,10]. Histones are basic proteins due to their N-terminal tail rich in lysine and arginine, which forms the basic nature of the histones [2]. Histones have an isoelectric point around 11 [16]. A study showed that total free histone concentration in sepsis patients who died within 28 days of ICU admission was 32.7 µg/mL, however, for survivors was 20.1 µg/mL. Total circulating histone level for healthy persons was 1.3 µg/mL [6].

Detecting genomic and proteomic biomarkers simultaneously can be challenging due to inherent differences in the nature of genetic material (genomic) and proteins (proteomic). Therefore, having a rapid and simultaneous method for detection of cfDNA (genomic biomarker) and circulating histones (proteomic biomarker) can be beneficial by offering a better understanding of the sepsis progression and aid physicians in prognosis. One of the methods that has been extensively used for detection and separation of biomolecules in microfluidics is gel electrophoresis [17]. Previously, we showed microfluidic devices containing dried agarose gels inside membranes for concentration and detection of biomolecules [18,19]. The dried gels can be reconstituted in the sample solution itself and function effectively, thereby eliminating the need to load the gels into devices at the time of testing making this approach suitable for point of care applications. These gels can be used in a variety of ways to either serve as an entangling and concentration medium for DNA or as gels loaded with specific pH to trap biomolecules at their isoelectric point [18,19].

Nevertheless, these devices still required premixing of fluorescent dyes with the sample solution prior to introduction into the device which is not suitable for point of care testing. Also, the dyes required for genomic and proteomic biomarkers are markedly different and integration of these dyes into the device itself and ensuring minimal cross reactivity can greatly facilitate their use in the field.

Here we introduce the design of a single microfluidic device with two dehydrated agarose gates and incorporated fluorescent dyes for accumulation and detection of histones and cfDNA from plasma sample in 20 minutes total. This device can be enhanced further as a point of care (POC) device for rapid quantification of histones and cfDNA as a prognostic biomarker in plasma of individuals with sepsis.

4.2 Device design and working principle

The goal of the device is to detect both cfDNA and total circulating histone in plasma of sepsis patients to quickly distinguish between survivors and non-survivors. This can be accomplished by tagging DNA and histone with different fluorescent dyes and isolating and accumulating each of them in agarose gel membranes embedded inside a microfluidic device. The fluorescent dyes are immobilized inside the sample reservoirs of the device which eliminates the need of premixing of the sample and dye outside the device. This was done by depositing and drying the dyes on the surface of a PET film in the location of sample reservoirs and positioning the film under the sample channel. The agarose gates are dehydrated agarose gels loaded onto porous PTFE membrane with pH 8.5 and pH 11 for cfDNA and histone trapping respectively. The porous PTFE membranes are beneficial for incorporating hydrogels during the device fabrication process. These membranes help preserve the structure of dehydrated hydrogels and facilitate rehydration as required [18].

The microfluidic device was made from pressure sensitive adhesives and films using xurography. Xurography has been used in all the fabrication steps from agarose integration to dye immobilization and device fabrication. Xurography is a rapid and low-cost method for fabrication of microfluidic devices by cutting and attaching different adhesives and polymer films [20]. The device consists of 6 layers which form four channels (two channels on top and two channels with one inlet in bottom) with a sandwiched layer containing dried agarose in between and a layer containing dried fluorescent dyes in the back (figure 4.1). A stack of four layers of hydrophilic porous PTFE membrane (36 μm thick each) was used as the scaffold for integration of agarose. These PTFE layers were sandwiched between two double sided adhesives, Kapton tape and a silicone-based adhesive (AR-94119). AR-94119 showed minimal auto-fluorescence with little non-specific binding of dye or labeled proteins to its surface. These two double sided adhesives have circular openings (1 mm in diameter) for filling the exposed PTFE membranes with agarose in those regions to form gel gates. Agarose solutions (3% w/v) made in CAPS buffer with pH 11 and TAE buffer with pH 8.5 were loaded in the open parts of porous membrane to create the gates for histone and DNA respectively. Qubit protein assay dye was used for labelling proteins and GelGreen for staining DNA. The fluorescent dyes were patterned on the surface of a hydrophilic PET film (3M-9984) using a screen made of Kapton tape with three rectangles cut-outs attached to the surface of the PET film for dye loading. After drying the dyes on the film in a desiccator, Kapton tape is peeled off, leaving patterned dried dyes at appropriate locations on the PET film. Top channels (buffer channels) layer was out of PVC film, and it was attached to the sandwiched layer containing agarose gates from the Kapton tape side. The top channels were sealed with a hydrophilic single sided adhesive (AR-93049) containing the inlets. The layer containing the bottom channels was cut out of Kapton tape and it was attached to the sandwiched layer from

silicone-based adhesive (AR-94119) side. Then, the electrodes were positioned at the two ends of bottom channels and one end of top channels. Finally, the device was sealed with the PET film layer containing immobilized dyes.

At the time of experiment, the top channels placed over agarose with pH 8.5 (made in TAE) and agarose with pH 11 (made in CAPS) gates were filled with 1X TAE and 0.2 M CAPS buffer with the same pH of the agarose gates respectively (figure 4.1a). After agarose rehydration with their corresponding buffer, the bottom channels were filled with the sample containing DNA and histones. The sample was pipetted several times in each of the reservoirs for better mixing the sample and the dried immobilized dyes. About 2 and 12 minutes waiting time was needed for DNA/GelGreen and proteins/Qubit labelling respectively (figure 4.1b). First, the objective was centered on the agarose membrane for DNA detection. After 2 minutes, 10 V was applied between the two ends of bottom channel under the agarose gate (pH 8.5) for DNA accumulation and top channel containing TAE buffer. Fluorescent images from the agarose membrane were taken every 30 seconds for a total of 5 minutes using a raspberry pi camera. By applying electric field, DNA tagged with GelGreen moved from bottom channel towards the positive electrode in buffer channel due to its negative charge. DNA gets accumulated in agarose gel inside the membrane as it provides a lower mobility environment (figure 4.1c). Based on the fluorescent intensity captured from the agarose gate after 5 minutes, the DNA concentration can be quantified for different samples.

After 12 minutes, the objective was centered on the other agarose gate (pH 11) and the filter cube was changed to the one matching Qubit dye. Electric field (30 V) was applied between the bottom channel under the agarose gate and buffer channel filled with CAPS buffer (figure 4.1d). The direction of the electric field was switched as the electrodes in sample channel were positive and the one in top channel was negative. Fluorescent images of the agarose gate were taken every 30

seconds for a total of 5 minutes using a raspberry pi camera. The device design was intended to prevent the entry of the majority of plasma proteins into the agarose membrane with pH 11, while histones get trapped in the isoelectric membrane. All the proteins were labeled with Qubit dye. Blood plasma has pH around 7.4. Therefore, pH 7.4 serves as a cut-off point for determining the charge of proteins and their direction of movement in the sample channel. In the presence of electric field, proteins with an isoelectric point lower than the sample pH acquire a negative charge and migrate towards the positive electrodes located in the reservoirs of the sample channel, consequently moving away from the agarose gate. However, proteins with an isoelectric point greater than that of the sample, such as histones, acquire positive charge, leading them to move toward the cathode in the upper channel. As histones enter the agarose gel membrane with a pH of 11, their charge diminishes, causing them to slow down and accumulate. Consequently, the quantification of histones is possible by assessing the fluorescent intensity in the agarose gate. As most of plasma proteins are acidic, they migrate towards the positive electrodes in the sample channels and others with pI higher than 7.4 which are much less abundant, migrate towards the agarose membrane. Hence, a significant portion of proteins is excluded from entering the gate. The proteins with pI greater than 7.4, they either pass through the gate or trap in the membrane depending on their pI values.

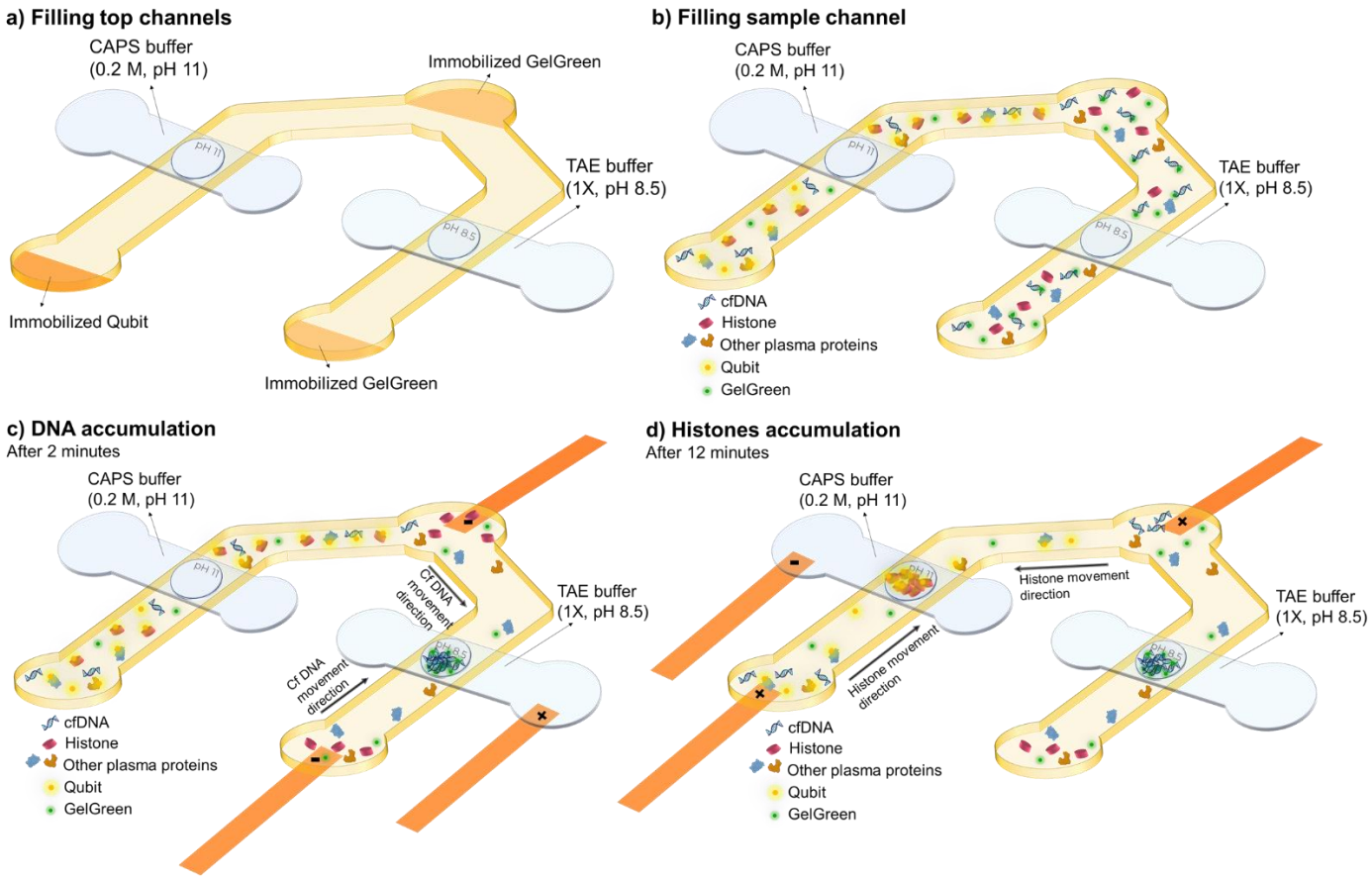

Figure 4.1 Working principle and steps of the device. a) Filling the top channels with the corresponding buffers for agarose rehydration. b) Filling the sample channels and waiting for labelling DNA and proteins with their corresponding dyes. c) DNA accumulation by applying 10 V to the channels connected to agarose gate with pH 8.5. d) Histone separation and detection by applying 30 V to the channels connected to the agarose gate with pH 11.

4.3 Materials and methods

4.3.1 Materials

Histone H3.1 human, histone from calf thymus type II-A, and bovine serum albumin (BSA) were acquired from Millipore Sigma. NoLimits 150 bp DNA fragment, Qubit protein assay kit, Tris-HCl (1M solution and pH 8.0) and CAPS buffer (0.5 M, pH 11) were obtained from Thermo Fisher Scientific. GelGreen nucleic acid gel stain, 10,000X in water was from Biotium. Pooled human plasma K2 EDTA was purchased from Innovative research. CAPS buffer (0.2 M, pH 11) was obtained from Bioworld. Agarose and 50x TAE buffer concentrate were purchased from BioShop Canada Inc, Burlington, ON. Hydrophilic PTFE unlaminated membrane (1 micron pore size) was

acquired from Sterlitech, Auburn, WA. Double-sided and double liner polyimide (Kapton) tape (100 μm thick) was purchased from Caplinq. A double-sided silicone-based pressure sensitive adhesive (ARcare-94119, 142 μm thick) and one-sided hydrophilic acrylic-based adhesive (ARflow-93049, 100 μm thick) were received from adhesive research, Glen Rock, PA. Surfactant free and hydrophilic polyester film (3M-9984, 99 μm thick) was received from 3M™, Maplewood, MN. Polyvinyl chloride (PVC) film (Clear-Lay, 127 μm thick) was from Grafix, Maple Heights, OH. Copper-polyimide composite foil (9 μm-Cu and 12 μm-PI thick) was obtained from DuPont.

4.3.2 Fabrication

The microfluidic device contains four channels, two agarose gates, and a layer containing dried fluorescent dyes. Two channels with a single inlet for sample are in the bottom and two channels are on top of each agarose gate for rehydration buffer. Agarose is loaded in the membranes between bottom and top channels. The layer containing immobilized dyes is the bottommost layer. Xurography was used as the main fabrication method in all the steps. Cutting plotter (FC8600, Graphtec America) with CB09UB blade was used for cutting different layers of the device. In the following, the process for agarose integration, dye immobilization, and device assembly is discussed in detail.

4.3.2.1 Integration of agarose into the device

In order to integrate the two agarose gates into the device; first two layers of silicone-based double-sided adhesives (Kapton tape and AR-94119) were patterned using xurography based on the design for agarose gates (1 mm diameter circular openings) and device inlets. Then, four layers of hydrophilic PTFE membrane (each layer; 36 μm thick and 2.5 mm wide) were stacked and sandwiched between these two layers of double-sided adhesives under the circular openings (figure 4.2a, i). The layers were aligned and laminated (figure 4.2a, ii). Then, 3% agarose was

made in two different buffers (0.5 M CAPS, pH 11 and 1X TAE buffer, pH 8.5). Each of the PTFE membrane circular openings was filled from both side of sandwiched layer with one of the agarose solutions made in CAPS and TAE buffer (figure 4.2a, iii). Following wicking the agarose solution into the membranes completely and its gelation, the excess amount of agarose was wiped off from the surface of the agarose containing layer and the agarose gates were allowed to dry.

4.3.2.2 Immobilization of fluorescent dyes into the device

GelGreen and Qubit were immobilized inside the microfluidic device by patterning and drying them on the surface of the bottom most layer of the device (hydrophilic PET film 3M-9984). To create the patterns of the dyes on the surface of the PET film, a layer of Kapton tape containing the cut-out patterns for dyes was used as a masking layer. The cut-out patterns were three rectangles; with 4.5 mm width and two with 1.8 mm and one with 2.3 mm height. This Kapton tape layer was attached to the PET film surface (figure 4.2b, i). Then, 2.5 µl of Qubit was pipetted into one of the smaller rectangular reservoirs and 2.5 µl of diluted GelGreen was pipetted into each of the other reservoirs (figure 4.2b, ii). Next, this layer containing the patterned dyes was put in a desiccator for assisting the evaporation of the dyes solvent (figure 4.2b, iii). After, drying the dyes completely in their locations (figure 4.2b, iv), the top Kapton tape layer was peeled off from the PET film (figure 4.2b, v), leaving behind the patterned dried dyes on the film (figure 4.2b, vi).

4.3.2.3 Assembly of the final device

The rest of the layers of the microfluidic device were cut using xurography as well. Top channels with 1.5 mm width and 4.15 mm height were cut out of PVC film (127 µm thick). This layer was aligned and attached to the layer containing dried agarose gates from the Kapton tape side. The bottom channels with a single inlet and 1.5 mm width were cut from double-sided Kapton tape with one liner removed (170 µm thick) and it was attached to the sandwiched dried agarose layer

from the AR-94119 adhesive side. Then, the channels were sealed from the top using a hydrophilic adhesive (AR-93049) with the inlets of the channels. The electrodes with 1.25 mm width were cut out of copper foil. They were placed in the reservoirs of the bottom channels and one of the reservoirs in the top channels. Then the hydrophilic PET film (3M-9984) containing the dried dyes, was attached to the bottom channels layer and electrodes. The arrangement of the layers of the device is shown in figure 4.2c. After alignment and assembly of the layers, the device passed through a lamination step for a good sealing. The schematic of the final device is demonstrated in figure 4.2d.

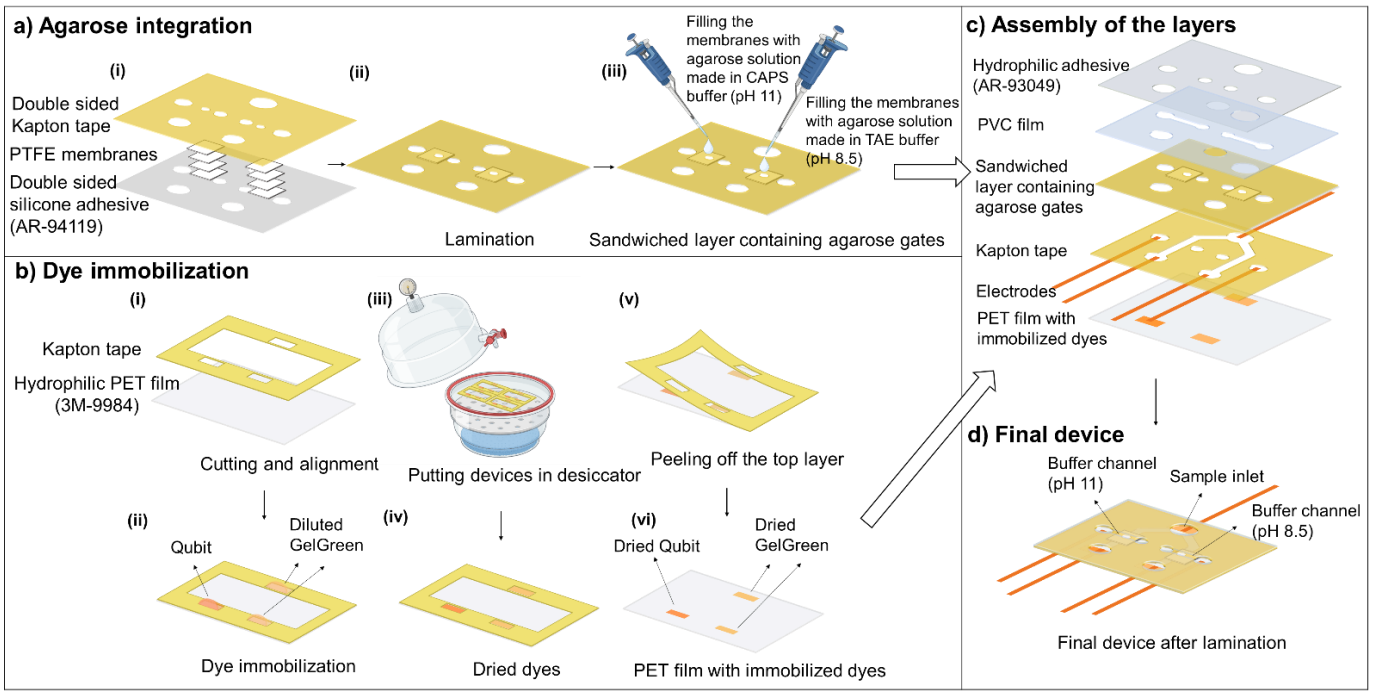

Figure 4.2 Fabrication steps of the final device. a) Integration of agarose gates into the device using PTFE membranes and double-sided adhesives. b) Steps for immobilization of the fluorescent dyes in the device. c) Alignment and assembly of the layers. d) Schematic view of the final device.

4.3.3 Experimental method

Histone from calf thymus and 150 bp DNA were used to test the labelling and accumulation in the devices with immobilized dyes. A solution containing histone from calf thymus at a concentration of 2 mg/mL was prepared by reconstituting the lyophilized histone powder in Milli-Q water. 150

bp DNA was used to be similar to the actual size of cfDNA (147 bp). Different concentrations of 150 bp DNA was made by diluting the 500 µg/mL stock solution. In case of Qubit immobilization, 2 µl of one-time diluted Qubit was immobilized in the inlets reservoirs similar to the method mentioned earlier. During the experiment, after rehydration of agarose gel with 10 µl of 0.2 M CAPS buffer, 1 mg/mL histone was added to the sample channel. The sample and dried Qubit were mixed by pipetting the sample several times in the inlets. The mixture was allowed to intercalate inside the channel for few minutes before starting the accumulation.

Human histone H3.1 was used for assessing the dye immobilized device with histone in the presence of BSA sample and human plasma spiked with histone samples. The sample containing histone mixed with BSA was made by diluting the 1 mg/mL stock histone H3.1 solution to 20 and 33 µg/mL and mix that with 40 mg/mL BSA (corresponding to average HSA concentration in plasma) in 50 mM Tris-HCl buffer pH 8.

In order to test the device function with dried immobilized GelGreen, 2 µl of 5X GelGreen was immobilized in the reservoirs of sample channel. 5X GelGreen was made by diluting the 10000X GelGreen in DI water. Then, buffer channel was filled with 10 µl of 1X TAE buffer for agarose rehydration. Next, sample containing 5 µg/mL of 150 bp DNA was added to the sample channel. Sample was pipetted into the reservoirs several times to help with the mixing of DNA and dried GelGreen. The mixture was allowed to sit inside the channel for few minutes before starting the accumulation. Similarly, different dilution ratio for GelGreen (5X, 10X, and 30X) was tested for the samples containing both DNA and histones.

In case of integrated device with two gates for DNA and histones detection from plasma samples, 2.5 µl Qubit with no dilution was deposited in one of the reservoirs connected to sample channel in histone accumulation section. Qubit was not diluted as more protein is present in plasma sample

(almost doubled the BSA concentration in previous sample). Also, 2.5 µl of 30X GelGreen was dried in the sample channel main inlet and outlet of the sample channel in DNA concentration section of the device. Histone and 150bp DNA spiked in plasma was made by spiking histone H3.1 and 150 bp DNA in plasma from healthy person to get final concentrations of 1 and 5 µg/mL of DNA and 20 and 33 µg/mL of histone. For each experiment 30 µl of sample was pipetted into the sample channels. The sample and dried dyes were mixed thoroughly by multiple pipetting inside the reservoirs.

4.3.4 Experimental setup

Each experiment was performed using a new device. The microfluidic device was positioned on a fluorescence microscope (Nikon Eclipse TE2000-S). Two different filter cubes, matching the excitation and emission wavelengths of each dye (GelGreen and Qubit) were used. A filter cube with excitation window of 472 ± 30 nm and an emission window of 520 ± 35 nm, matching the excitation and emission of GelGreen dye was used for the DNA accumulation part. Another filter cube with excitation window of 455 ± 25 nm and an emission window of 600 ± 30 nm, according to the excitation and emission of Qubit dye was used for the histone part of experiment. The light source for the microscope was X-Cite 120LED and it was operated with 30% of the maximum exposure. The microscope was connected to a Raspberry Pi camera, programmed to activate the light source one second prior to capturing each image. Images were taken at 30 seconds intervals, with an exposure time of 4 seconds and an ISO setting of 400. To minimize interference from external background light, a black cloth covered the device during the imaging process. For each image the objective was centered on the agarose gates of the device. The experimental set up for DNA and histone accumulation is shown in figure 4.3. First, dried agarose gates were rehydrated by filling the top channels with the corresponding buffers. For the first part of the experiment

(DNA accumulation), the filter cube suitable for GelGreen dye was utilized. The device electrodes linked to sample and buffer channels for DNA concentration were connected to a power supply (Keithley 2410). Then, sample channels were filled. After 2 minutes waiting for staining DNA with GelGreen, 10 V was applied between the sample channel under the agarose gate with pH 8.5 and its buffer channel (figure 4.3a). Images were taken every 30 seconds for 5 minutes. When DNA accumulation was completed the filter cube was changed to the one matching the Qubit and objective was centered on the agarose gate with pH 11. Electrodes were also connected to the channels of the agarose gate with pH 11 for histone accumulation. After 12 minutes waiting time for Qubit and sample proteins labelling, 30 V was applied between the channels (figure 4.3b). Images were taken every 30 seconds for 5 minutes.

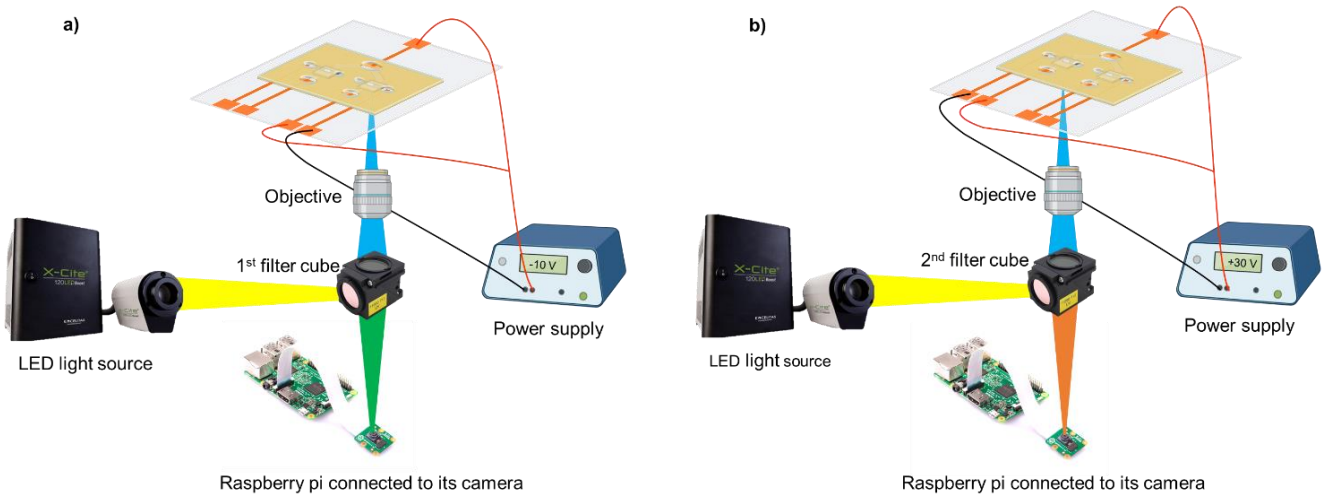

Figure 4.3 Experimental setup for each part of experiment. a) The setup for DNA detection part. b) The setup for histone detection.

4.3.5 Image analysis

The captured images by raspberry pi camera through both filters were analyzed using ImageJ. Original images were converted to grayscale. A region of interest (ROI) was defined around the agarose gates, represented by a slightly larger circle encompassing the original gate to account for any misalignment of the adhesive layers and cover all accumulations in the membrane. After

deducting the grayscale value obtained for each image from the initial grayscale value (background), the new value was used for representing the fluorescence intensity at that time point. The background value for each part of the experiments (DNA and histone accumulation) was determined as the average ROI value for all devices at the time when the agarose was completely rehydrated.

4.4 Results and discussion

4.4.1 Tagging and accumulating histone and DNA in the devices with immobilized dye

To demonstrate the possibility of immobilizing Qubit and GelGreen in dried state inside the device and still efficiently tagging and accumulating proteins and DNA, experiments using two samples of histones and DNA in buffer were performed. First, two devices with two perpendicular overlaid channels, one containing agarose in TAE buffer (pH 8.5) with immobilized GelGreen in sample reservoirs (5X diluted) and another one with agarose in CAPS buffer (pH 11) and immobilized Qubit in reservoirs were fabricated. The devices were tested the next day. A 1 mg/mL calf thymus histone was diluted from the stock solution in 50 mM Tris-HCl buffer, pH 8. For testing the device with immobilized Qubit, at the time of experiment for agarose rehydration, the top channel was filled with CAPS buffer with pH 11 similar to the pH of agarose isoelectric gate. An image was taken from the agarose gate after the rehydration (figure 4.4a). As a result of agarose rehydration, the membrane section turns transparent. Then, bottom channel was filled with the 1 mg/mL histone in buffer sample. Sample was pipetted several times in the sample inlet for enhancing mixing between the sample and immobilized Qubit. After 5 minutes waiting for binding Qubit and histones, 30 V was applied between the channels. When electric field is applied, histones tagged with Qubit, possessing a positive charge in the sample solution (pH 8), start to move toward the cathode and the agarose gate. Upon reaching the agarose gate with pH of 11, histones largely lose

their charge and become trapped. Figure 4.4a shows the change in fluorescence intensity in the gate at the time of applying voltage and after 5 minutes. At 0 minute, there is a slight fluorescence increase from filling the channel with sample and mix that with Qubit. The fluorescent intensity starts to increase by applying electric field.

Similar experiment was designed for accumulation of DNA in a device with immobilized GelGreen. After filling the top channel with 1X TAE buffer for agarose rehydration, the bottom channel was filled with 5 µg/mL of 150 bp DNA diluted from stock solution in 50 mM Tris-HCl buffer. Sample was pipetted several times in the sample channel reservoirs for better mixing of dried GelGreen and DNA. After 2 minutes waiting, 10 V was applied. By applying electric field, DNA due to its negative charge migrates towards anode in buffer channel and it traps inside the agarose loaded membrane as the agarose mobility is lower. Figure 4.4b shows the change in fluorescence intensity in the membrane at the time of applying voltage and after 5 minutes. At 0 minute, there is a small fluorescence increase from filling the channel with DNA sample and its binding with GelGreen. The fluorescent intensity starts to increase after applying the electric field.

Therefore, it was shown that both Qubit and GelGreen can be immobilized and stored inside the microfluidic device, eliminating the need for premixing the sample and dye outside the device. Both histone and DNA can be tagged efficiently with dried Qubit and GelGreen respectively and get accumulated inside the rehydrated agarose. However, sample and dye still need to get mixed inside the device for getting a homogeneous mixture of biomolecules labelled with their respective dyes. Failure to mix in the reservoir can result in uneven distribution of substances and suboptimal biomolecules labeling, leading to a poor signal. To enhance mixing in the future, several improvements such as incorporating mixing elements and electrokinetic mixing can be considered.

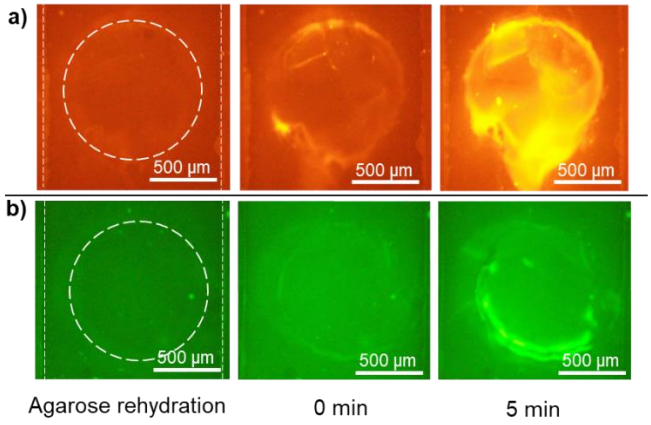

Figure 4.4 Tagging and concentration of a) histone and b) 150 bp DNA in the devices with integrated dried fluorescent dyes.

4.4.2 Trapping histones in the presence of high concentration of other background proteins (BSA) in a device with immobilized Qubit

The capability of the device with immobilized Qubit to detect histones in the presence of other proteins, such as a high concentration of albumin, was examined. Samples were prepared by mixing 40 mg/mL of BSA with different concentrations of histone. BSA was chosen due to its similarities in properties such as isoelectric point and weight to human serum albumin (HSA). Albumin constitutes a significant portion of blood plasma proteins, with a concentration ranging from 35 to 50 mg/mL and an isoelectric point around 5. Consequently, BSA with concentration of 40 mg/mL was chosen to mimic albumin in plasma. Considering the isoelectric point of BSA to be around 5 and histones around 11, they acquire opposite charges in the sample solution with pH of 8. BSA acquires negative charge, while histones obtain positive charge in the solution. Thus, when subjected to an electric field, they migrate in different directions.

A similar device with 2 µl of one-time diluted Qubit dried in the sample channels reservoirs was used. A new device was used for each repeat of the experiment. After filling the top channel with CAPS buffer, the bottom channel was filled with the sample containing 40 mg/mL BSA and 0, 20, and 33 µg/mL of histone. The sample was mixed several times with dried Qubit inside the

reservoirs by repeated pipetting. After 5 minutes waiting time for binding the proteins and Qubit, 30 V was applied between the channels. Images are demonstrated in figure 4.5a for the sample contains only BSA and BSA mixed with 20 and 33 µg/mL of histone at 0 and 5 minutes. In all the cases, the bottom channel shows a high fluorescence intensity, after filling and mixing the sample in the channel. This is because of the high concentration of BSA (40 mg/mL). After waiting time for complete binding proteins and Qubit dye, electric field was applied. In a pH 8 environment, BSA, gains negative charge and it moves away from the agarose membrane toward the positive electrodes at the ends of the sample channel. Meanwhile, histones move toward the gate and become trapped. The average intensity in the gate after 5 minutes for samples with 0, 20, and 33 µg/mL of histone is plotted in figure 4.5b. As depicted in the images, after 5 minutes the fluorescence intensity is highest in the gate for the 33 µg/mL sample. The intensity reduces with decreasing concentration of histone in the sample. In the control sample, nearly all of the BSA migrated toward the electrodes, and the membrane region got almost cleared of BSA after applying an electric field for 5 minutes. This indicates that the device with immobilized dried Qubit, effectively distinguishes between various levels of histones even in the presence of a high amount of albumin.

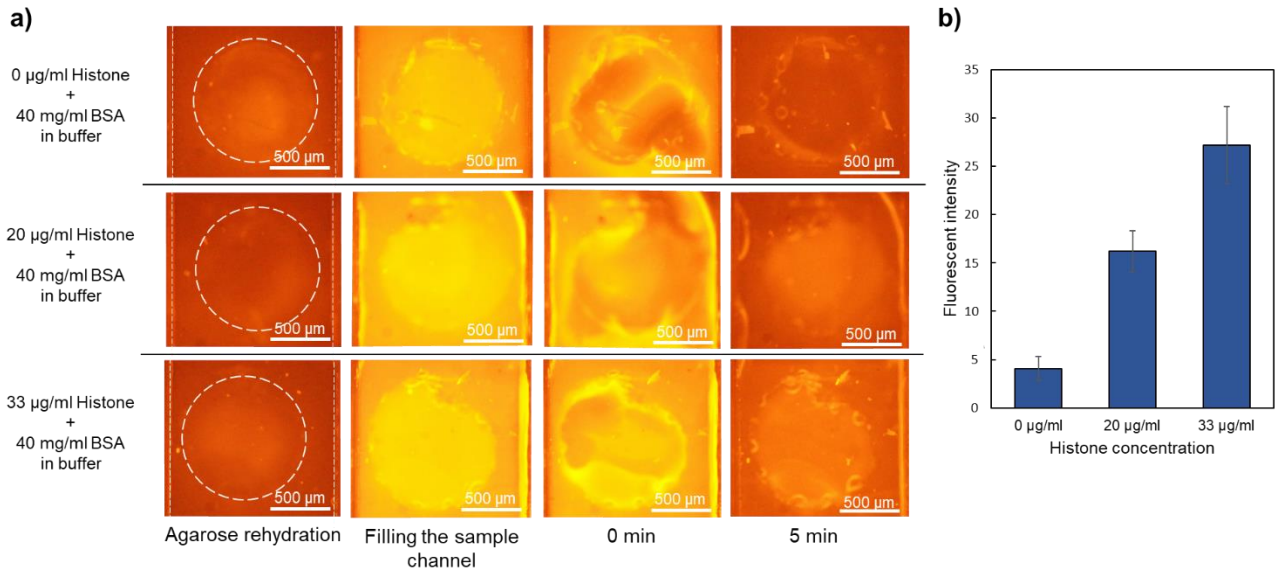

Figure 4.5 Trapping histones in the presence of 40 mg/mL BSA in the devices with immobilized Qubit. a) Images captured at the time of filling the sample channel, at the time of applying voltage (0 minute), and after 6 minutes for different samples. b) Fluorescence intensity values for each concentration of histone in the sample containing BSA (N=3).

4.4.3 Accumulation of DNA in the presence of histone in a device with immobilized GelGreen dye

In the next step, we studied the interference to DNA accumulation from presence of histones in a sample containing both. There will be binding of DNA to histone due to their natural function and charges. In order to identify whether free DNA is present in a mixture sample, a gel electrophoresis was performed. Four samples; only Qubit, mixture of 150 bp DNA tagged with GelGreen and histone tagged with Qubit with the similar weight ratio between cfDNA and histone in case of non-survivors, only 150 bp DNA tagged with GelGreen, and only histone tagged with Qubit were made. These samples were loaded in four wells of a 2% agarose gel and electrophoresis was performed with 75 mA for 45 minutes. As it is shown in figure 4.6a, a DNA band still formed from the sample containing both DNA and histone, however, the band in smaller compared to its corresponding DNA weight in the sample containing only 150 bp DNA. This shows that only a small portion of DNA in the mixture sample has been affected by electrostatic interaction between

DNA and histone and major part of the DNA or DNA bound histone, remained negatively charged. This shows that the designed device can be used for accumulating DNA and histone from a mixed sample in agarose gates with the mentioned working conditions.

We also tested this separation in the device containing immobilized GelGreen to investigate the functionality of the device with immobilized dye for the samples containing both DNA and histone. However, 5X diluted GelGreen which was used before, was not providing enough dye for the mixture of 150 bp DNA and histone. Therefore, less diluted immobilized GelGreen was used. Devices with 2 µl of 10X and 30X GelGreen deposited in the reservoirs were fabricated. The bottom channel was filled with the sample containing 5 µg/mL of 150 bp DNA and 30 µg/mL of histone. After waiting for staining DNA with GelGreen, 10 V was applied between channels. Following 5 minutes applying voltage, devices with 30X GelGreen demonstrated enough dye for tagging 5 µg/mL of 150 bp DNA in the presence of 30 µg/mL of histone (figure 4.6b). This dilution ratio was selected for the rest of the experiments.

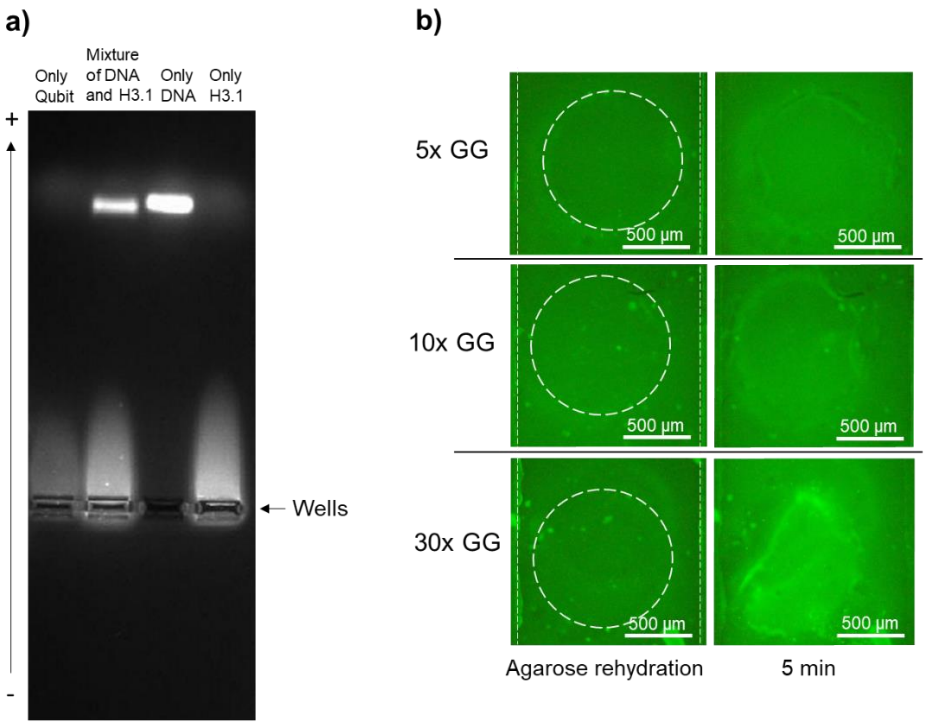

Figure 4.6 Accumulation of DNA in the presence of histones. a) Gel electrophoresis of DNA, histone, and mixture of DNA and histone. b) Tagging and separating DNA in the presence of histone with different dilution ratios for immobilized GelGreen.

4.4.4 Accumulation of DNA spiked in plasma in the presence of histone in the device with immobilized GelGreen

After testing the device with immobilized GelGreen with mixture of DNA and histone in buffer, devices with two regions of immobilized 30X GelGreen were made for accumulation of 150 bp DNA spiked in plasma in the presence of histone. Three samples with the corresponding concentration of cfDNA and histone in plasma for healthy person (no DNA or histone spiked), survivor (1 µg/mL 150 bp DNA and 20 µg/mL of histones), and non-survivor of sepsis (5 µg/mL 150 bp DNA and 33 µg/mL histones) were made. After rehydration of agarose by TAE buffer in top channel and filling the sample channel, we waited for 2 minutes. Then, 10 V was applied for initiating the migration of DNA towards the agarose gate. As it is shown in figure 4.7a, after 5 minutes, the fluorescent intensity in the agarose gate was higher for the sample containing 5 µg/mL 150 bp DNA compared to the sample with 1 µg/mL of DNA. Therefore, using the device with

immobilized 30X GelGreen for tagging cfDNA, survivors and non-survivors of sepsis, can be differentiated based on the fluorescent intensity in the agarose membrane (figure 4.7b).

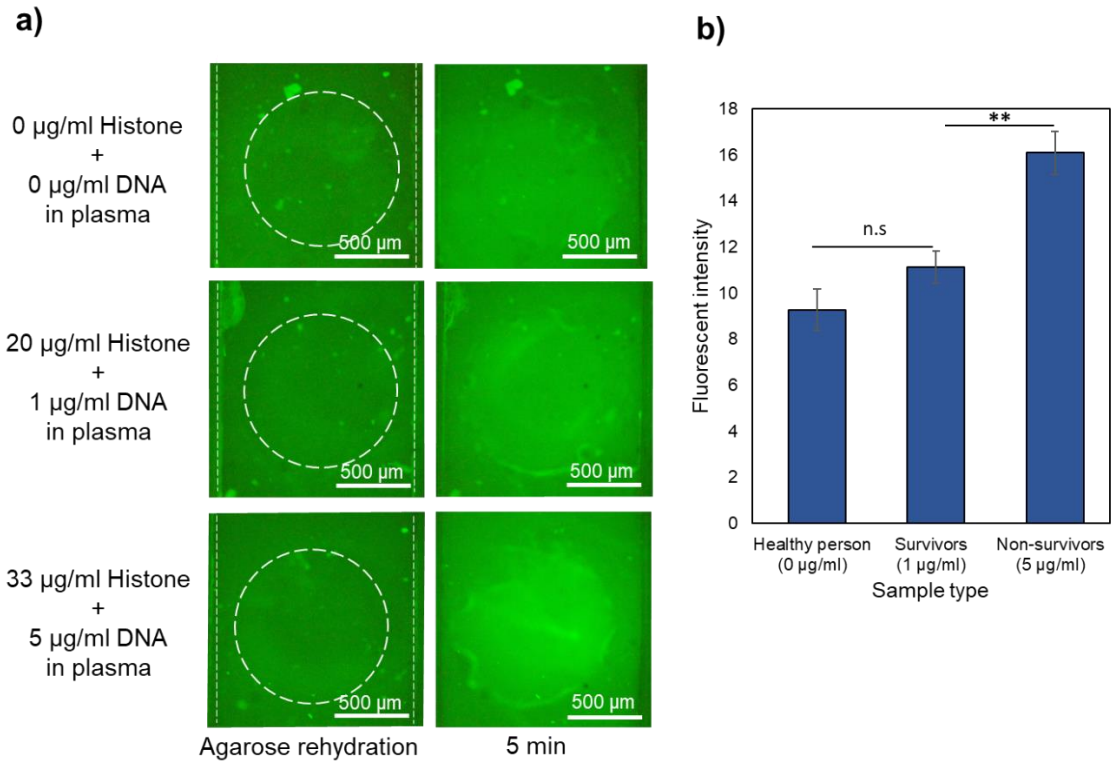

Figure 4.7 Accumulation of 150 bp DNA spiked in plasma in the presence of histone in the devices with 30X GelGreen. a) Images captured after agarose rehydration and after 5 minutes applying 10 V for samples representing healthy person, survivors, and non-survivors. b) Fluorescence intensity values for DNA concentrations corresponding to survivors and non-survivors (N=3). Statistical significance for samples calculated by two-tailed t-test (** $p < 0.01$).

4.4.5 cfDNA and Histone detection from human plasma samples in fully integrated device

After showing that 150 bp DNA and histone can be tagged with their dried immobilized fluorescent dyes and get accumulated in their corresponding agarose gates separately, we showed the possibility of integrating both of these accumulations in a same device with a single inlet for the sample and two agarose gates for concentrating DNA and histone. One of the challenges for integrating both of detections in a single device was the overlapping between the excitation and emission wavelengths of GelGreen and Qubit which can cause difficulty in fluorescent imaging if both are present in the sample at the same time. It was shown that if the plasma sample is mixed

with both GelGreen and Qubit, the fluorescent intensity coming from DNA/GelGreen get blocked due to the high concentration of plasma proteins tagged with Qubit (figure 4.8). Therefore, dyes need to be immobilized in different locations to minimize the chance of their mixture. Consequently, Qubit was deposited inside only one of the reservoirs of the sample channel under the agarose gate with pH 11. GelGreen was deposited in the main inlet as well as the other outlet of the sample channel separated from Qubit. With this deposition arrangement, Qubit only gets mixed with the sample part connected to pH 11 agarose gate for histone accumulation and it would not affect the fluorescent signal from DNA/GelGreen in the other channel. It should be noted that in case of histone accumulation, the movement of histone and DNA is in the opposite direction and therefore the presence of GelGreen in the channel for histone detection would not affect the final fluorescent signal from the agarose gate with pH 11.

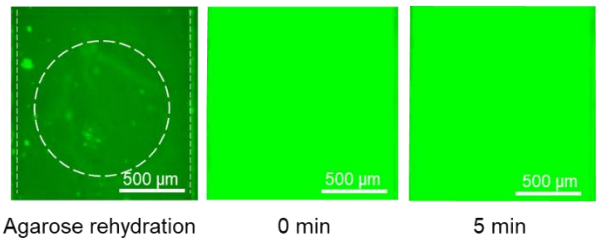

Figure 4.8 Fluorescence saturation inside the channel for DNA detection due to interference from plasma proteins tagged with Qubit when both dyes are mixed with the sample.

The final design for the integrated device consists of two agarose gates and immobilized fluorescent dyes with the optimized dilution ratio in separate reservoirs. The device is used for accumulating of both 150 bp DNA and histone from plasma. Three different samples resembling the plasma samples for healthy person, survivor, and non-survivor of sepsis were tested. To prepare the samples similar protocol as previously mentioned was followed. The deposited Qubit was not diluted in this case as the total plasma protein level can be up to 80 mg/mL. Also, 30X GelGreen was deposited in the sample main inlet and the outlet of the channel connected to agarose gate with

pH 8.5 during device fabrication. The experimental setup and conditions were like before. After 2 minutes waiting time for staining DNA and 5 minutes applying 10 V for DNA accumulation, the objective was centered on the other agarose gate for histone detection. The filter cube was also changed to the other one, suitable for Qubit. After 12 minutes waiting for tagging proteins with Qubit, 30 V was applied for 5 minutes between the channels for histone accumulation. The experiment was repeated 3 times for each concentration with a new device used in each repeat.

As it is shown in figure 4.9a, the fluorescent intensity in the agarose gate for both 150 bp DNA and histone after 5 minutes applying electric field is higher for samples simulating non-survivor condition compared to survivor, and survivor is greater than healthy person. Figure 4.9b also demonstrates the fluorescent intensity values for each of the biomarkers. This shows the device capability for differentiating between healthy persons, sepsis survivors and non-survivors based on the concentration of two biomarkers in less than 20 minutes using their plasma samples. For developing this device to a POC device for sepsis prognosis additional characterization is needed with clinical patients blood samples. Calibration with a range of cfDNA concentrations is also necessary to establish the device accuracy across different sample. Also, further modifications are required to enhance the device sensitivity and resolution, contributing to its effectiveness as a robust tool for sepsis prognosis.

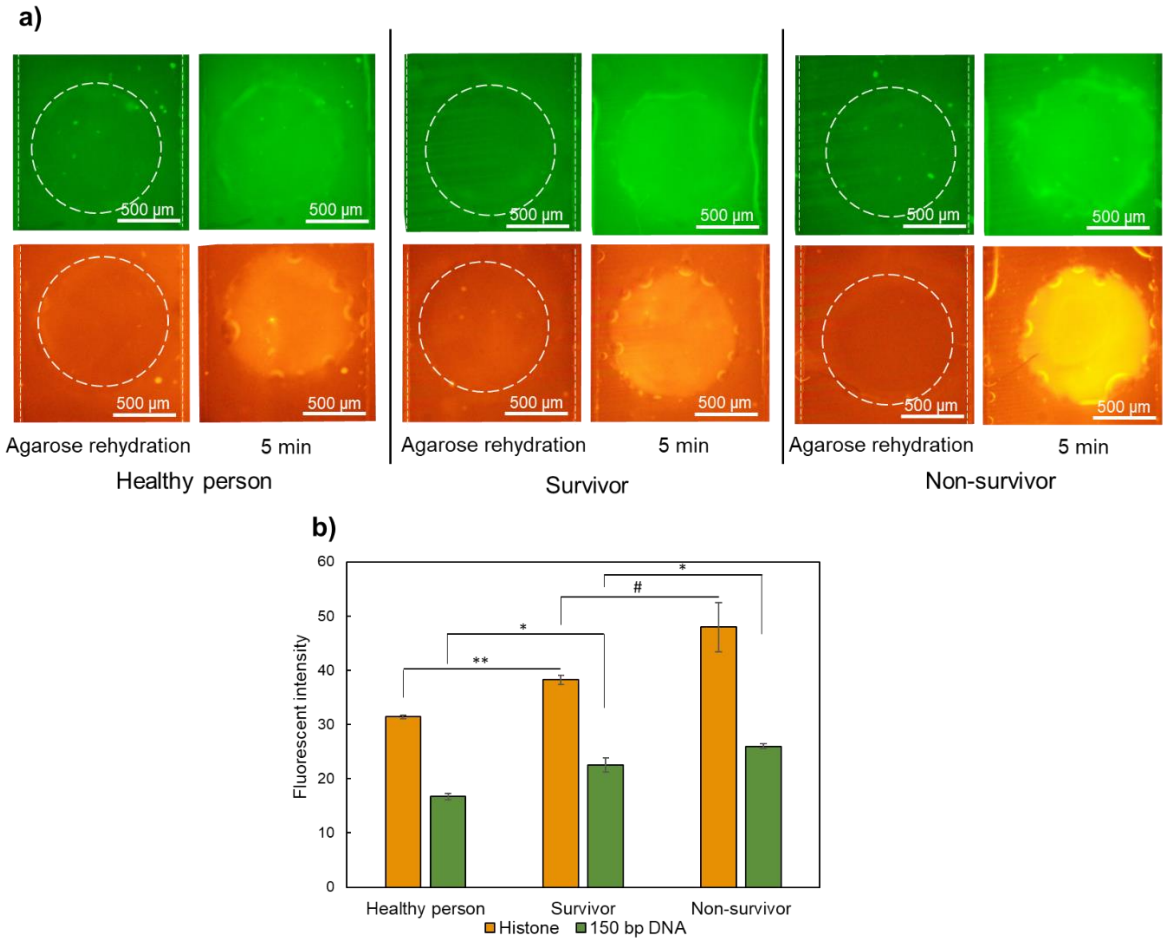

Figure 4.9 Trapping and concentrating 150 bp DNA and histone from spiked plasma sample in a fully integrated device. a) Images captured after agarose rehydration and after 5 minutes applying 10 V for DNA detection and 30 V for histone detection in the plasma samples representing healthy persons, survivors, and non-survivors. b) Plot showing changes in measured fluorescent intensity for DNA and histone for samples corresponding to healthy person, survivors, and non-survivors (N=3). Statistical significance for samples calculated by two-tailed t-test (** $p < 0.01$, * $p < 0.05$, # $p < 0.1$).

4.5 Conclusion

This paper presents a rapid, low-cost, and fully integrated microfluidic device for detection of cfDNA and free histone as prognostic biomarkers for sepsis. This microfluidic device detects both cfDNA and histones in a single platform by addressing previous limitations, such as the need for sample pretreatment and off-chip dye mixing. The study demonstrates the feasibility of immobilizing fluorescent dyes, Qubit for histones and GelGreen for DNA, in a dried state within the device while efficiently tagging and accumulating the respective biomolecules. The

incorporation of dehydrated agarose gates and immobilized fluorescent dyes enhances efficiency and simplifies the process. Xurography, a rapid and cost-effective microfluidics fabrication technique, is employed for all device fabrication steps. The device was tested with 30 µl of samples containing both 150 bp DNA and histones spiked in plasma, representing healthy individuals, sepsis survivors, and non-survivors. Results demonstrated the device ability to differentiate between these groups based on the concentration of the two biomarkers within less than 20 minutes. This suggests the device potential as a point-of-care tool for sepsis prognosis, offering rapid assessments of multiple biomarkers from patient plasma samples. However, more characterization is needed for using clinical patients samples and the device needs to be calibrated with other concentrations. Additionally, for a point-of-care device, the DC power supply needs to be substituted with batteries. Moreover, simplifying the fluorescent microscope can be achieved by incorporating a LED light source and optical filters.

References

1. Singer, M.; Deutschman, C.S.; Seymour, C.W.; Shankar-Hari, M.; Annane, D.; Bauer, M.; Bellomo, R.; Bernard, G.R.; Chiche, J.-D.; Coopersmith, C.M. The Third International Consensus Definitions for Sepsis and Septic Shock (Sepsis-3). *Jama* **2016**, *315*, 801–810.

2. Li, Y.; Wan, D.; Luo, X.; Song, T.; Wang, Y.; Yu, Q.; Jiang, L.; Liao, R.; Zhao, W.; Su, B. Circulating Histones in Sepsis: Potential Outcome Predictors and Therapeutic Targets. *Frontiers in Immunology* **2021**, *12*, 650184.

3. McGregor, C. Improving Time to Antibiotics and Implementing the" Sepsis 6". *BMJ Open Quality* **2014**, *2*, u202548-w1443.

4. Charoensappakit, A.; Sae-khow, K.; Rattanaliam, P.; Vutthikraivit, N.; Pecheenbuvan, M.; Udomkarnjananun, S. Cell-Free DNA as Prognostic and Diagnostic Biomarkers for Adult Sepsis: A Systematic Review and Meta-Analysis. **2023**.

5. Kim, M.-H.; Choi, J.-H. An Update on Sepsis Biomarkers. *Infection & chemotherapy* **2020**, *52*, 1.

6. Cheng, Z.; Abrams, S.T.; Alhamdi, Y.; Toh, J.; Yu, W.; Wang, G.; Toh, C.-H. Circulating Histones Are Major Mediators of Multiple Organ Dysfunction Syndrome in Acute Critical Illnesses. *Critical care medicine* **2019**, *47*, e677–e684.

7. Dwivedi, D.J.; Toltl, L.J.; Swystun, L.L.; Pogue, J.; Liaw, K.-L.; Weitz, J.I.; Cook, D.J.; Fox-Robichaud, A.E.; Liaw, P.C. Prognostic Utility and Characterization of Cell-Free DNA in Patients with Severe Sepsis. *Critical care* **2012**, *16*, 1–11.

8. Eichhorn, T.; Linsberger, I.; Lauková, L.; Tripisciano, C.; Fendl, B.; Weiss, R.; König, F.; Valicek, G.; Miestinger, G.; Hörmann, C. Analysis of Inflammatory Mediator Profiles in Sepsis Patients Reveals That Extracellular Histones Are Strongly Elevated in Nonsurvivors. *Mediators of Inflammation* 2021, ***2021***.

9. Jing, Q.; Leung, C.H.C.; Wu, A.R. Cell-Free DNA as Biomarker for Sepsis by Integration of Microbial and Host Information. *Clinical Chemistry* **2022**, *68*, 1184–1195.

10. Wildhagen, K.C.; Wiewel, M.A.; Schultz, M.J.; Horn, J.; Schrijver, R.; Reutelingsperger, C.P.; van der Poll, T.; Nicolaes, G.A. Extracellular Histone H3 Levels Are Inversely Correlated with Antithrombin Levels and Platelet Counts and Are Associated with Mortality in Sepsis Patients. *Thrombosis research* **2015**, *136*, 542–547.

11. Gould, T.; Lysov, Z.; Liaw, P. Extracellular DNA and Histones: Double-edged Swords in Immunothrombosis. *Journal of Thrombosis and Haemostasis* **2015**, *13*, S82–S91.

12. Marsman, G.; Zeerleder, S.; Luken, B.M. Extracellular Histones, Cell-Free DNA, or Nucleosomes: Differences in Immunostimulation. *Cell death & disease* **2016**, *7*, e2518–e2518.

13. van der Meer, A.J.; Kroeze, A.; Hoogendijk, A.J.; Soussan, A.A.; van der Schoot, C.E.; Wuillemin, W.A.; Voermans, C.; van der Poll, T.; Zeerleder, S. Systemic Inflammation Induces Release of Cell-Free DNA from Hematopoietic and Parenchymal Cells in Mice and Humans. *Blood advances* **2019**, *3*, 724–728.

14. Zeerleder, S.; Stephan, F.; Emonts, M.; De Kleijn, E.D.; Esmon, C.T.; Varadi, K.; Hack, C.E.; Hazelzet, J.A. Circulating Nucleosomes and Severity of Illness in Children Suffering from Meningococcal Sepsis Treated with Protein C. *Critical care medicine* **2012**, *40*, 3224–3229.

15. Rhodes, A.; Wort, S.J.; Thomas, H.; Collinson, P.; Bennett, E.D. Plasma DNA Concentration as a Predictor of Mortality and Sepsis in Critically Ill Patients. *Critical care* **2006**, *10*, 1–7.

16. Gargano, A.F.; Shaw, J.B.; Zhou, M.; Wilkins, C.S.; Fillmore, T.L.; Moore, R.J.; Somsen, G.W.; Paša-Tolić, L. Increasing the Separation Capacity of Intact Histone Proteoforms Chromatography Coupling Online Weak Cation Exchange-HILIC to Reversed Phase LC UVPD-HRMS. *Journal of proteome research* **2018**, *17*, 3791–3800.

17. Kailasa, S.K.; Kang, S.H. Microchip-Based Capillary Electrophoresis for DNA Analysis in Modern Biotechnology: A Review. *Separation & Purification Reviews* **2009,** *38*, 242–288.

18. Shahriari, S.; Selvaganapathy, P.R. Integration of Hydrogels into Microfluidic Devices with Porous Membranes as Scaffolds Enables Their Drying and Reconstitution. *Biomicrofluidics* **2022**, *16*, 054108.

19. Shahriari, S.; Damodara, S.; Selvaganapathy, P.R. Isoelectric Trapping and Discrimination of Histones from Plasma in a Microfluidic Device Using Dehydrated Isoelectric Gate. *Microchimica Acta* **2024**, *191*, 131.

20. Shahriari, S.; Patel, V.; Selvaganapathy, P.R. Xurography as a Tool for the Fabrication of Microfluidic Devices. *Journal of Micromechanics and Microengineering* **2023**.

5 Chapter 5 Conclusion and Future work

5.1 Conclusion

In this thesis, first, a new approach to integrate hydrogels into microfluidic devices using a combination of porous membranes and xurography was introduced. The developed technique allows for the creating of multiple hydrogel locations with different shapes and sizes as small as 200 μm during the fabrication of the microfluidic device. Currently, the most popular method for integration of gels into microfluidic devices is photopolymerization. However, the required post-processing steps such as rinsing the channels from un-crosslinked precursor, make this technique relatively complicated. Also, by using porous membranes for hydrogel integration, the hydrogel can be stored for prolonged amount of time within the device. Rehydration can occur around the membrane fibers while maintaining a seal. Demonstration of usefulness of this technique for hydrogel integration was achieved by making microfluidic devices for electrophoretic accumulation and detection of two sepsis biomarkers (cfDNA and histones) in rehydrated agarose. This highlights the method potential utility in point-of-care diagnostics where long storage of hydrogels is needed.

Sepsis is a serious medical condition which needs an immediate attention. Several biomarkers such as Procalcitonin (PCT), C-reactive protein (CRP), cfDNA, and histones have been found to be useful, either by themselves or as a panel for sepsis prognosis. cfDNA and total circulating histones which are released during cell death as the result of sepsis serves as prognostic indicators for sepsis ICU mortality. Therefore, the development of devices for rapid and cost-effective detection of cfDNA and free histones in plasma samples enable a more accurate prognosis for severe sepsis patients.

Creating a tool that can detect such diverse biomarkers (a genomic biomarker and a proteomic biomarker) poses challenges due to the varying detection methods required for each. However, here a fully integrated microfluidic device capable of analysing both genomic (cfDNA) and proteomic (total circulating histones) biomarkers using a unified detection platform was demonstrated. In order to develop the final device, first, two microfluidic devices composed of dehydrated agarose membranes were developed for accumulation of cfDNA and histones separately. In the microfluidic device for detecting cfDNA, the fluorescently labelled DNA was electrophoretically trapped inside the rehydrated agarose. There was a clear difference in the fluorescent intensity of the agarose region between 1 and 5 μg/mL of DNA, representing cfDNA concentration in survivors and non-survivors of sepsis.

For detecting total free histones, a similar microfluidic device containing a dehydrated agarose gate with pH 11 for isoelectric trapping of histones was fabricated using xurography. Incorporating agarose gate with specific pH without the need for a specifically targeted dye greatly reduces the cost of histone detection. It was shown that dehydrated and rehydrated agarose membrane gate still behaves effectively to achieve isoelectric trapping. Separation and accumulation of histones tagged with a non-specific fluorescent dye in a dehydrated agarose membrane with pH 11 was demonstrated. The microfluidic device used 30 Volts for differentiating between healthy individuals, sepsis survivors, and non-survivors in less than 10 minutes.

Finally, a fully integrated microfluidic device for simultaneous detection of both cfDNA and histones was introduced. The possibility of immobilizing fluorescent dyes, Qubit for histones and GelGreen for DNA, in a dried state within the device was also investigated. It was shown that dried dyes still could effectively tag and accumulate the respective biomolecules. This immobilization overcomes the need for off-chip sample and dye premixing. It was illustrated that the integration

of dehydrated agarose gates and immobilized fluorescent dyes, simplify workflow in testing and enable the use of the device with minimal training. The microfluidic device was tested with 30 µl samples containing both 150 bp DNA and histones spiked in plasma, representing healthy individuals, sepsis survivors, and non -survivors. The device could differentiate between these groups in less than 20 minutes using low voltages. These findings suggest the device potential as a point of care tool for sepsis prognosis.

5.2 Future directions

In the following, some works for continuing and further developing the proposed devices are suggested:

1- The preliminary experiments demonstrated the device promising potential for detecting both cfDNA and histones. However, to validate its effectiveness in a clinical setting, further experiments are required with clinical patient samples. Here, DNA and histone spiked plasma samples were used to simulate survivors and non-survivors severe septic patients plasma samples as proof of concept. Moreover, device need to be calibrated with varied concentrations of both biomarkers to ensure its accuracy across different levels of biomarker presence. Also, the sensitivity and resolution of the device should be tested and enhanced.

2- In order to develop a POC device, enhancements to the experimental method and setup are crucial. One critical aspect involves making the device more compact and portable to enhance its usability across various settings. This can be done by replacing the DC power supply with batteries, thereby eliminating the need for a constant power source. Also, simplifying the fluorescent microscope by incorporating a LED light source and optical filters, reducing complexity and cost. These enhancements improve the practicality and accessibility of the POC device.

3- Another limitation of current device is the requirement of manual mixing of the sample with the dried immobilized dyes in the reservoirs by means of several pipetting, which is not desirable in a POC device. Therefore, the manual mixing can be substituted by an automated mixing process which enhances mixing efficiency and reliability. One possible solution is to implement electrokinetic mixing, a technique that utilizes electric fields to induce fluid motion and promote mixing of the sample with the immobilized dyes. Alternatively, integrating mixing elements directly into the device design can also facilitate automated mixing. By incorporating these automated mixing mechanisms, the need for manual intervention is eliminated.

4- Detection of other sepsis biomarkers can be incorporated in the device as well. The current device can be expanded by adding more isoelectric gates for separation and detection of other sepsis biomarkers from the sample. This can be helpful for simultaneous detection of multiple biomarkers using a single device. Also, the application of the device can be extended for other medical conditions such as cancer where quantification of similar biomarkers is required. Therefore, the device with some modifications can be applied for other purposes.

Overall, this thesis presents a promising platform for rapid and low-cost detection of sepsis prognostic biomarkers using dehydrated and rehydrated agarose gates. The techniques and devices that have been developed have the potential for further improvement to suit their current application or other potential applications that may be explored in the future.